LMS/RUL/S08716

Modeling of Flow and Transport Induced by Gas Production Wells near the Project Rulison Site, Piceance Basin, Colorado

June 2013

Approved for public release; further dissemination unlimited

U.S. DEPARTMENT OF ENERGY | Legacy Management

Available for sale to the public from:

U.S. Department of Commerce
National Technical Information Service
5301 Shawnee Road
Alexandria, VA 22312
Telephone: 800.553.6847
Fax: 703.605.6900
E-mail: orders@ntis.gov
Online Ordering: *http://www.ntis.gov/help/ordermethods.aspx*

Available electronically at *http://www.osti.gov/scitech/*

Available for a processing fee to U.S. Department of Energy and its contractors, in paper, from:

U.S. Department of Energy
Office of Scientific and Technical Information
P.O. Box 62
Oak Ridge, TN 37831-0062
Phone: 865.576.8401
Fax: 865.576.5728
Email: reports@adonis.osti.gov

LMS/RUL/S08716

Modeling of Flow and Transport Induced by Gas Production Wells near the Project Rulison Site, Piceance Basin, Colorado

June 2013

This page intentionally left blank

Contents

Figures

Tables

Appendixes

Abbreviations

BCF	billion cubic feet
^{14}C	carbon-14
DOE	U.S. Department of Energy
DRI	Desert Research Institute
ft	feet
g/mol	grams per mole
^{85}Kr	krypton-85
LM	Office of Legacy Management
m	meters
MCF	thousand cubic feet
MMCF	million cubic feet
N/S	north/south
psi	pounds per square inch
THO	tritiated water

Executive Summary

The 1969 Project Rulison test in western Colorado, the second natural gas stimulation experiment in the Plowshare Program, was conducted to determine if a nuclear device could be used to fracture low-permeability, gas-bearing rock to enhance natural gas production. Following the detonation, testing on the reentry well produced gas at rates significantly greater than those of conventional wells of the time; however, the presence of radionuclides in the produced gas persisted above acceptable levels, and the reentry well was shutin in April, 1971 and site wells were plugged and abandoned in 1976 and 1977 (Austral 1977). Recent advances in hydrofracturing technology have made it feasible to extract natural gas from low-permeability reservoirs and have led to a significant increase in drilling in the area. Drilling activity near the Rulison site has raised concerns that remnant radioactivity in the detonation zone could migrate to nearby producing wells and enter the natural gas distribution system.

Radionuclides that can exist in the gas phase and were created in significant amounts by the detonation are of primary concern because of their potential mobility. The relative permeability of the gas phase is orders of magnitude greater than that of liquids in the natural-gas-producing reservoirs at the Rulison site. Gas-phase radionuclides other than tritium were largely removed by production testing. The depletion of tritiated methane by the production testing leaves tritiated water vapor as the primary mobile contaminant of concern at Rulison. Tritiated liquid water in the detonation zone acts as a source that partitions from the low-mobility aqueous phase to the higher-mobility gas phase.

Numerical modeling can be used to make predictions about a site's flow system and contaminant transport potential by quantitatively replicating the site conceptual model and various aspects of the system, allowing past, current, and future scenarios to be tested. A limitation of the previous Rulison models was the computational constraint that limited the size of the volume that could be included in the model domain. The modeling effort has been continued using a multiprocessor version of the modeling code to allow the model domain to be extended to include current gas production wells 0.75 mile west of the site and to span the entire productive interval. The Rulison model was initialized to conditions following the detonation and used to simulate the reentry well production testing, the subsequent pressure recovery after testing ended, migration of contamination from the detonation zone to its current extent, and the effects on the flow system of recently installed gas wells. The new Rulison model was calibrated to not only the historical reentry well data, but to production data from the current producing wells. Attempts were made to be more conservative than previous models by elongating the detonation zone, both the chimney and surrounding nuclear fractured region, in the direction of the natural fracture trend in the area. The extended domain made it possible to simulate the effects of the enactment of the Rulison Path Forward document (DOE 2010), which recommends a conservative, staged approach to drilling in the area. This study confirmed the results of the previous Rulison modeling in that it predicts that contamination, in the form of tritiated water, is contained within the institutional control boundary of Lot 11. Simulations of future wells producing in the lot adjacent to the site do not induce migration, though a small pressure gradient develops between the detonation zone and the hydrofractured intervals at the same depth as the detonation zone. The modeling provides quantifiable results that allow the effects of gas production on the flow system and the potential for contaminant migration to be visualized at the Rulison site.

This page intentionally left blank

1.0 Introduction

The Piceance Basin in western Colorado contains significant reserves of natural gas in poorly connected, low-permeability (tight) sandstone lenses of the Mesaverde Group. The ability to enhance the production of natural gas in this area has long been a goal of the oil and gas industry. The U.S. Atomic Energy Commission, predecessor agency to the U.S. Department of Energy (DOE) and the U.S. Nuclear Regulatory Commission, participated in three tests using nuclear detonations to fracture gas-bearing formations in an effort to enhance gas production. The tests were conducted under Project Plowshare, a program designed to identify peaceful, beneficial uses for nuclear devices. The first, Project Gasbuggy, was conducted in 1967 in the San Juan Basin of New Mexico. The 29-kiloton fission-fusion device produced significant amounts of tritium (38,000 curies, Sokol 1970) in the subsurface. The two subsequent tests in the Piceance Basin of Colorado (Figure 1), Project Rulison in 1969 and Project Rio Blanco in 1973, were designed to limit the amount of tritium produced by using fission devices and enhanced shielding. The 40-kiloton (DOE 2000) Rulison device produced 10,000 curies of tritium (Reynolds 1971), and the three simultaneously detonated 33-kiloton devices (DOE 2000) at Rio Blanco produced 1,000 curies each, for a total of 3,000 curies (Toman 1974). Among the many radionuclides created by the detonations, tritium is considered the most likely radionuclide that could feasibly migrate to nearby gas producing wells due to its occurrence in both the gas and liquid phases, its abundance relative to other mobile radionuclides, and its relatively long half-life (12.3 years) as compared to the many short-lived (half-lives on the order of days or less) radionuclides produced by the detonation.

The ability to enhance natural gas production from tight sands has become practical through advances in hydrofracturing technology. Fluids with entrained sand are pumped into gas reservoirs at high pressure, creating fractures that extend outward from the wellbore. After fracturing, the fluid is pumped out, and the sand remains, keeping the fractures propped open, enhancing reservoir permeability and gas flow to a well. The ability to hydrofracture tight sandstones has enabled gas development in the Piceance Basin. An increase in drilling activity near the Rulison site has raised concerns that contamination (specifically, radionuclides produced by the detonation) currently contained in the subsurface could be released through a gas well drilled too close to the site.

As wells are drilled nearer the Rulison site, the DOE Office of Legacy Management (LM) has taken the approach outlined in the June 2010 Rulison Path Forward document (DOE 2010, available on the LM website: http://www.lm.doe.gov/Rulison/Documents.aspx). The Path Forward recommends that drillers adopt a conservative, staged approach to gas development. They are encouraged to drill wells in areas with a low likelihood of encountering contamination (both distance and direction from the detonation zone are factors) and to collect data from these wells prior to drilling nearer the site's institutional control boundary. The Path Forward relies in part on the results from a numerical modeling effort that has been refined over time. The modeling results indicate that contamination has been contained within the 40-acre institutional control boundary, Lot 11 (Figure 2). The Path Forward document also couples the model predictions with the monitoring of gas and produced water from the gas wells and the monitoring of shallow groundwater near the site (see the Monitoring Plan on the LM website). In coordination with the Colorado Oil and Gas Conservation Commission, DOE reviews applications to drill within 3 miles of the site.

Figure 1. Delineation of the Piceance Basin
(based on the contact between Tertiary and Upper Cretaceous rocks, Green 1996)

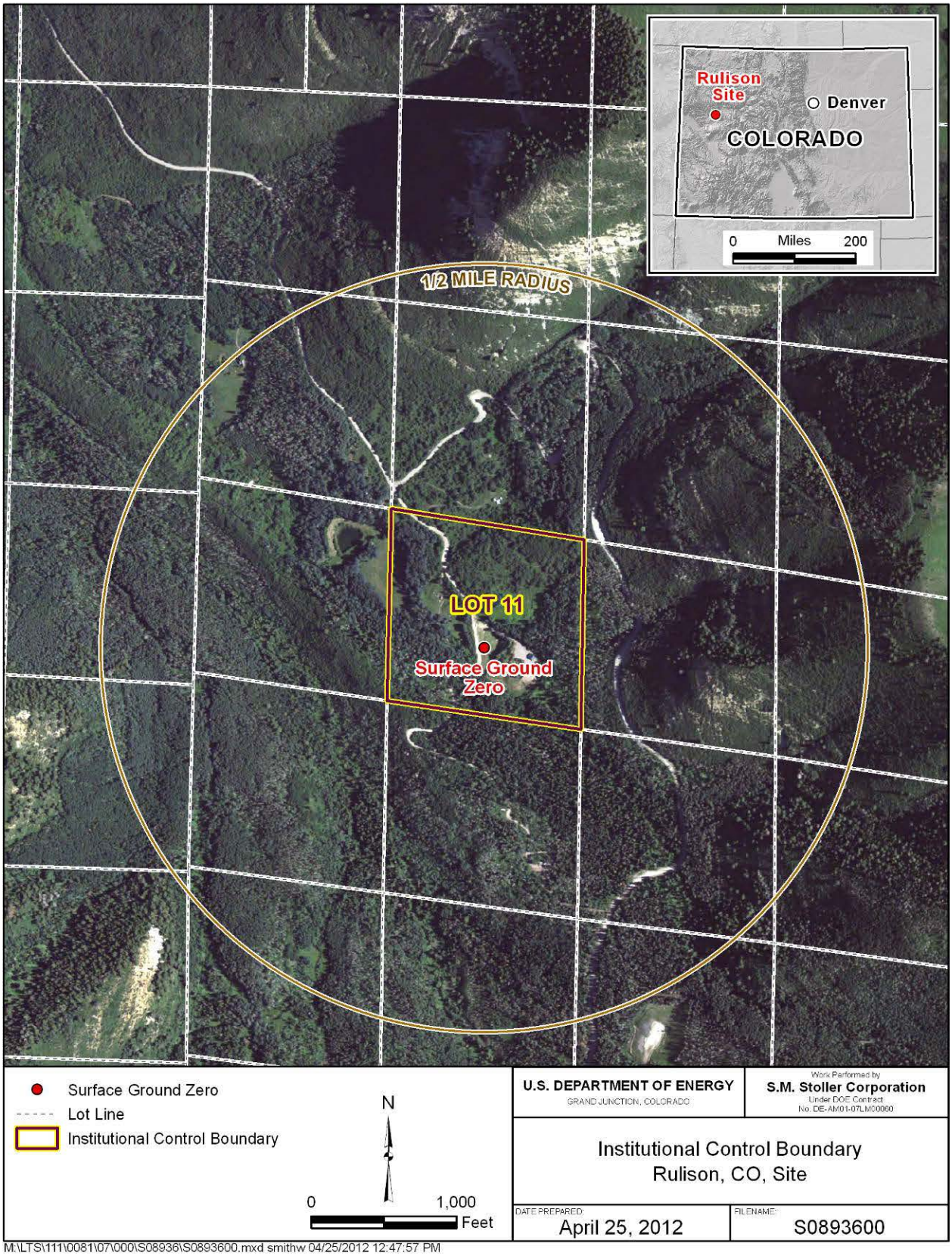

Figure 2. Lot 11, 40-Acre Institutional Control Boundary

1.1 Modeling Objectives

A numerical model is a tool that incorporates hydrogeologic data for a given site to make quantitative predictions on fluid flow and potential contaminant transport. The various models of both Rulison and Rio Blanco were used to estimate the current extent of contamination, simulate the flow of fluids to one or more producing wells as they are drilled nearer the detonations, and evaluate the potential for contaminant migration from the detonation zone to the wells.

1.1.1 Summary of Past Modeling

The original Rulison flow and transport modeling performed by Desert Research Institute (Cooper et al. 2007) indicated that contamination (specifically tritium) was unlikely to migrate beyond Lot 11 even with a gas production well only 200 feet (ft) from the lot boundary. Reviews of the model results identified concerns with the value of the partitioning coefficient controlling the distribution of tritiated water between the liquid and vapor phases, the assignment of effective porosity to hydraulically generated fractures surrounding a hypothetical production well, and the treatment of molecular diffusion in the partially saturated reservoir. These concerns were addressed in the Model Addendum (Cooper et al. 2009) through additional computer simulations testing the impact of these model features on the degree to which tritium is transported away from the detonation zone. A concern not addressed by the addendum was the limited use of data from the site in constructing the model. The model was updated in 2010, the Rulison Model Update (Cooper et al. 2010), to address this concern. The updated model used sandstone and shale ratios from nearby wells (less than 0.5 mile from the model domain) and was calibrated to historical data from the reentry well production tests performed in 1970 and 1971. A detailed summary of three of the previous modeling reports by DRI (from Rio Blanco through Rulison) is provided in Appendix A of this report and the concurrent Rio Blanco modeling report. The three previous modeling reports (Cooper et al. 2007, 2009, 2010) are included on the accompanying DVD.

1.1.2 Rationale for Additional Rulison Modeling

A limitation of the previous Rulison models was the computational constraints that limited non-isothermal models to about 100,000 elements (grid blocks). This limits the vertical and horizontal extents of the model domain, given that individual elements need to be sufficiently small to represent the heterogeneity of the producing formation in order to realistically simulate flow and transport. Previous models simulated production from one to several perforation intervals in a single hypothetical well opposite the detonation. With the advent of a massively parallel version of the modeling code (TOUGH2_MP), problems requiring several million elements can now be simulated. The modeling effort has been continued with an extended model domain that includes current gas production wells to the west and spans the entire productive interval. This new Rulison model was calibrated to not only the historical reentry well data, but to production data from current producing wells. The extended domain made it possible to simulate the effects of the enactment of the Rulison Path Forward (DOE 2010).

1.2 Geologic Setting

The Tertiary and Cretaceous strata of the Piceance Basin contain significant hydrocarbon reserves. The Green River Formation is estimated to contain up to 1.45 trillion barrels of oil in

place (http://www.ogj.com/articles/2011/10/green-river-shale-oil-in-place-put-at-1-45-trillion-bbl.html), half of which is in the Piceance Basin. Gas reserves in the Upper Cretaceous Mesaverde Group (Figure 3), primarily the Williams Fork Formation in which the Rulison nuclear test occurred, are estimated at 300 trillion cubic feet (http://oilshalegas.com/piceancebasin.html). The Williams Fork Formation is composed of low-permeability, discontinuous, interbedded fluviodeltaic sandstones and shales. The tight sandstones in the lower two-thirds of the Williams Fork can be stimulated by hydrofracturing to enhance production. Sandstones in the upper one-third of the Williams Fork are not production targets due to their higher water content, which lowers the relative permeability of the gas phase and causes water production to be excessive compared to the amount of gas that can be produced. Wells near Rulison are being located on 10 acre-centers, about 400 ft north-south and about 1,320 ft east-west of adjacent wells. The east-west trend of natural fractures in the Williams Fork causes the hydrofracturing and drainage patters to be elongated in that direction.

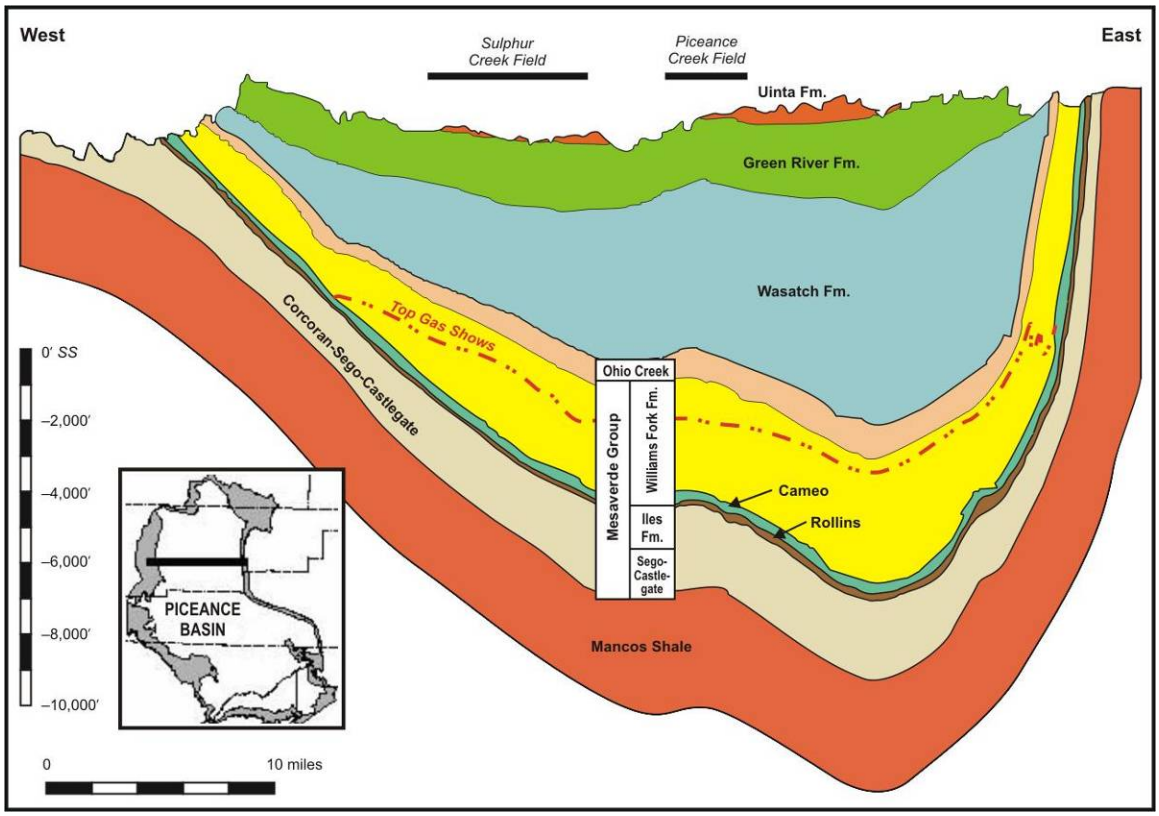

(modified from Yurewicz 2003)

Figure 3. Piceance Basin Cross Section

1.3 Nuclear Test Description

The extremely high temperatures associated with a subsurface nuclear detonation vaporize a volume of rock and produce a roughly spherical cavity surrounding the detonation point. A high-pressure shock wave spreads from the blast, fracturing the rock beyond the cavity wall to a distance related to the yield of the device, depth of burial, and the rock properties. As the high temperatures decrease, the vaporized rock condenses to a liquid melt that flows to the base of the cavity. Within minutes to hours after the detonation, the fractured rock above the cavity usually

collapses, forming a rubble-filled chimney. The chimney region extends upward from the base of the former cavity to where open fractures end and a stable vaulted ceiling forms. The rubble zone with rock fragments entrained in a glassy matrix forms when the cavity collapses into the basal melt zone. The relatively rapid rate of cooling causes the solidified melt rock to have a vitreous texture (melt glass).

The Rulison test consisted of a single 40-kiloton detonation at a depth of 8,425 ft below ground surface. A cavity with a 76 ft radius (AEC 1973) was created within milliseconds of the detonation, and the chimney formed as the overlying fractured rock collapsed from 1 minute to 9 hours after the detonation (Frank 1971). The top of the chimney was picked at a depth 8,151 ft below ground surface, the depth at which the reentry well lost circulation, and 275 ft above the detonation, making the chimney/cavity complex 350 ft high. Based on modeling after the detonation, the formation permeability was increased 33-fold to a distance of 2.75 cavity radii, or 209 ft. This was interpreted as the extent of the nuclear fracturing (Montan 1971).

1.4 Radionuclide Source and Potential Migration Pathways

An underground nuclear detonation produces a number of radionuclide contaminants with the potential to migrate with passing fluids (liquid and gas). The radionuclides include unburned fissile fuel such as uranium and plutonium isotopes, fission products such as cesium-137 and strontium-90, activation products from neutron bombardment of device hardware and the surrounding lithology, and tritium (Bowen et al. 2001). Not all radionuclides produced by a detonation pose a long-term hazard. Radionuclides with short half-lives that quickly decay to undetectable levels and those produced in amounts so small that they never exceed regulatory limits can safely be disregarded. Radionuclides with properties that make them essentially immobile in certain geologic environments are also of less concern than those that are more mobile in the subsurface. Each radionuclide exists as a solid, liquid, or gas under various temperature and pressure conditions depending on its chemical properties. For instance, most radionuclides have a high melting point, causing them to solidify with and become entrained in the melt rock as it cools. In water-saturated environments, the melt rock can be subject to dissolution, which could potentially lead to the slow release of radionuclides into passing groundwater. Many radionuclides strongly sorb to mineral grains, causing their migration rate to be much slower than the rate of groundwater movement. The migration of radionuclides from melt rock dissolution has been shown to be limited in saturated environments, and in unsaturated environments where formation water is practically immobile (as at the Rulison site), dissolved radionuclides are not expected to move beyond the detonation zone. For all practical purposes, isotopes of uranium, plutonium, cesium, and strontium are immobile in the geologic environment surrounding the Rulison detonation zone and are protected from direct access by the existing institutional control areas.

Radionuclides that can exist in the gas phase (Table 1) and were created in significant amounts by the detonations are of primary concern because of their potential mobility. The relative permeability of the gas phase is orders of magnitude greater than that of liquids in the natural-gas-producing reservoirs of the Williams Fork Formation. The gas phase largely consists of methane with smaller amounts of ethane, propane, carbon dioxide, water vapor, and other minor constituents. Gas-phase radionuclides produced by the Rulison detonation (Reynolds 1971) in order of abundance were estimated at approximately 10,000 curies of tritium (an isotope of hydrogen with two neutrons), approximately 1,100 curies of krypton-85 (^{85}Kr, a noble gas), and

minor amounts of argon isotopes and carbon-14 (^{14}C) (AEC, 1973). Mobile radionuclides other than tritium were largely removed by production testing (described below) and radioactive decay. The depletion of tritiated methane by the production testing leaves tritiated water (as vapor or liquid) as the primary mobile contaminant source for the Rulison site.

Table 1. Gas-Phase Components and Potential Radionuclides

Gas Component	Possible Radionuclides
Carbon dioxide (CO_2)	$^{14}CO_2$
Natural gas (methane (CH_4), water vapor (H_2O)	THO, $^{14}CH_4$, CTH_3
Hydrogen gas (H_2)	HT
Noble gases	^{85}Kr, ^{37}Ar, ^{39}Ar

THO = tritiated water; CTH_3 = tritiated methane; HT = tritiated hydrogen gas; Ar = argon

The most likely transport mechanism to the surface for tritiated water vapor in or near the detonation zone is with natural gas extracted from a nearby production well. To be of concern, the well would have to be close enough to interact with the potentially contaminated region. Wells in the Piceance Basin near Rulison are located on a 10-acre spacing to drain an area of roughly 1,200 ft by 300 ft (10 acres), with the long axis oriented east-west, along the natural fracture trend in the Williams Fork Formation. In practice, this requires four wells per quarter-quarter section (centered east-west and aligned north-south) to drain each 40-acre parcel. The majority of wells installed at this spacing do not interact with one another or with wells in adjacent 40-acre lots. It is evident that wells east and west of the detonation zone would be in the most susceptible transport direction due to the increased permeability in that direction and the tendency of fractures to propagate in that direction.

Production data continue to support 10-acre spacing for wells near the Rulison site, though no wells at this spacing have produced for an entire life-cycle of 20–25 years. If this history holds, material within Lot 11 (the institutional control area) should not be impacted by wells located in adjacent lots, including those to the east and west. Shortly after the detonation, gas-phase contaminants were spread through the nuclear chimney and likely through the adjacent nuclear fractured region. Reentry well production testing following the detonation removed about two chimney volumes of gas and created an inward pressure gradient that persisted for years, drawing contaminants from the nuclear fractured region back to the chimney (and out the wellbore during testing). It is predicted that as the inward pressure gradient of the testing dissipated, tritium likely spread by gaseous diffusion back throughout the region of increased permeability and possibly beyond.

1.4.1 Radionuclides Removed by Production Testing

A reentry well was drilled into the Rulison chimney and tested to determine the success of the detonation at improving gas production. The well produced 455 million cubic feet (MMCF) of gas in 107 days of testing that took place from October 1970 through April 1971 in four separate flow tests. The produced gas was flared to the atmosphere, and samples of the produced gas and produced water (much of which was condensed water vapor) were collected and analyzed to determine the degree to which radioactivity levels changed as testing progressed. All releases during drilling and testing were monitored by the U.S. Environmental Protection Agency

National Environmental Respiratory Center and the Colorado Department of Health to protect workers at the site, the public, and the environment (AEC 1973).

As expected, the radioactivity levels decreased throughout the testing as gas from the chimney region was produced, burned, and replenished by uncontaminated gas from the surrounding formation. Sample analysis indicated that approximately 1,060 of the 1,100 curies of ^{85}Kr were removed by the production testing (Smith 1971). The concentration of ^{85}Kr in the produced gas (assumed well-mixed throughout the detonation zone due to its inert nature) was closely monitored throughout the testing to determine when radioactive gas from the detonation zone was depleted. Due to radioactive decay, less than 7 percent of any ^{85}Kr that was not removed by testing would remain in 2009. Table 2 provides an estimate of the ^{85}Kr inventory for Rulison and the inventory of Rio Blanco for comparison. Sample results also indicate that the estimated 2.5 curies of ^{14}C produced by the detonation was removed during the production testing.

Table 2. Krypton-85: Created by Detonation, Removed by Testing, Remains in 2012 After Decay

^{85}Krypton (Curies)	Created	Testing Removed	Remains in 2012
Rulison	1,113[a]	1,062	trace
Rio Blanco (upper)	775[b]	775	0
Rio Blanco (middle)	775[c]	0	75
Rio Blanco (lower)	775[c]	244	55

[a] Precise number from integration of concentration data (AEC 1973), typically rounded to 1,100 curies
[b] Estimate for upper chimney, ± 80 curies (Toman 1974)
[c] Estimate for upper chimney used for middle and lower chimneys

Approximately 3,000 of the original 10,000 curies of tritium were removed by the production testing, leaving 7,000 curies of tritium that would have decayed to 600 curies by 2012. Tritium was initially present in hydrocarbons (mostly methane with lesser amounts of ethane and propane), hydrogen gas, and water (vapor and liquid). Production testing data indicate that essentially all gas-phase tritium was removed from the detonation zone. The remaining tritium is likely present in liquid water and in minerals that make up the melt rock. Table 3 provides an estimate of the tritium inventory for Rulison and Rio Blanco for comparison. Tritium does not exchange with normal hydrogen atoms in hydrocarbons except at the very high temperatures that occur during and soon after the detonation. If a significant portion of the remaining tritium is in the melt rock, the source of mobile radionuclides at Rulison will be decreased. However, the tritium present in liquid water in the detonation zone will be a long-term source (until it decays) that evaporates to form mobile tritiated water vapor.

Table 3. Tritium: Created by the Detonation, Removed by Testing, Remains in 2012 After Decay

Tritium (Curies)	Created	Testing Removed	Remains in 2012
Rulison	10,000	3,000	600
Rio Blanco (upper)	1,000	202[a]	80
Rio Blanco (middle)	1,000	0	100
Rio Blanco (lower)	1,000	51[b]	100

[a] 150 curies injected into Fawn Creek Govt #1 well (CER 1975)
[b] 28 curies injected into Fawn Creek Govt #1 well
20 of the 178 tritium curies injected would remain in 2012 after decay

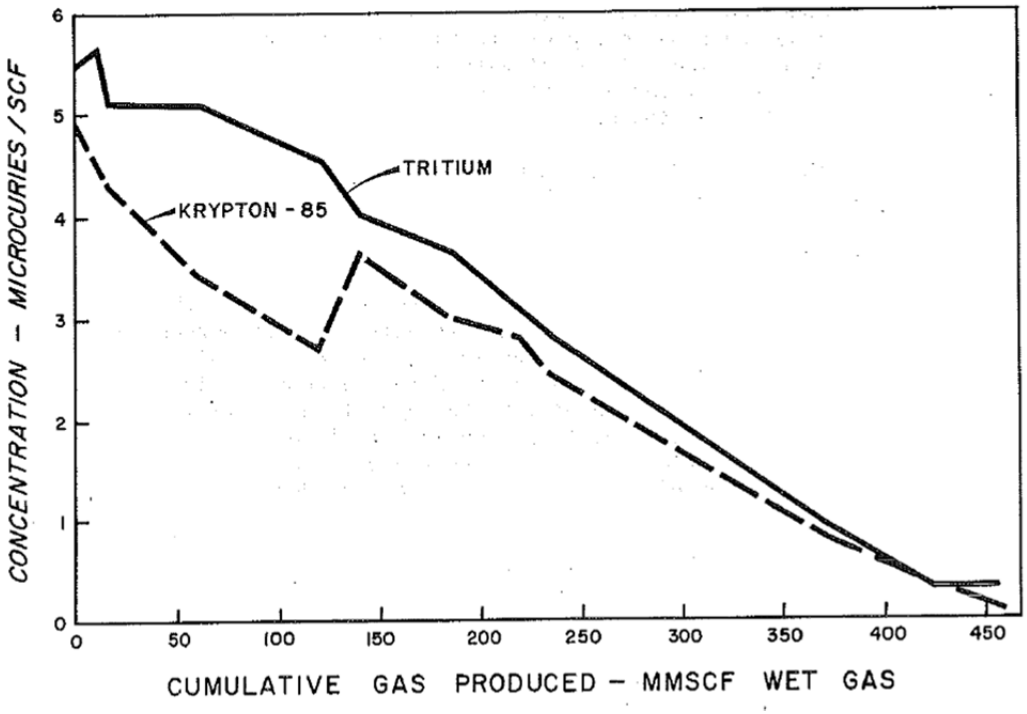

Note: MMSCF = million standard cubic feet Source: AEC 1973

Figure 4. Concentration of Tritium and Krypton-85 During the Reentry Well Production Testing

2.0 Conceptual and Numerical Model of Flow and Transport within the Mesaverde

The very low permeabilities of the Williams Fork Formation, on the order of microdarcys for the sandstones and even less for the shales, indicate that there is no appreciable flow of gas or liquid within the time frame of concern (hundreds to thousands of years). Non-stimulated wells produce from only a short distance from the wellbore, and for a well to produce enough gas to warrant drilling, formation permeability has to be increased to allow flow. The nuclear detonation at Rulison effectively created a highly stimulated zone with an extremely permeable chimney and a surrounding fractured region of increased permeability. The calculated dimensions of the cavity, chimney, and nuclear fractured region are based on data from drilling the reentry well and its production testing. Current methods stimulate wells by fracturing the surrounding formation through the injection of fluids with entrained sand under high pressure. There is a limit to the distance from the wellbore that this is effective, and that distance varies with lithology and other factors. In the Williams Fork Formation near Rulison, it has been shown that stimulated wells recover gas from an area of about 10 acres without influencing adjacent wells. The typical drainage pattern and area has been confirmed by over a hundred wells drilled near the Rulison site. The wells are expected to produce about a billion cubic feet (BCF) or more of gas on average over a 20−25-year life.

A numerical model is a tool that attempts to quantitatively replicate the site conceptual model and various aspects of the system to allow different scenarios to be tested. At the Rulison site, an important scenario is the minimum distance a producing gas well can be located from the nuclear

test cavity without inducing contaminant migration. The modeling code is selected based on its ability to simulate the important processes at a site. For instance, the code selected for this study must be able to simulate multiphase flow and transport of a radionuclide (tritium as tritiated water) that is present in both the aqueous and gas phases and to simulate the production of natural gas from wells in the Williams Fork Formation. To improve confidence in the reliability of results, the model is calibrated to site data to test whether it can reproduce what is already known and thus ensure that parameters such as permeability are within reasonable ranges.

The model uses an equivalent porous media approach even though flow is predominantly through a fractured system. The approach is justified in that the fractures through which flow occurs are assumed to be frequent with limited extents in the low permeability formation, and not rare and extensive, such that they would short-circuit the flow system. The mechanical forces that create the nuclear fractured and hydrofractured regions rubblize the formation to increase permeability.

2.1 Numerical Modeling Code

The TOUGH2_MP code (Transport of Unsaturated Groundwater and Heat_Massively Parallel processing) (Zhang et al. 2008), was selected for the modeling. It is a multiphase, multicomponent, non-isothermal code that allows components to partition between phases depending on thermophysical properties. The equation of state selected was EOS7R, which allows for five components (water, brine, parent radionuclide [RN1], daughter radionuclide [RN2], and air) and two phases (aqueous and gas). The code was modified to calculate a temperature-dependent Henry's law constant based on the vapor pressure. The code was also modified to change the properties of the "air" component to those of methane to better represent the gas reservoirs of the Williams Fork Formation. Simulations were run remotely on a supercomputer at Clemson University. The earlier Rulison and Rio Blanco models used the single processor version of TOUGH2. The versions of the code are essentially the same except for the ability of TOUGH2_MP to handle much larger problems with many more elements in significantly faster simulation times.

3.0 Rulison Model Construction

A number of steps are involved in constructing a numerical model. First, the specific size and location of the area to be modeled has to be selected, then it has to be discretized into individual elements. The elements have to be populated by material types that represent the domain lithology as closely as data permit. For Rulison, this includes separate types for the detonation zone and hydrofractured regions near wells. The material types are differentiated based on assigned parameters such as permeability, porosity, and capillary properties. Appropriate boundary conditions and initial conditions have to be determined and assigned. And finally, the handling of sources and sinks for simulating extraction of material from the domain.

3.1 Rulison Model Domain and Discretization

The horizontal and lateral extents of the Rulison model domain were increased from the previous DRI models to include existing gas production wells 0.75 mile west of the site (Figure 5 and Figure 6) and to include the entire gas-productive lower two-thirds of the Williams Fork

Formation. The horizontal extent is 6,000 ft in the east-west direction and 4,000 ft in the north-south direction (Figure 7). The vertical extent of the model domain is 2,200 ft—the 2,000 ft thick lower two-thirds of the Williams Fork Formation and an additional 200 ft into the non-producing upper third of the Williams Fork (Figure 8). This allows data from the recently installed (2010) producing wells to be incorporated into the model to support historical data from the emplacement well and the re-entry well (included in previous models). The three-dimensional model is discretized into elements that are 50 ft (15.24 meters [m]) in the horizontal *x* and *y* directions (element centers shown on Figures 6 and 7) and 20 ft (6.1 m) in the vertical *z* direction, for a total of 1,056,000 elements (120*x*, 80*y*, 110*z*). Subsets of the model (Figure 5) were extracted to reduce simulation times for calibrating to the historical post-shot production testing data and current gas well production data.

3.2 Formation Lithologic Distribution

Model elements have to be populated with `ROCK` types that realistically represent the subsurface at the site. `ROCK` is the keyword in the TOUGH2 input file that identifies the block with information about the different material types. Each `ROCK` type is assigned a set of parameters (see Section 3.5) that affect flow and transport throughout the model. The Williams Fork Formation at the Rulison site is primarily composed of discontinuous interbedded shale and sandstone lenses. The sandstones vary in clay content; the cleaner sandstones (the producing sandstones) are the main candidates for perforating and hydrofracturing. Data from Noble Energy, the primary operator in the area, indicate that about 42.5 percent of the targeted Williams Fork section near Rulison can be considered producing sandstones. The remaining 57.5 percent is considered shale for the purposes of the model. Figure 9 shows a vertical slice through a sandstone-shale realization with the detonation zone.

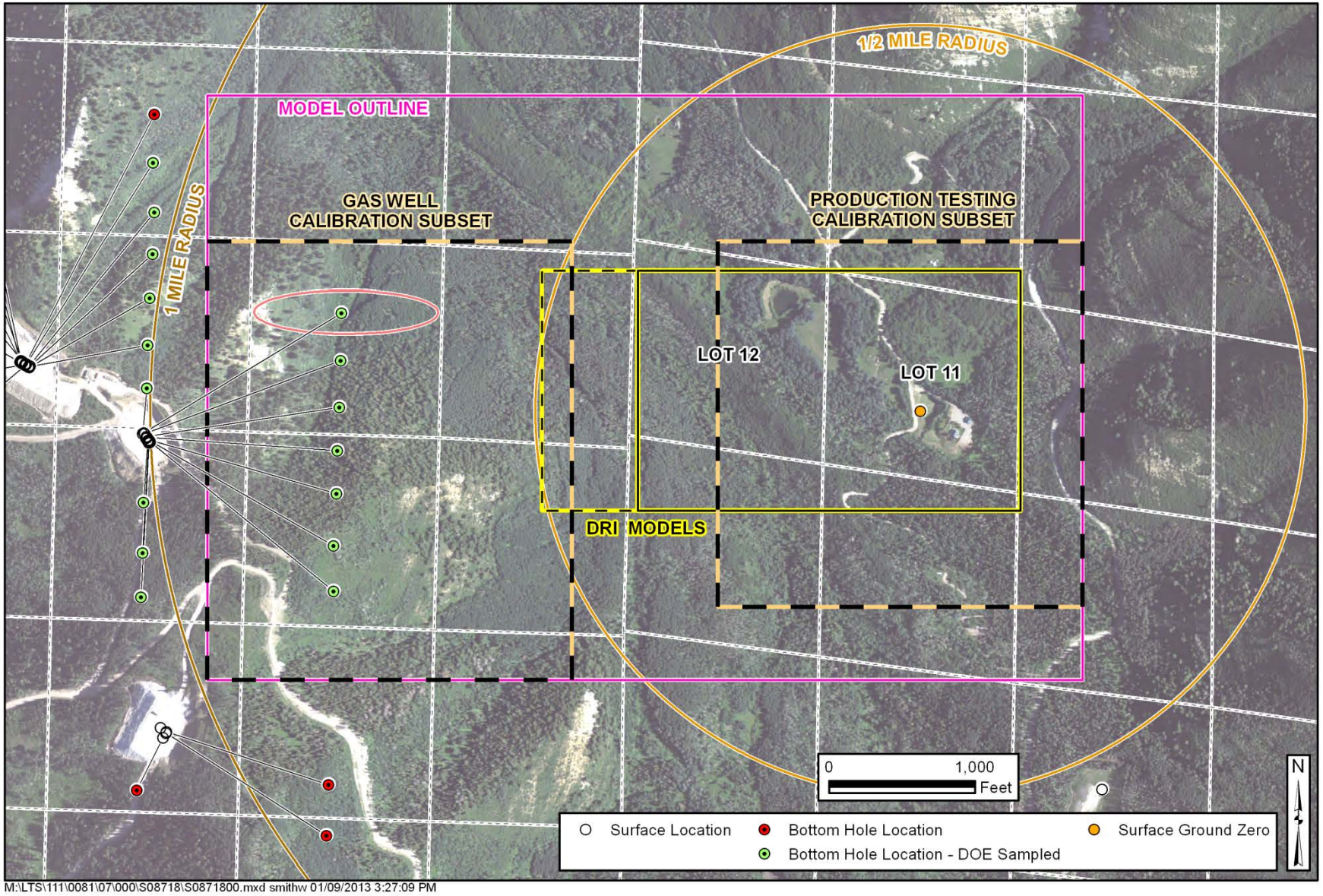

Figure 5. Horizontal Extent of Current and Previous Model Domains

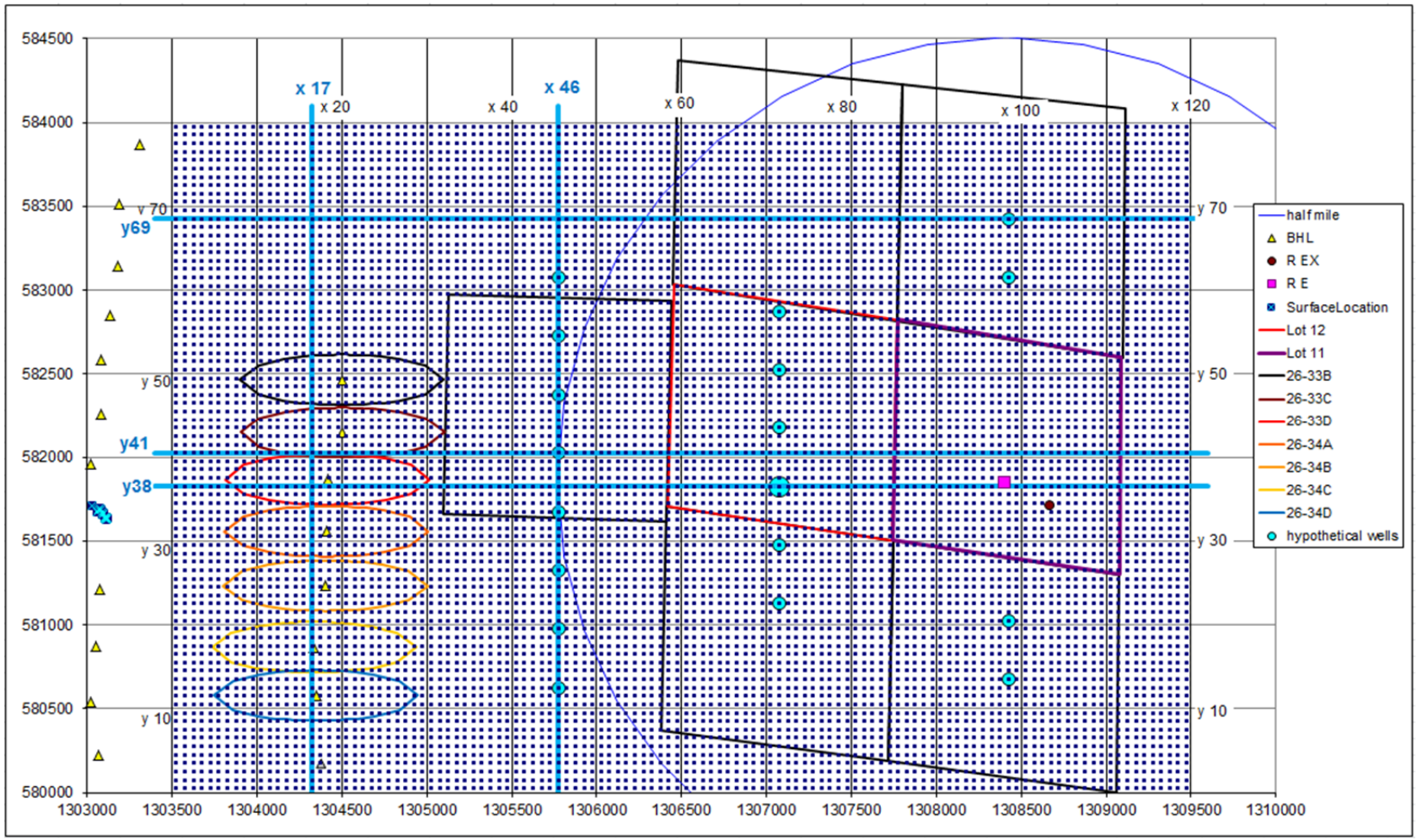

Figure 6. Map of the Rulison Model in Real Coordinates
(feet, State Plane Colorado central, NAD 27) including lot boundaries, current wells with diagrammatic drainage extent, simulated hypothetical wells (light blue), and element centers (dark blue). Blue lines are reference for section 5.2.

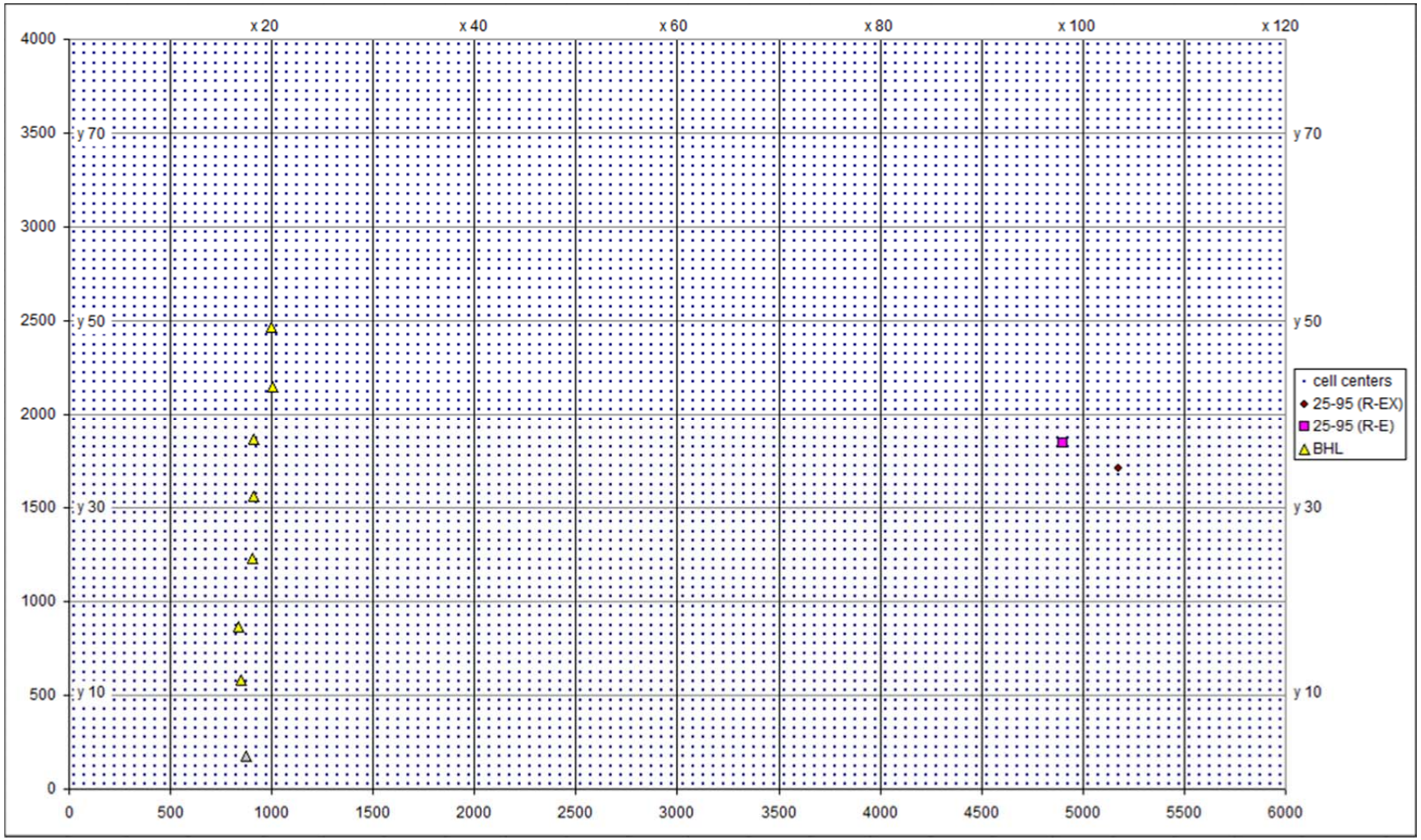

Figure 7. Map of the Rulison Model in Model Coordinates Including Current Wells, Simulated Hypothetical Wells, and Element Centers

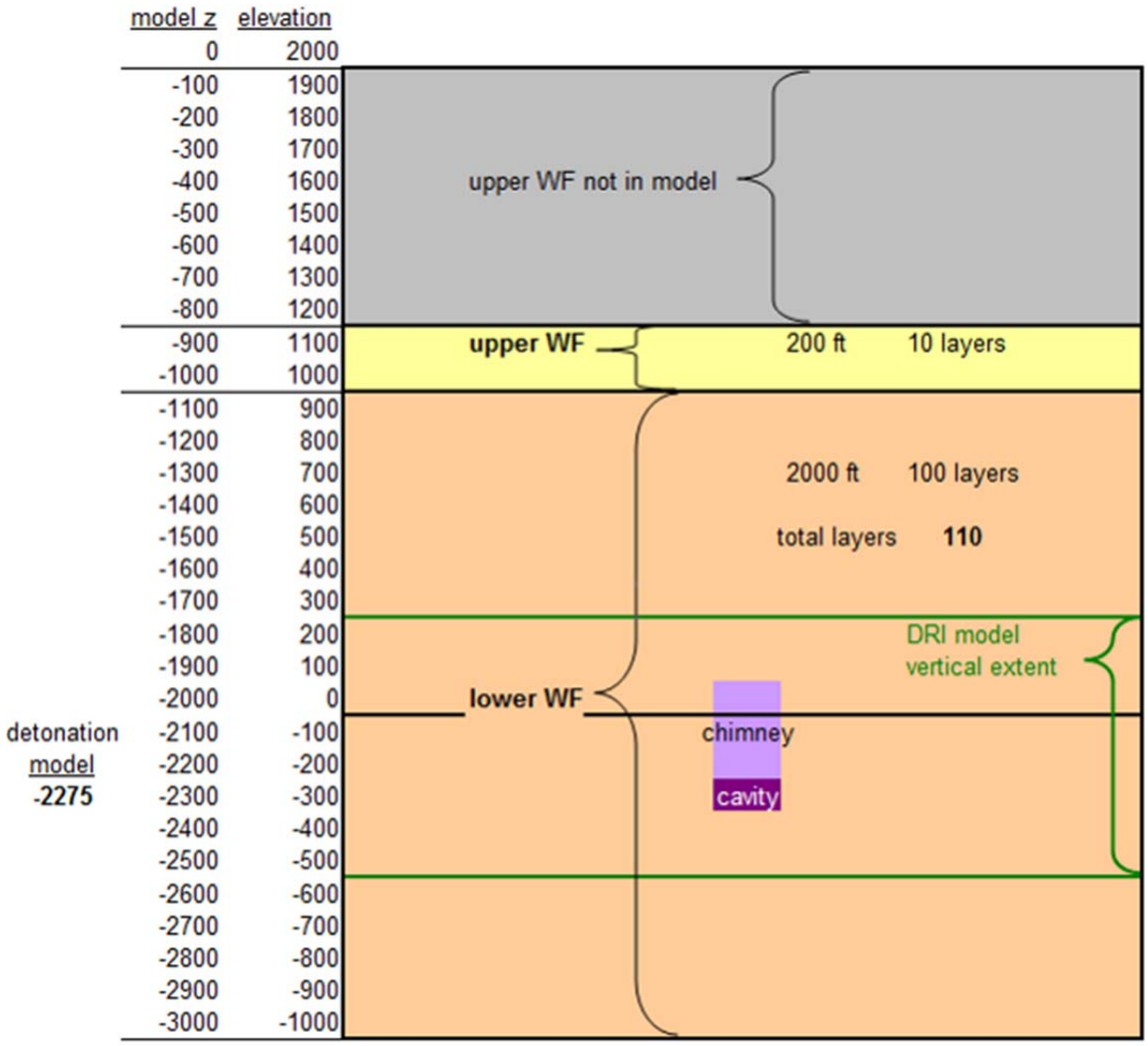

Figure 8. Vertical Extent of the Rulison Model with Model Depth, Elevation, and Vertical Extent of Previous Models

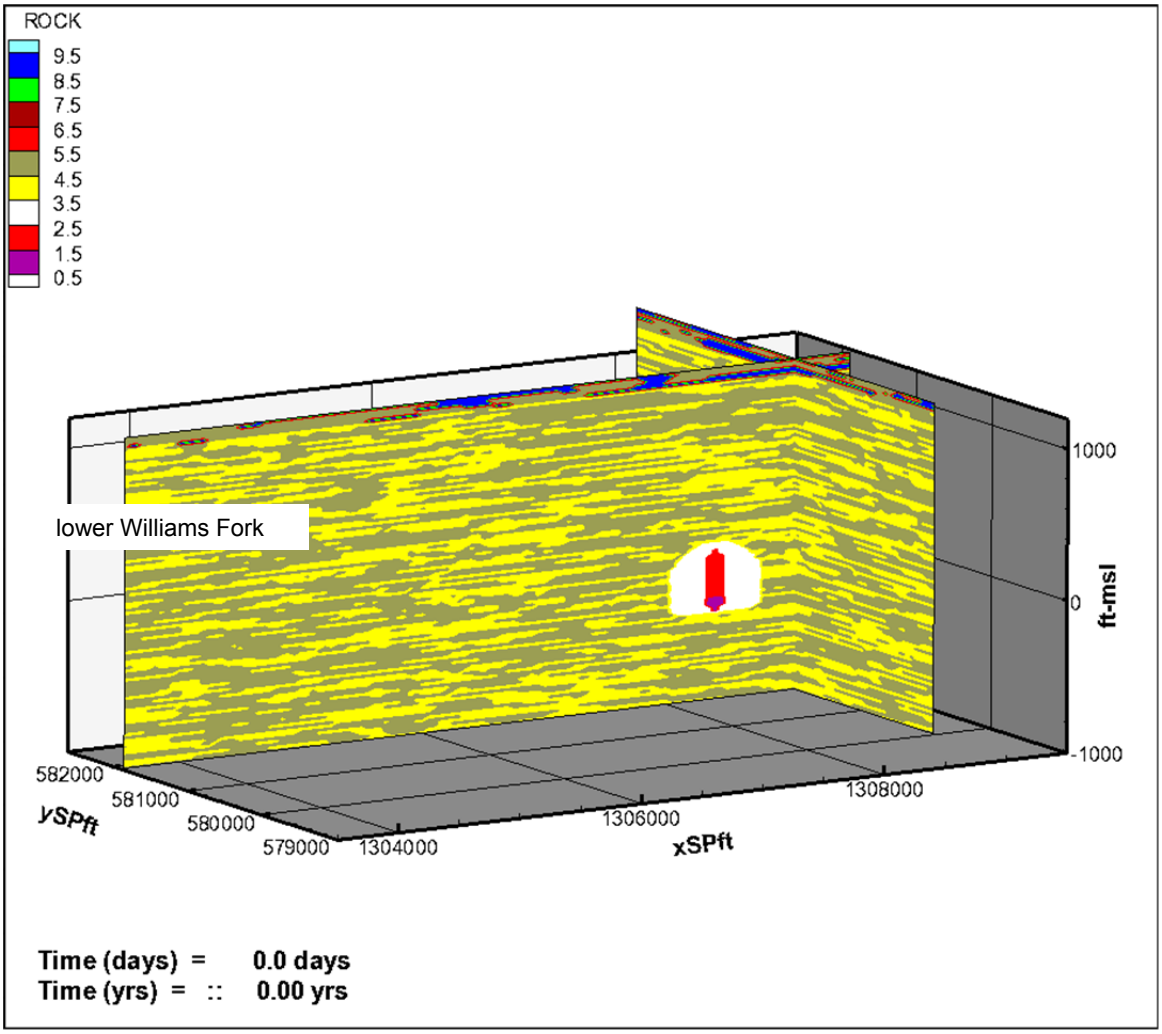

Figure 9. Rulison Model Lithologic Distribution
ROCK color numbers match with the order of ROCK type in section 3.5, yellow = lower Williams Fork sandstone, olive = shale, white = nuclear fractures, red = chimney, purple = melt glass, blue = upper Williams Fork sandstone

Geophysical and lithologic logs from the exploratory and emplacement wells were used with published statistics on sand body sizes and correlation lengths to generate multiple realizations of sand-shale distributions for the previous Rulison models. The increased size of the current model domain allowed data from current production wells to be included in generating sand-shale distributions. Ten realizations were generated for the large domain and 3 were used for the simulations. At locations within the model domain where well data are available (the vertical columns of elements at the seven existing well locations in the domain), the ROCK type is known and assigned based on the well data. These are conditioning points (known values) that do not change for any of the different geostatistical realizations. The remainder of the domain is populated randomly within the constraints of the geostatistics. The log correlations and subsequent geostatistical realizations were generated by DRI (David Gillespie, log correlations; and Yong Zhang, geostatistical distributions) using the same method that was used for previous models. A thorough discussion of the method is provided in Appendix B. Note that even though

the wells in the domain were directionally drilled, they are vertical within the productive section to intersect as many of the discontinuous sands as possible.

3.3 Rulison Detonation Zone

The cavity was assumed to be essentially spherical (as with earlier models), and the subsequent collapse chimney complex was assumed to be a vertical ellipsoid (similar to the cylindrical chimney of earlier models). The nuclear fractured region in earlier models radiated spherically from the detonation to a distance of 230 ft. For this modeling effort, the nuclear fractured region was defined as a truncated (at depth) ellipsoid with a longer east-west axis (aligned with the higher permeability natural fracture trend of the formation) to be conservative. The equation used to calculate a 3-dimensional ellipsoid is given in Equation 1, and the variable values used to calculate the chimney and nuclear fracture extent are in Table 4. Locations on the surface of the ellipsoid have equation values equal to 1; element centers within the ellipsoid have equation values less than 1.

$$\frac{x^2}{x_r^2} + \frac{y^2}{y_r^2} + \frac{z^2}{z_r^2} = 1 \qquad \text{Equation (1)}$$

Where x, y, z = Distance from an element center to the ellipsoid center in the x,y,z directions,
x_r, y_r, z_r = Ellipsoid radius in the x,y,z directions.

Table 4. Model Coordinates and Ellipsoid Radii (ft) of Chimney and Nuclear Fracture Extent

	x ellipsoid center	y ellipsoid center	z ellipsoid center	x_r ellipsoid radius	y_r ellipsoid radius	z_r, ellipsoid radius	Truncated below
Chimney	4875	1850	−2210	85	80	220	−2320
Nuclear fractures	4875	1850	−2250	400	200	300	−2420

Elements with coordinates that total less than 1 using Equation 1 are within the ellipsoid. The detonation zone was designed using calculations with Microsoft Excel prior to modifying the TOUGH2 MESH. Side view and top view slices of the model chimney and nuclear fractured region are shown in Figure 10 and Figure 11.

This conceptualization assumes that the fracturing caused by the nuclear detonation will occur preferentially with the natural fracture trend that controls the predominant hydrofracturing direction and that fracturing will preferentially propagate upward, toward the surface. The truncation depth for the nuclear fracture ellipsoid assumes no fracturing below that depth. This approach is more conservative than previous models, allowing the nuclear fractured region to extend nearer to the institutional control boundary of Lot 11. Elements within the nuclear fracture ellipsoid are assigned the `ROCK` type `NFrac`, and elements within the chimney ellipsoid are assigned the `ROCK` types `chimn` or `glass` (`ROCK` type parameters are given in Section 3.5). The truncation depth for the chimney assumes melt glass below that depth within the chimney ellipsoid.

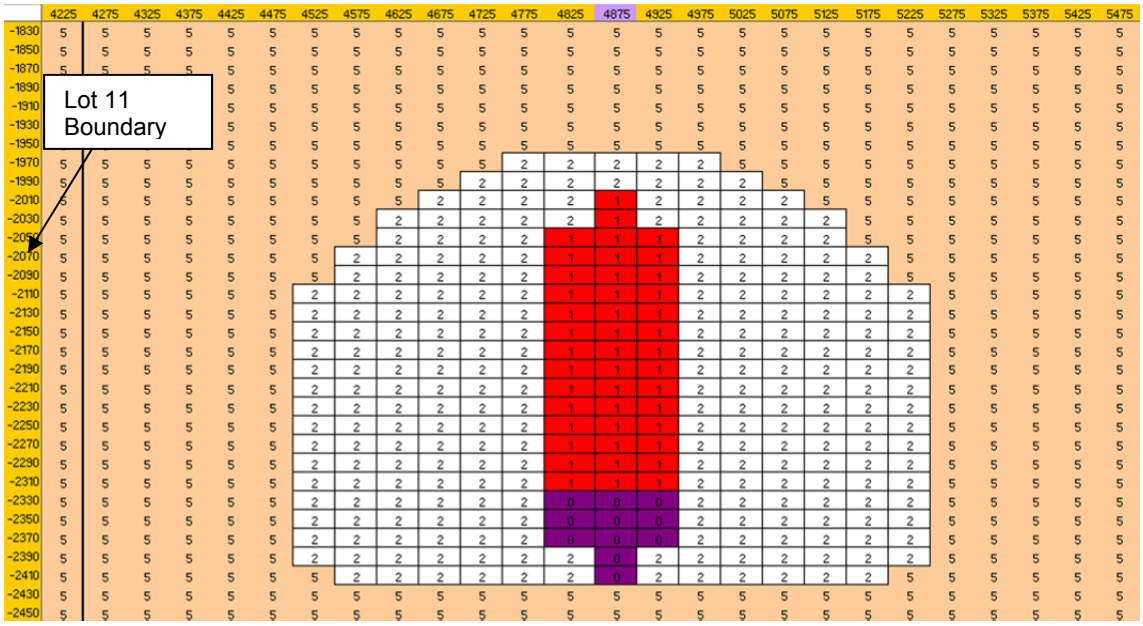

Figure 10. Vertical (Side View) Slice of the Model Chimney and Nuclear Fractured Region (y = 1825 ft; purple represents melt glass, red represents the chimney, and white represents the nuclear fractured region)

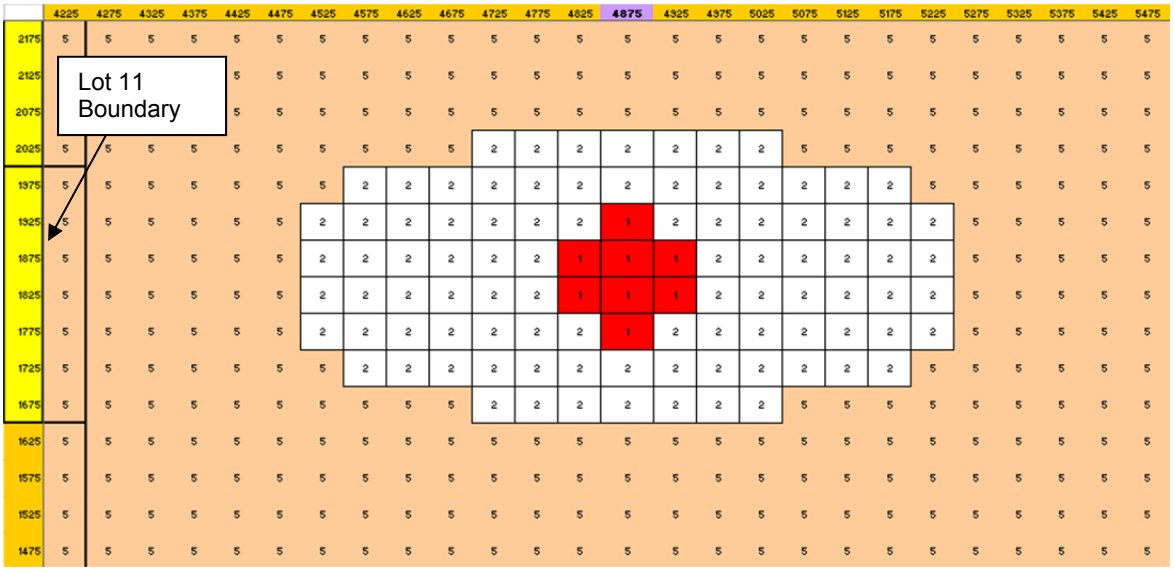

Figure 11. Horizontal (Top View) Slice of the Model Chimney and Nuclear Fractured Region (z= -2275 ft; red represents the chimney and white represents the nuclear fractured region)

3.4 Hydrofracturing of Wells

The method of selecting production intervals for both existing wells (yellow triangles in Figure 6) and future wells (blue circles in Figure 6) within the model were the same. Sandstones within the lower Williams Fork Formation that were 40 ft or more in thickness (model layers are 20 ft thick, so two or more consecutive elements in the vertical column at each well) were

simulated as being hydrofractured. Much like an actual well, no information about how laterally extensive the sandstone was away from the wellbore was used to decide which interval would be hydrofractured. And, like an actual well, the horizontal distance that hydrofracturing extended from the wellbore was to a degree controlled by the lithology surrounding the wellbore. Hydrofractures were assumed to extend farther in sandstones than in shales, and it was assumed that hydrofracturing would be more effective in the sandstones. The extent of hydrofracturing was determined using two nested ellipsoids to calculate a near and a far hydrofracture extent. Elements within the near ellipsoid, both sandstones and shales, were hydrofractured. Sandstone elements were changed to hydrofractured near sandstone (`HFnsd`), and shale elements were changed to hydrofractured shales (`HFshl`). Initially (prior to gas well calibration), the permeability of `HFnsd` elements were set at 100× the permeability of lower Williams Fork sandstones (`LWFsd`), and the permeability of the shale increased 10×. Outside the inner ellipsoid but within the far ellipsoid, only the sandstone elements were hydrofractured. They were changed from sandstone to hydrofractured far sandstone elements (`HFfsd`) with a permeability increase of 10× that of the previous `LWFsd` elements. The axes of the ellipsoids were elongated east-west in the direction of the natural fracture trend of the formation. The model *x*, *y* locations of existing gas producing wells within the model domain are given in Table 5 along with the near and far ellipsoid radii in the *x* and *y* directions.

Table 5. Model Coordinates and Hydrofracture Ellipsoid Radii of Existing Wells (measurements in ft, xnr = radius in the x direction of the near ellipsoid, yfr = radius in the y direction of the far or outer ellipsoid). Well locations can be seen in Figure 5 and Figure 6 and are ordered from north to south in the table.

Well Name	xwell	ywell	xnr	ynr	xfr	yfr
26-33B	975.	2475.	250.	60.	400.	60.
26-33C	1025.	2125.	250.	60.	400.	60.
26-33D	925.	1875.	250.	60.	400.	60.
26-34A	925.	1575.	250.	60.	400.	60.
26-34B	925.	1225.	250.	60.	400.	60.
26-34C	825.	875.	250.	60.	400.	60.
26-34D	825.	575.	250.	60.	400.	60.

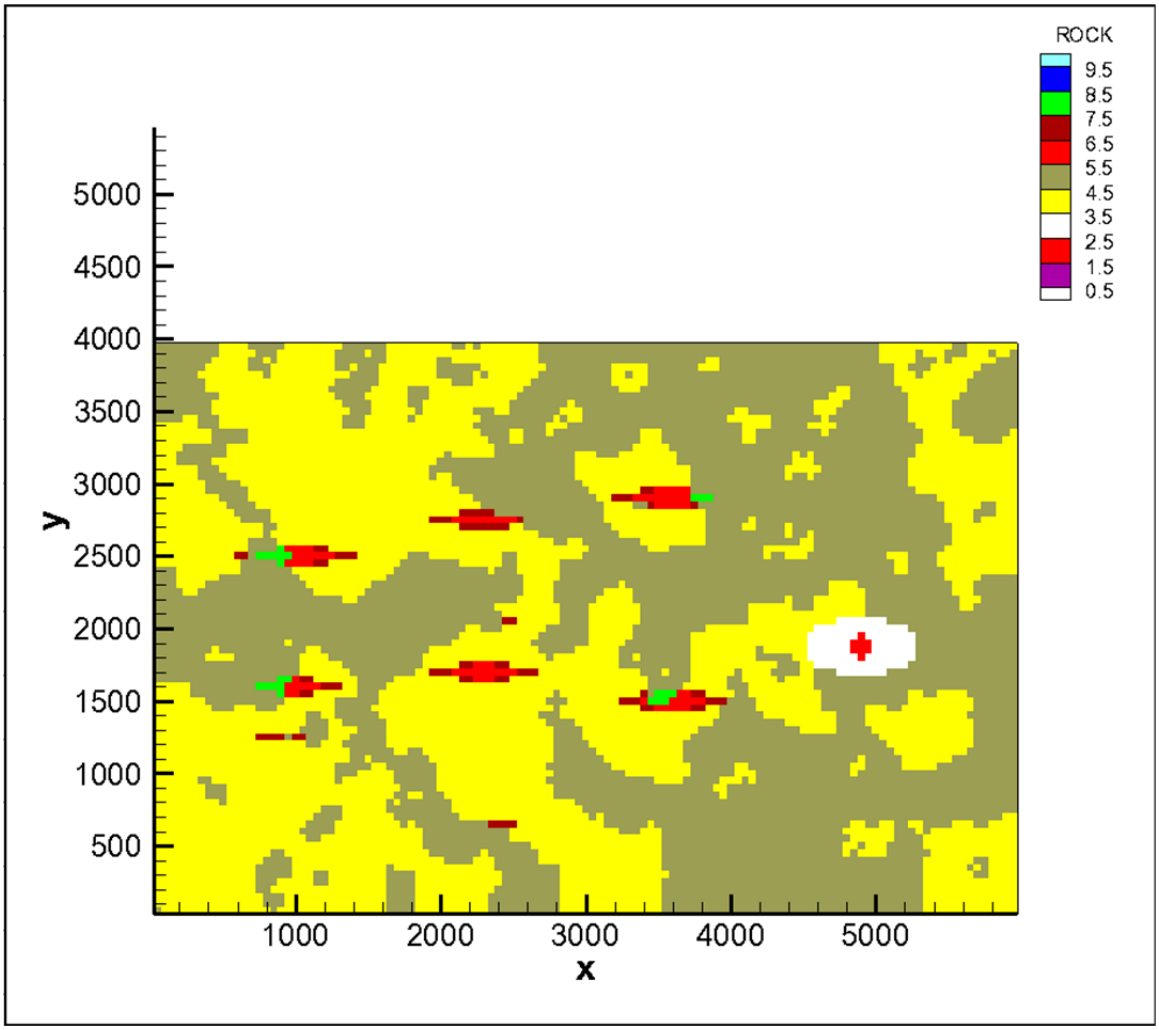

Figure 12. Horizontal Slice Through the Domain Showing Several Hydrofractured Wells (Existing and Possible Future) and Detonation Zone
(yellow = lower Williams Fork sandstone, olive = shale, white = nuclear fractures, red = chimney or HFnsd, dark red = HFfsd, green = HFshl)

3.5 ROCK (Material) Parameters

Porosity, permeability (for the *x*, *y*, and *z* directions), capillary pressure curves, and relative permeability curves are specified for each material or ROCK type (Table 6). ROCK type names are limited to five characters.

Table 6. ROCK types used in the Rulison and Rio Blanco Models

Order	ROCK Type	Description
1	glass	Melt glass, allows constant heat source at base of chimney
2	chimn	High-permeability and high-porosity chimney
3	NFrac	Nuclear fractured
4	LWFsd	Lower Williams Fork sandstone, gas reservoirs
5	shale	Shale, any formation in the section
6	HFnsd	Hydrofractured sandstone near a well, max permeability increase
7	HFfsd	Hydrofractured far sandstone, less permeability increase
8	HFshl	Hydrofractured shale, restricted to the near region (as HFnsd)
9	UWFsd	upper Williams Fork sandstone, gas-bearing but nonproductive
10	FtUsd	Ft. Union sandstone, gas-bearing but nonproductive (Rio Blanco)

3.5.1 Permeability and Porosity

A reasonable range of permeability and porosity values for the various ROCK types were determined by calibrating the Rulison model to production and pressure data from the reentry well and to gas wells within the domain. The Rulison detonation was in the lower Williams Fork Formation, and the Rulison model domain covers the entire lower Williams Fork plus 200 ft of upper Williams Fork (to separate the productive lower Williams Fork from the boundary). Calibrating the Rulison model to the reentry well data determined reasonable parameters for the permeability and porosity of the chimney, nuclear fractured region, and the lower Williams Fork sandstones. Calibrating the Rulison model to the production well data determines reasonable parameters for the permeability and porosity of the lower Williams Fork sandstones, and the hydrofractured sandstones and shale near producing wells. A discussion of the model calibration is in Section 4.0.

3.5.2 Capillary Pressure and Relative Permeability

Capillary pressure and relative permeability values for each ROCK type were based on published information about the Mesaverde in Byrnes and Cluff (2009). Charts (modified from Byrnes and Cluff [2009]) of capillary pressure and relative permeability curves for Mesaverde rocks of different permeabilities are shown in Figure 13 and Figure 14. The capillary pressure curves assigned to different ROCK types in the models are overlain on the chart in Figure 13 and are based on the TRUST capillary function (Narasimhan et al. 1978). The relative permeability curves assigned to different ROCK types in the models are overlain on the chart in Figure 14 and are based on Corey (1954), except the curve for shale which is based on the van Genuchten-Mualem model (Mualem 1976; van Genuchten 1980). Values for unique ROCK types in the model (chimn, NFrac, HFnsd, HFfsd, and HFshl) were estimated considering the effects that hydrofracturing would have on the unfractured rock (tend to increase relative gas permeability and decrease capillary pressure relative to the published Mesaverde values).

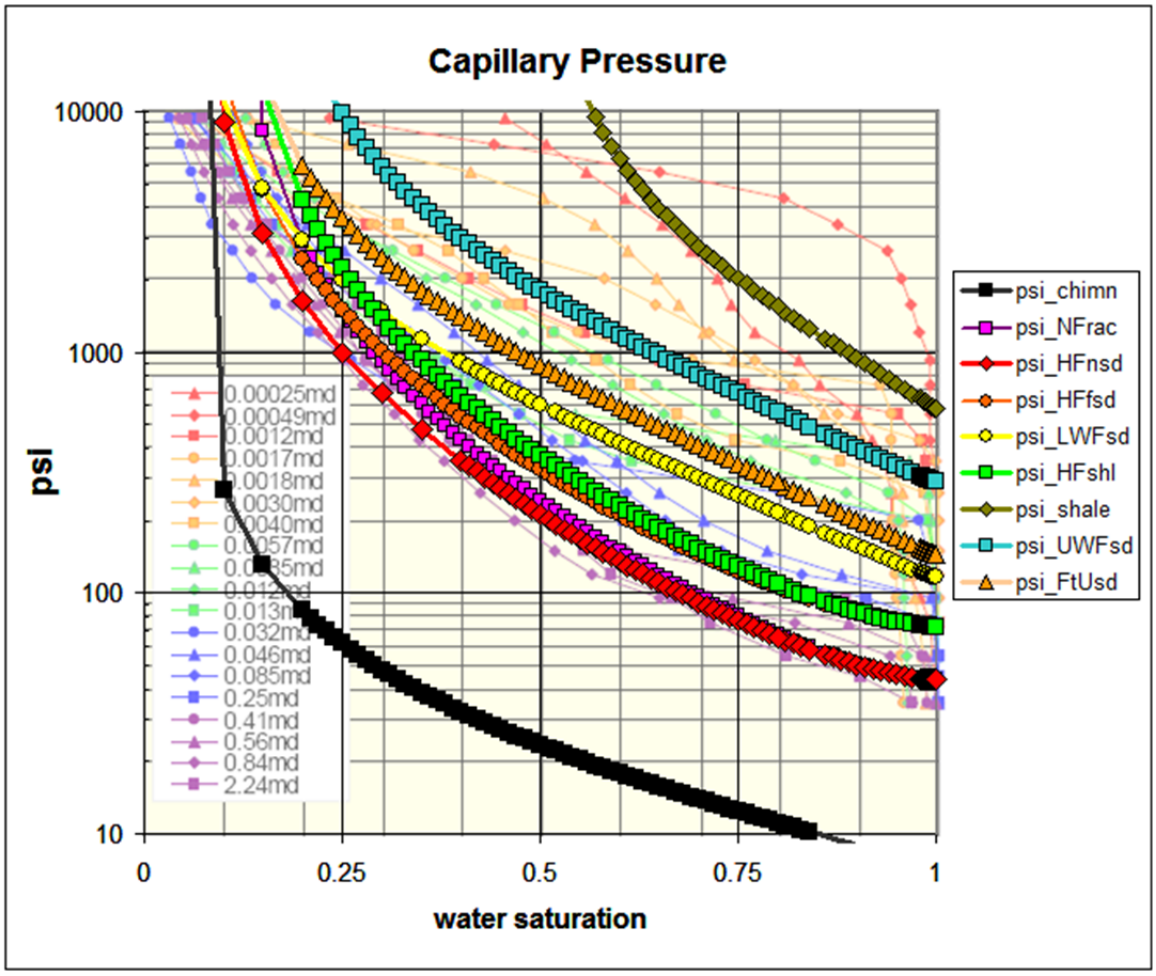

Source: Byrnes and Cluff 2009

Figure 13. Capillary Pressure Curves for the Modeled ROCK Types Superimposed on the Chart of Air-Mercury Capillary Pressure Curves for Selected Mesaverde Samples

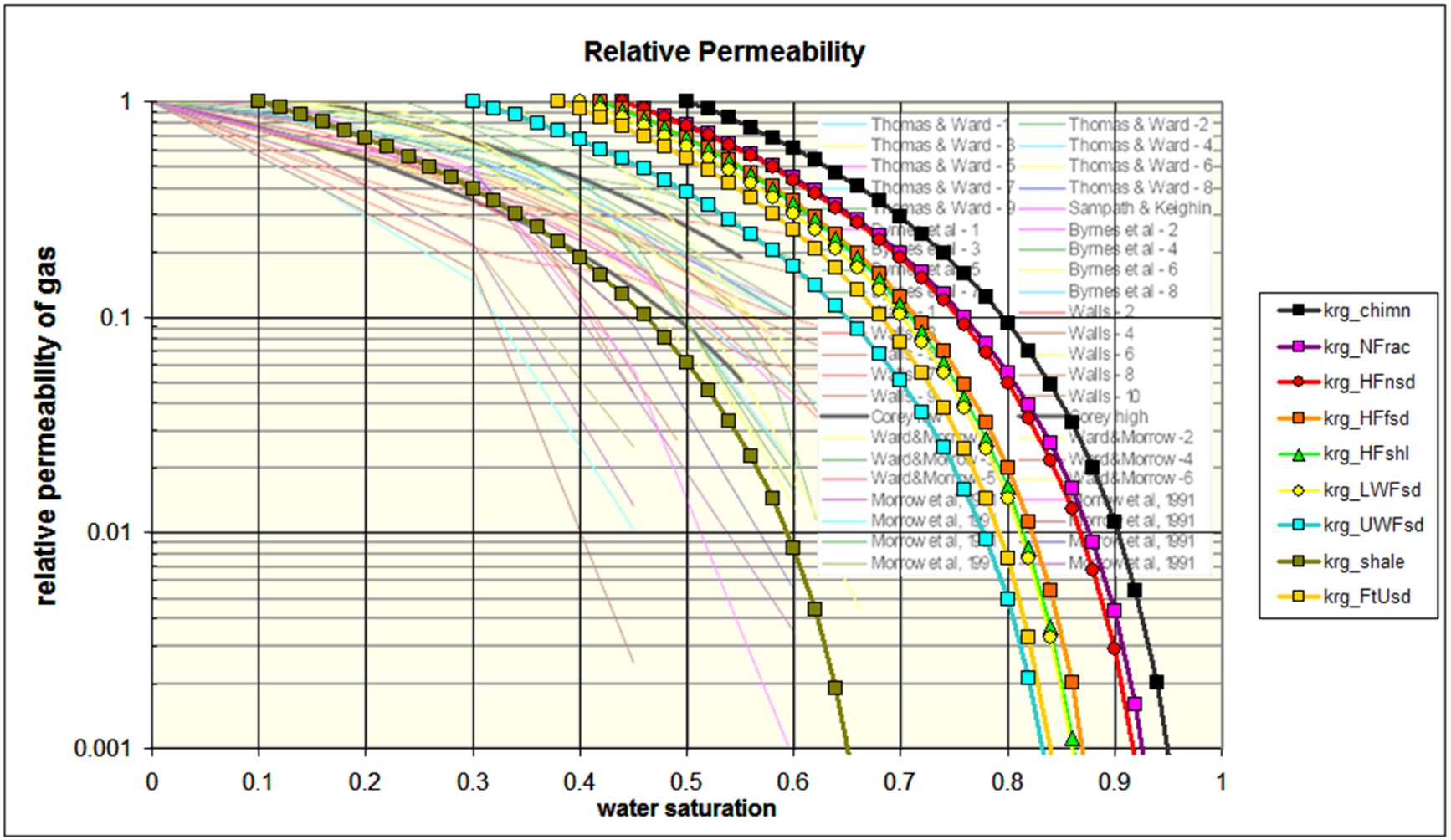

Source: Byrnes and Cluff 2009

Figure 14. Relative Permeability to Gas Curves for the Modeled ROCK Types Superimposed on the Chart

Capillary pressure and relative permeability can significantly affect the movement of fluids in a multi-phase system. For partially saturated gas reservoirs, the presence of a wetting phase (water) impedes the movement of the non-wetting (gas) phase because the gas must overcome the capillary pressure of the water. For example, at a water saturation of 50 percent, gas in the nonproductive upper Williams Fork sandstones would require nearly 2,000 pounds per square inch (psi) to displace water from capillary forces alone (Figure 13). Additionally, the presence of water partially blocks openings, reducing the area through which gas can flow and reducing the permeability of the gas phase. For example, at a water saturation of 50 percent, the relative permeability of the nonproductive upper Williams Fork sandstones would be about 40 percent of the intrinsic permeability of the formation due to the presence of water (Figure 14). A good contrast is the capillary pressure and gas permeability of the shale (gas is essentially immobile) to that of the chimney, where gas can move freely (Figure 14). Note that the relative permeability curves were selected at the high-permeability range to be conservative by erring towards increased flow.

3.6 Boundary Conditions

The size of the model domain in combination with the very low native permeabilities of the formations allows for no-flow boundaries on all sides without significantly altering the flow field, even for wells near boundaries. The majority of flow within the model domain is from regions that have been fractured to allow flow, the nuclear fractured region or hydraulically fractured regions surrounding gas wells. These regions are separated from boundaries by the very low permeability formation, and any significant interaction with boundaries over the time frame of the simulations would in itself indicate that the model is not calibrated to observed real-world conditions. This is a conservative formulation in that any well–boundary interaction would increase the pressure decline at the well, increase the pressure gradient, and increase the potential for transport of radionuclides from the detonation.

3.7 Initial Concentration and Partitioning of Tritiated Water (THO) Between Gas and Aqueous Phases

The Henry's Law constant is used to describe the partitioning of a compound between the gas and aqueous phases. A common example is the group of compounds known as VOCs (volatile organic compounds). For instance, the air above a container of water that contains dissolved benzene (the aqueous phase) will have a detectable odor from the benzene vapor and humidity from the water vapor (the gas phase) because of their tendency to evaporate, which is quantified by their vapor pressure. This partitioning provides a method to calculate the mass fraction of THO in the gas phase using the vapor pressure of water, assuming that THO is in molecular equilibrium with the gas and liquid phases. This is not precise, but within a few percent, because the THO molecule is heavier than regular H_2O (20 vs. 18 grams per mole [g/mol]), causing it to be slightly under-represented in the more energetic gas in the real system relative to the simulations. The Henry's Law constant used to calculate the partitioning of THO between the two phases is simply the water vapor pressure.

The water vapor pressure is directly related to temperature (Figure 15), and the code was modified to calculate a temperature-dependent Henry's Law constant based on the vapor pressure (enacted in the code as the inverse of the vapor pressure, HCRN1 [Henry's Constant

Radionuclide 1]). The inverse pressure form of the Henry's Law constant is developed in Equation 2 and was used to reproduce published values (Smiles et al. 1995) for confirmation.

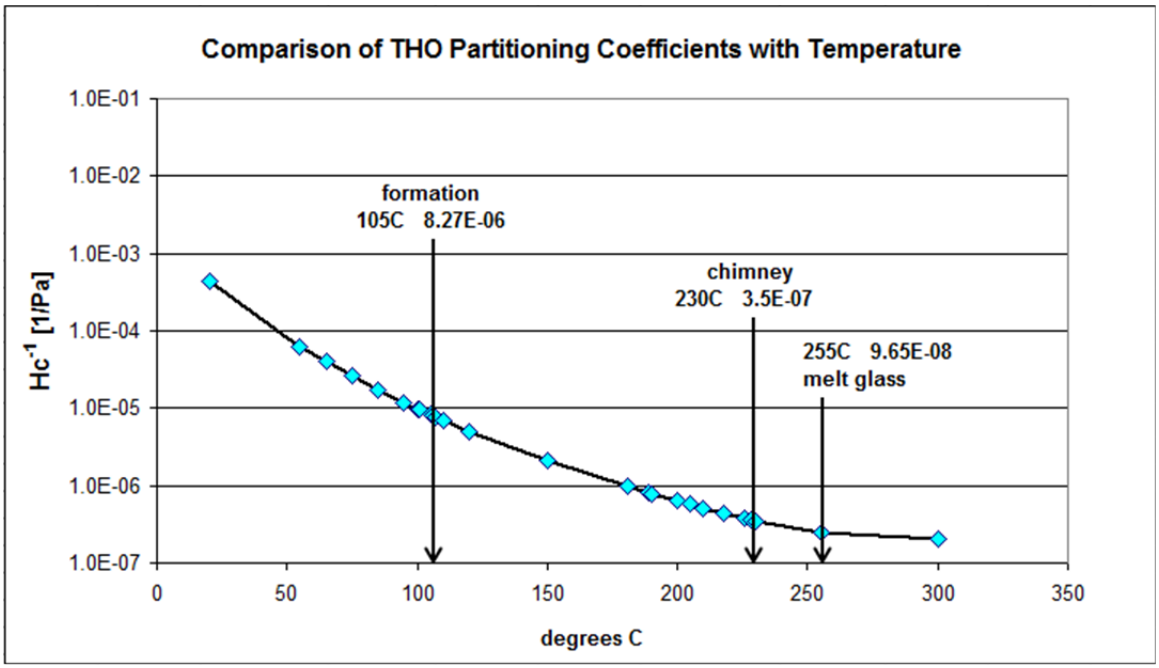

Figure 15. Inverse Vapor Pressure of Water Relative to Temperature

Inverse Henry's Law constant: $HCRN1 = \frac{\chi_l^{THO}}{P_g^{THO}}$ Equation (2)

Gas and aqueous phases should have same ratio of molecules:

$$\frac{P_g^{THO}}{P_g^{H_2O}} = \chi_g^{THO} = \chi_l^{THO}$$

Substitute to get HCRN1, same pressure units (pascals [Pa]) as TOUGH2 EOS7R (1/Pa)

$$HCRN1 = \frac{\chi_l^{THO}}{P_g^{THO}} = \frac{\frac{P_g^{THO}}{P_g^{H_2O}}}{P_g^{THO}} = \frac{1}{P_g^{H_2O}}$$

Where:

χ_l^{THO} = mole fraction of tritiated water in the aqueous phase

P_g^{THO} = partial pressure of tritiated water vapor in the gas phase

The remaining tritium at the Rulison site is present in water as THO and within crystals in the melt rock (about 40 percent [Toman 1974]). The tritiated methane created by the nuclear test was removed by the production testing. The percentage of tritium in the melt rock is uncertain, and to be conservative, all remaining tritium is assumed to be present as THO. The initial concentration was assigned to chimney elements (1.0×10^{-9} for Rulison) as a mass fraction of THO in the aqueous phase (a primary variable). The gas-phase mass fraction of THO (a secondary variable)

is calculated (partitioned) with the first time step of the simulations based on the initial thermophysical properties for the chimney elements. The code was also modified to replace air with methane. This was necessary to get the initial partitioning correct because the molecular weight of air (29 g/mol) is greater than that of methane (16 g/mol). The mass fraction of THO in the gas phase will be higher if it partitions into a less-dense gas phase (methane rather than air). Figure 16 shows the effects of molecular weight and temperature on the initial partitioning of THO from the aqueous phase to the gas phase. Simulations were run on a small set of elements (50 in a vertical column) to show this effect. Two additional molecular weights (35 and 23 g/mol) are shown in addition to those for air and for methane.

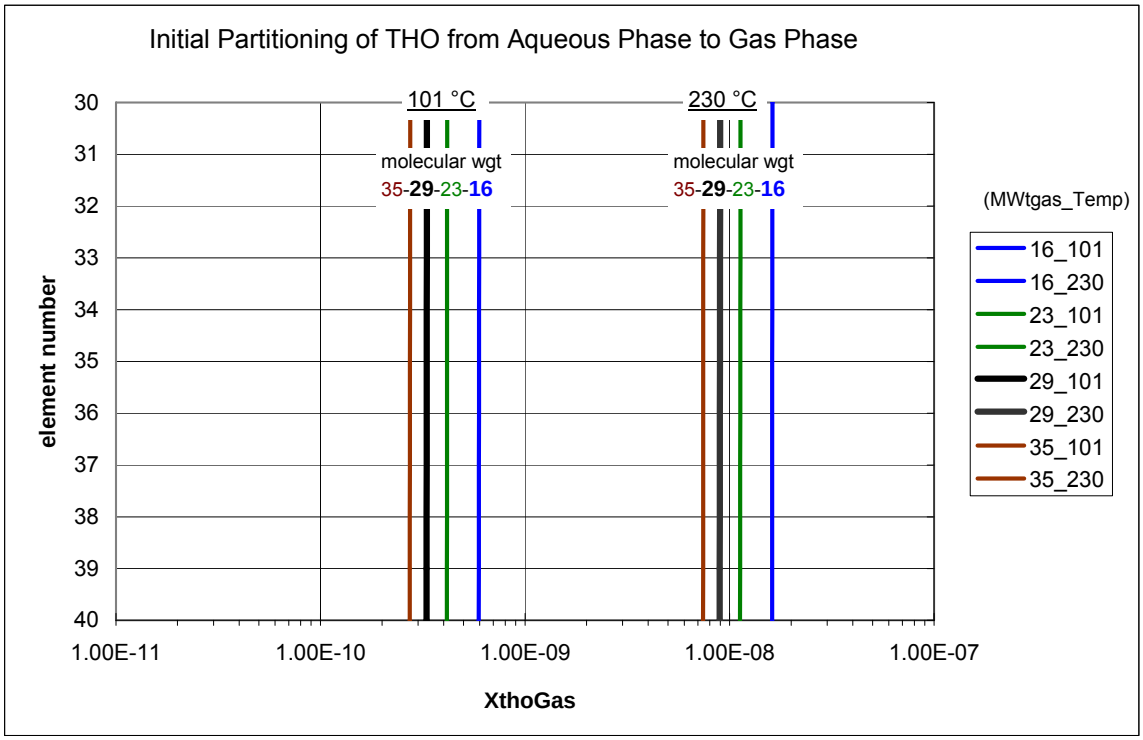

Figure 16. Effects of Molecular Weight and Temperature on the Initial Partitioning of THO from the Aqueous Phase to the Gas Phase

Partitioning of THO between the aqueous and gas phases is important beyond the initial partitioning. In order for THO in the gas phase to migrate an appreciable distance from the detonation zone (higher temperature than the formation), it will have to pass through the surrounding cooler formation. The water saturation in the formation is about 0.50, and any tritiated water vapor that comes into contact with the water will be depleted in THO due to the preferential partitioning of THO at lower temperatures into the aqueous phase. Considering that the relative permeability of liquid in the formation is orders of magnitude less than that of gas, this acts as an effective retarding mechanism to THO migration.

Earlier models calculated the concentration in the chimney by looking at the remaining tritium after production testing, the pore volume of the chimney elements, and volume of water in the chimney. A value of 1.57×10^{-10} mass fraction of THO in the aqueous phase was used for earlier models (Cooper et al. 2007). The appropriate mass fraction of THO is uncertain and depends on

the volume of water in the chimney, which is a function of the number of chimney elements, their porosity, and their water saturation (all unknowns with their own associated uncertainties). To maintain a bias toward conservative estimates, a higher value (more than an order of magnitude) was used for the current model to alleviate any concern that the initial concentration was being underestimated. Tritium does not exchange between water and methane molecules except at very high temperatures. In experiments, no exchange was observed at temperatures up to 300 °C (Frick et al. 1971).

3.8 Initial Conditions

A set of initial conditions has to be supplied for every model element prior to running simulations. Ideally, they represent the undisturbed natural conditions of the system. Initial conditions are specified for each element in TOUGH2 as a set of primary variables (in the file INCON) from which all secondary variables can be calculated. For the EOS7R equation of state, the primary variables for two-phase conditions are gas-phase pressure, brine mass fraction, mass fraction of THO, mass fraction of helium-3, gas saturation, and temperature. The gravity capillary equilibrium initial conditions were calculated analytically using the TRUST capillary function (Narasimhan et al. 1978). Initial conditions were first calculated for the entire MESH with no detonation zone. Elements in the MESH located in the detonation zone were converted to the `ROCK` types `NFrac`, `chimn`, and `glass` to simulate the detonation. Initial conditions for those elements were changed to be more representative of the new `ROCK` types that have significantly different parameters than either sandstone or shale. Tests of varying the initial condition of hydrofractured elements by increasing their water content (due to remnant injected water from the hydrofracturing process) indicated that the water content quickly dropped in the simulations and was not significant beyond the initiation of production, so the step was not included. This is consistent with actual initial production period from wells which is designed to remove the water introduced during the hydrofracturing process.

3.8.1 Formation

The initial pressure at the bottom of the Rulison domain was specified as 22 megapascals (MPa) and resulted in an initial pressure range of 19.7 to 22 MPa (about 2,850 to 3,190 psi) from the top to the bottom of the domain. Shut-in pressures through the productive interval from drill-stem tests in the pre-shot exploratory well ranged from 2,250 to 3,050 psi (Nork and Fenske 1970). Water saturations in the sandstones are about 0.50 and about 0.65 in the shales, with the variation due to the capillary pressure curve used for each and some variation with depth (Figure 17). Reported formation temperatures ranged from 214 °F (DeGolyer and MacNaughton 1971) to 220 F (Montan 1971), or 101 °C to 105 °C. A temperature of 101 °C was used for earlier models, and a formation temperature of 105 °C was used for this model. The higher temperature favors partitioning of THO to the mobile gas phase, thereby increasing any potential transport.

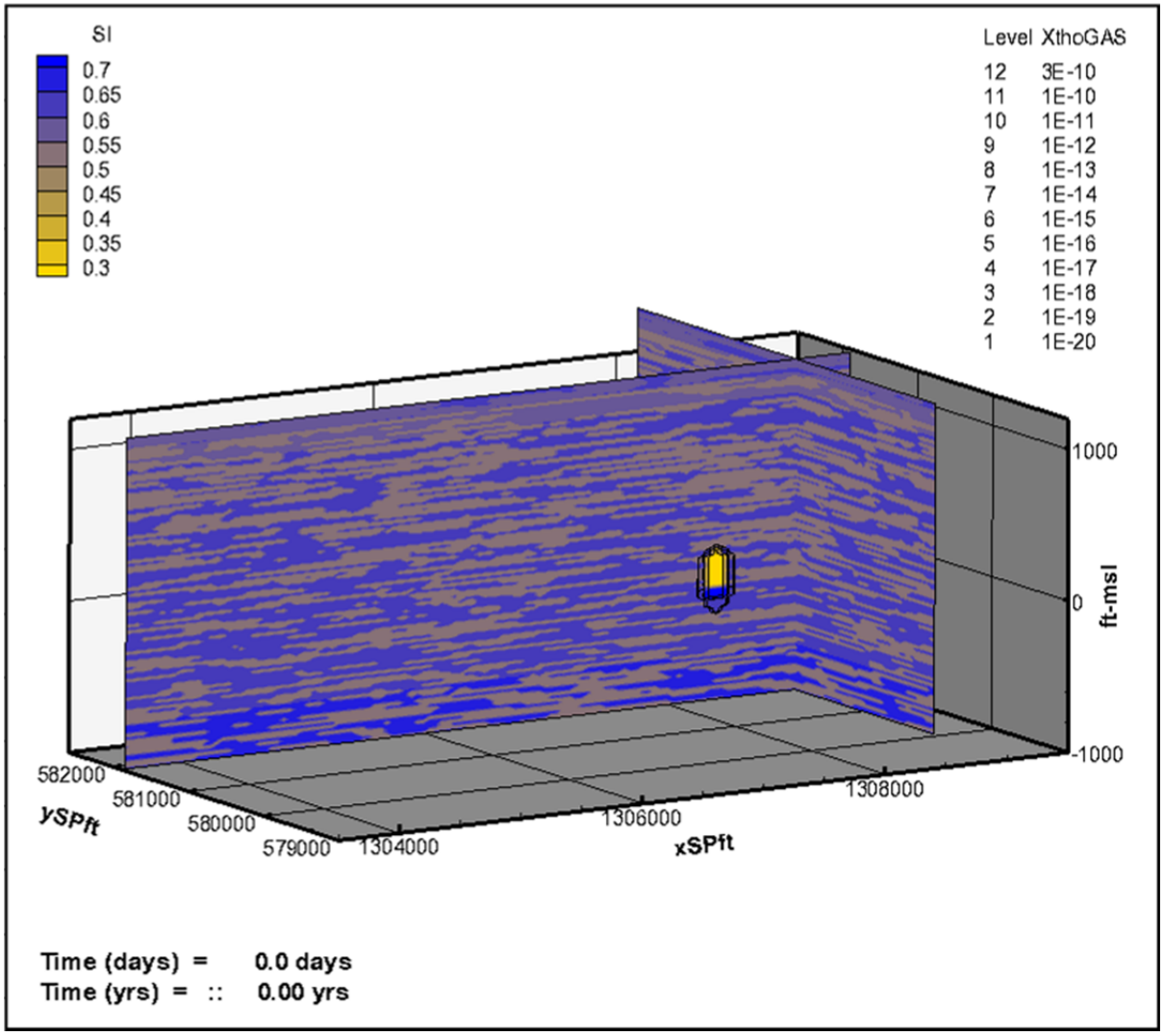

Figure 17. Initial Liquid Saturation Conditions (Flood): lower water saturation in the chimney (yellow), moderate water saturation in the sandstone (tan), higher water saturation in the shale (blue) Mass Fraction of THO in the Gas Phase (Contours): Initial distribution with contours crowded at the chimney

3.8.2 Detonation Zone

The detonation created a chimney (a cavity and subsequent rubble-filled collapse chimney) with properties significantly different from those of the native formation and surrounded by a fractured zone of increased permeability. The initial water saturation of most chimney elements was assigned a value of 0.25, with water content increasing at the base of the chimney. The initial water content of nuclear fracture elements was not changed from that of the original sandstone or shale. The temperature of the chimney was assigned an initial value of 230 °C (445 °F from DeGolyer and MacNaughton 1971), and the nuclear fractures were assigned a temperature of 155 °C (assumed to be 50 °C hotter than the formation to reduce THO partitioning from the gas phase to the much less mobile aqueous phase). The melt glass elements at the base of the chimney were assigned a temperature of 255 °C (491 °F) and given very low permeability and porosity to act as a constant heat source. The initial pressure in the chimney

was increased above initial formation pressures to account for the first pressure of the first production test, 3,321 psi (22.9 MPa) (DeGolyer and MacNaughton 1971).

3.9 Decay and Diffusion

The majority of the tritium produced by the detonation has been removed from the subsurface through the decay of tritium to stable helium-3. The half-life of tritium is 12.32 years, or 4,500 days (Lucas and Unterweger 2000). An easy way to visualize the effect of decay is that for every 40-year period, the amount of tritium decreases by an order of magnitude. For instance, the approximately 7,000 curies of tritium remaining after the Rulison nuclear test in 1969 (about 3,000 of the original 10,000 curies were removed by production testing) will have decayed to 700 curies in 2009 and to 70 curies in 2049.

The handling of diffusion and the associated parameter tortuosity was done as a constant diffusivity model for these simulations. This method was adopted for the 2009 Model Addendum (Cooper et al. 2009) as a more conservative approach (favors more diffusive transport) and has been used in all subsequent modeling. A detailed description is provided in the 2009 Model Addendum, which is included on the DVD accompanying this report.

3.10 Well Treatment (Sources and Sinks)

Several different methods are available in TOUGH2 to simulate wells (sinks), and the one that is chosen depends not only on what is to be produced but also on the available data about production. Sinks and sources are specified in the `GENER` block of the input file.

3.10.1 Reentry Well

Production from the reentry well was simulated using a `MASS` extraction (Pruess et al. 1999) rate in kilograms per second (kg/s) of combined of gas and water based on the historical data that recorded both the amount of gas and water extracted over time and the resulting pressure decline (Figure 18). Production testing took place over a total of 107 days during four separate tests from October 3, 1970, to April 23, 1971. Pressure data were collected for another 157 days until September 27, 1971. A total of 455 MMCF of gas (430 MMCF dry gas) was produced along with 20,244 barrels of water during the testing. The observed data of million cubic feet of gas plus barrels of water was converted to a kilogram per second rate for model input. The gas volume and water volume were converted to kilograms using the ideal gas law ($PV = nRT$). For example, the first production test was simulated as a 3 day 0.988 kg/s `MASS` extraction rate.

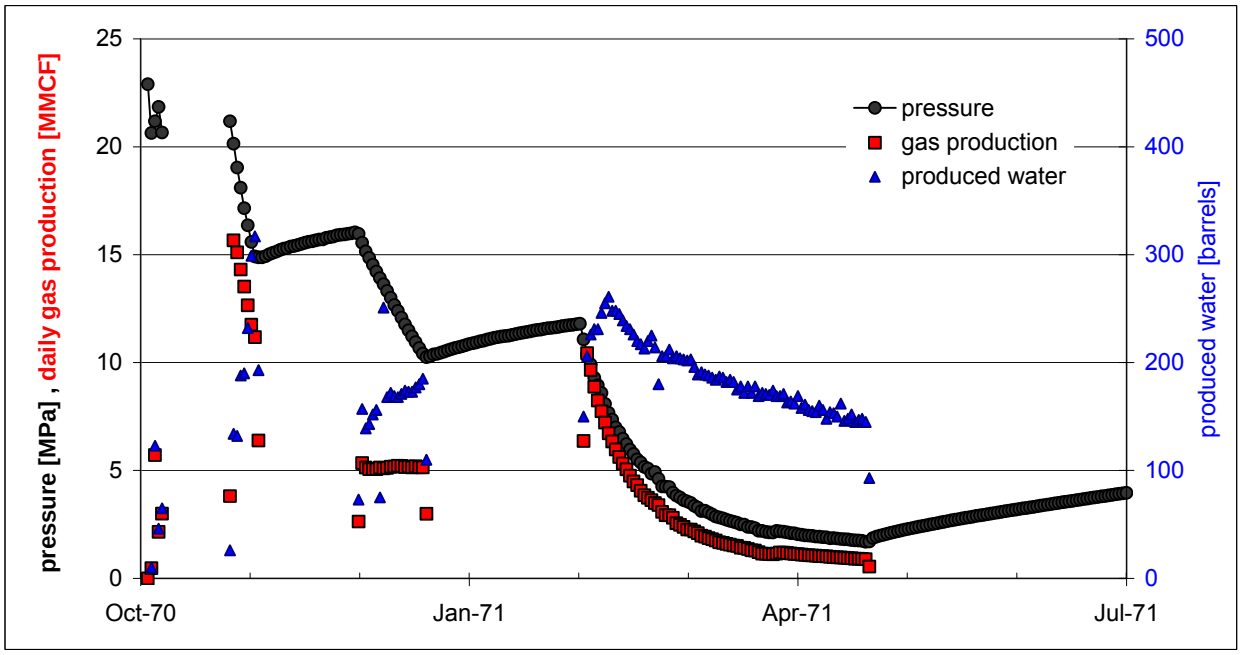

Source: DeGolyer and MacNaughton 1971

Figure 18. Pressure Decline Curve for the Reentry Well Production

Ideal gas law ($PV = nRT$) and calculations for the rate for the first test (3 days):

$$\frac{P\,Mwt}{R\,T} = \frac{101{,}325\,[Pa]\,16\left[\frac{g}{mol}\right]}{8.314\left[\frac{Pa\;m^3}{mol\;K}\right]\,288\,[K]} = 677\left[\frac{g}{m^3}\right] = 0.677\left[\frac{kg}{m^3}\right]$$

$$1\,[MCF]\quad 1000\left[\frac{ft^3}{MCF}\right] 0.3048^3\,\frac{m^3}{ft^3}\,0.677\left[\frac{kg}{m^3}\right] = 19.2\,[kg]$$

$$\text{first test over 3 days}\quad \frac{11{,}343\;MCF}{3\;days} = \frac{217{,}433\;kg}{3\;days} = 0.839\,\frac{kg}{s}\;gas$$

Calculations for the water mass rate:

$$1\,[barrel]\quad 42\left[\frac{gallons}{barrel}\right] 8.33\left[\frac{lb}{gallon}\right] 0.454\left[\frac{kg}{lb}\right] = 159\,[kg]$$

$$\text{first test over 3 days}\quad \frac{244\;barrels}{3\;days} = \frac{38{,}737\;kg}{3\;days} = 0.149\,\frac{kg}{s}\;water$$

A single element in the upper part of the chimney was selected as the reentry well extraction location. The reentry well stopped drilling after losing circulation fluids in the high-permeability chimney or in adjacent fractures. The `MASS` production option (kilograms per second combined gas and water) was used in the model with 13 different rate step changes to simulate the four production tests and the declining production rate during the last test (Figure 19).

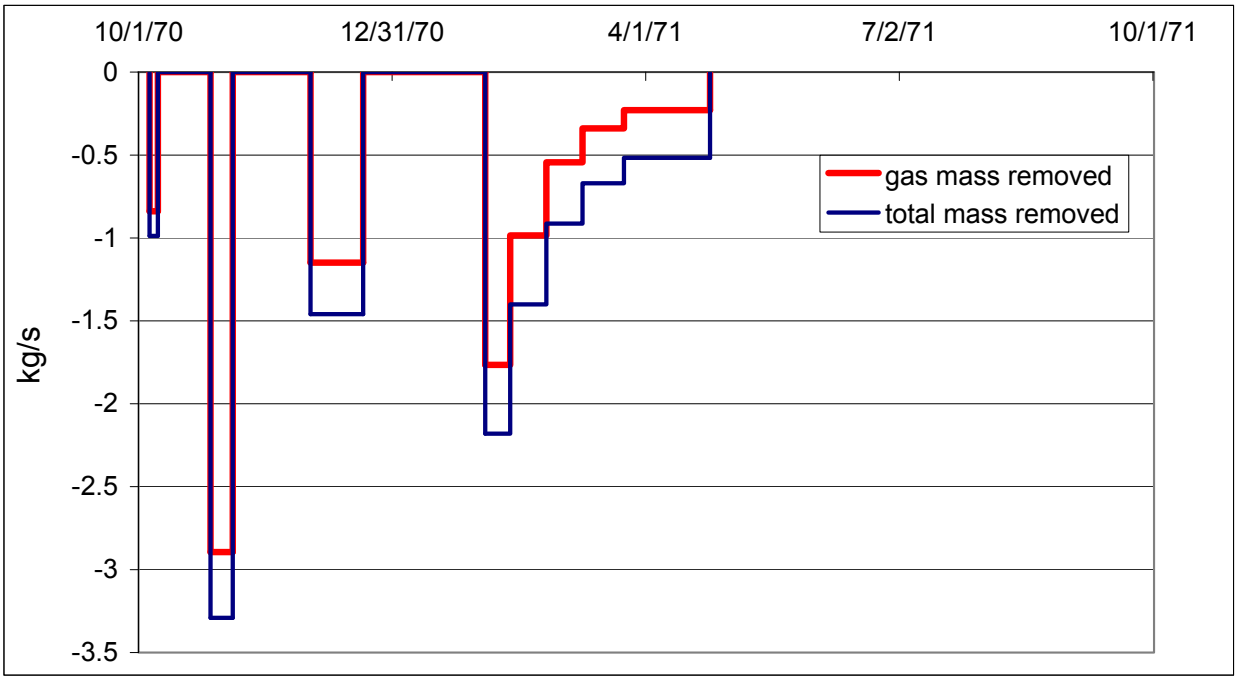

Figure 19. Simulated Mass Rate Removed

3.10.2 Gas Wells

Production from current and future gas wells was simulated as production against a specified wellbore pressure (well on deliverability, Pruess et al. 1999). A pressure of 600 psi (estimated down-hole pressure at the perforated interval) was used based on discussions with Noble Energy engineers (operator of gas wells within the model domain). The specified pressure was assigned to perforated well elements using the `DELV` option in the model, and fluids flowed into the well due to the pressure differential. The pressure difference (about 2,300 psi; 2,900 − 600) and production rate are highest when a well begins production and then declines over time as fluids (primarily gas) are depleted. The simulated production rate was compared to the actual production rate from existing producing wells within the model domain to determine how well the model simulated actual production (see Section 4.0, "Model Calibration").

4.0 Model Calibration

Simulations were initially run with model parameters from previous modeling efforts to test how well the model could reproduce the pressure data from the historical reentry well production testing. Parameter values were adjusted to achieve the best match with the new model. The specific parameter values arrived at during the calibration process should be considered in a general context or as a limited range and not taken as absolutes. The parameters that achieve the best match will change slightly depending on the sand/shale realization and even more so with changes to the conceptual model, like the elongated nuclear fractured region. With the expanded model domain, a second calibration method was used to test how well the model could reproduce production rate data from current gas producing wells.

4.1 Reentry Well Calibration

The primary calibration of the model was based on the historical reentry well data. The calibration simulations were conducted on a subset of the model domain from the vicinity of the detonation (275,000 elements) to reduce computation time to allow for the numerous simulations required for calibration. Parameters adjusted during the calibration process were the permeability and porosity of the chimney, nuclear fractured region, and the lower Williams Fork sandstone. The best fit is shown on Figure 20, and the fit parameters are given in Table 7. The permeability of the lower Williams Fork sandstone in the horizontal direction of the natural fracture trend (k*x*) was assumed to be 10× that of the permeability normal to the trend (k*y*) and that of the vertical permeability (kz). This anisotropy ratio was constant for all simulations.

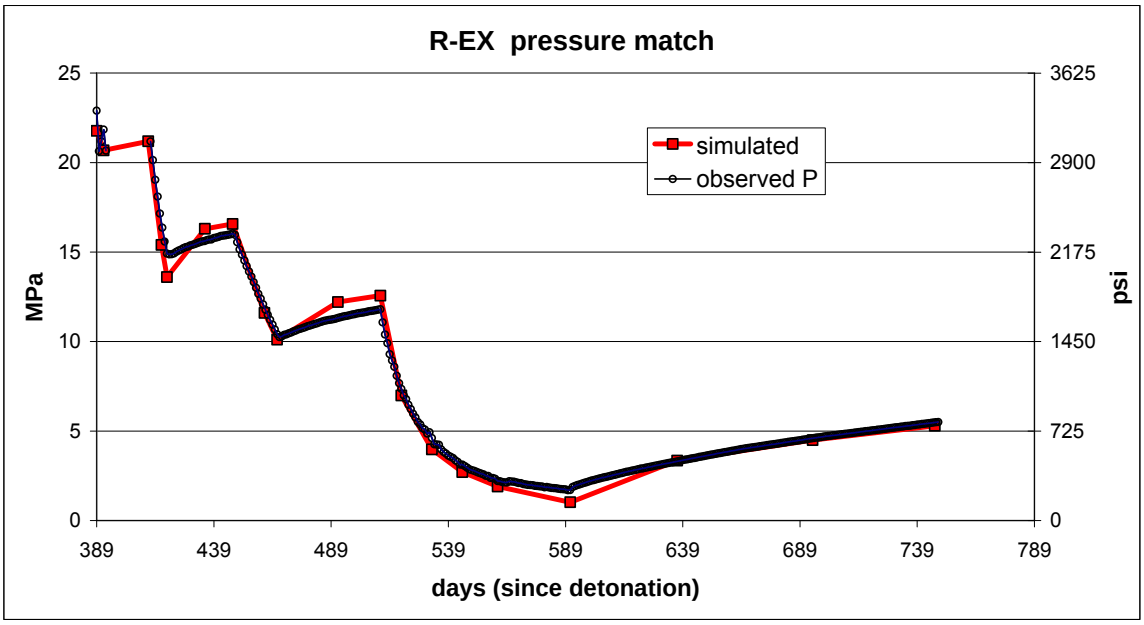

Figure 20. Overlay of Calibrated Simulated Pressure Curve with Observed Pressure

Table 7. Parameters from Calibration That Provided the Best Fit for One Realization

Unit	Permeability[b] (k*x*) [m^2]	Permeability (k*y*, kz) [m^2]	Porosity
`chimn`	0.4×10^{-11}	0.4×10^{-11}	0.33
`NFrac`	0.6×10^{-15}	0.6×10^{-15}	0.06
`LWFsd`	0.5×10^{-17}	0.5×10^{-18}	0.05
`shale` [a]	0.1×10^{-19}	0.1×10^{-19}	0.06

[a] shale properties provided for comparison (not adjusted for calibration)
[b] for comparison, a darcy is about 0.1×10^{-11} (1.0×10^{-12})

A series of simulations were run using a good fit case as the base and varying calibration parameters within a range to show the sensitivity of the simulated pressure results to parameter changes (Table 8). The two test simulations that caused the greatest pressure drop were the low `LWFsd` porosity and the low `NFrac` permeability (Figure 21). This would be expected in that

the permeability of the chimney is orders of magnitude greater than the surrounding material and acts effectively as an enlarged wellbore. Lowering or raising it by and order of magnitude should have minimal effect. It is also expected that the permeability of the nuclear fractured region would be a sensitive parameter because it envelopes the chimney which is an effectively large well bore. The low porosity `LWFsd` simulations would increase the pressure drop at the production well, especially later in the testing, because there would be less gas available to replenish the gas removed from detonation zone by the production testing. The two test simulations that caused the least pressure drop were the high `NFrac` porosity (more gas volume readily available adjacent to the chimney) and the high `LWFsd` permeability (gas in the sandstones surrounding the detonation zone could migrate more quickly) (Figure 21).

Table 8. Range of Parameters Used in the Sensitivity Runs

Unit	kx (low)	kx (high)	Porosity (low)	Porosity (high)_
`chimn`	0.1×10^{-12}	0.1×10^{-10}	0.17	0.34
`NFrac`	0.7×10^{-17}	0.7×10^{-15}	0.03	0.09
`LWFsd`	0.3×10^{-18}	0.3×10^{-16}	0.01	0.06

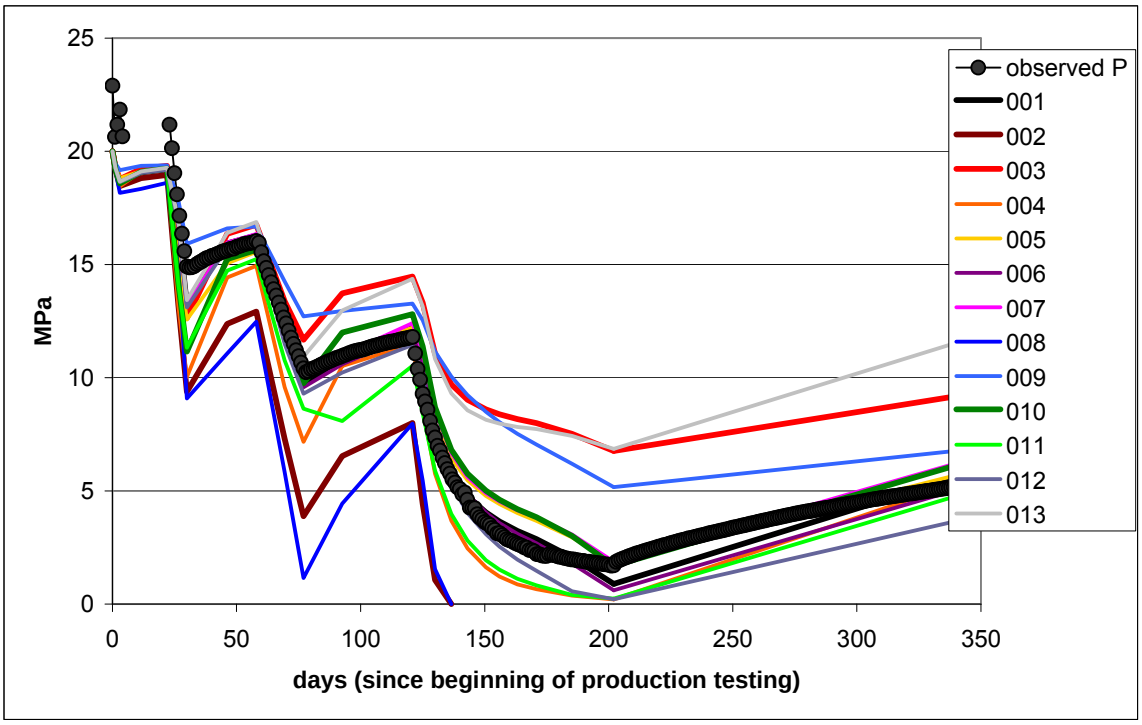

Figure 21. Plot of Results of Parameter Sensitivity Simulations

4.2 Gas Well Calibration

Extending the model domain to include current gas production wells allowed a secondary model calibration method to be used. These calibration simulations were conducted on a 330,000 element-subset of the model domain to reduce computation time to allow for the numerous simulations required for calibration. The subset was also taken from a different

sandstone–shale realization than that used for the reentry well calibration. The simulated gas wells produce against a specified wellbore pressure (Section 3.10, "Well Treatment [Sources and Sinks]"), requiring that production rates be used for the calibration data instead of pressures (used for reentry well calibration).

Parameters adjusted during the calibration process were the permeability and porosity of the lower Williams Fork sandstone (`LWFsd`), the hydrofractured sandstone near the well (`HFnsd`), the hydrofractured sandstone far from the well (`HFfsd`), and the hydrofractured shale near the well (`HFshl`). Three wells, two with many sand layers perforated (26-33B, 26-34C) and one with few sand layers perforated (26-34D), were chosen for the calibration. The best fit (solid lines) plus two other simulation results are shown on Figure 22. The best fit parameters are given in Table 9. Figure 22 also has production rates for the other wells within the domain. Figure 23 shows the simulated production extended to 20 years. The permeability of the lower Williams Fork sandstone and the hydrofracture `ROCK` types was assumed to be 10× greater in the horizontal direction of the natural fracture trend (k*x*) than horizontally normal to the trend (k*y*) or in the vertical direction (kz). This anisotropy ratio was constant for all simulations.

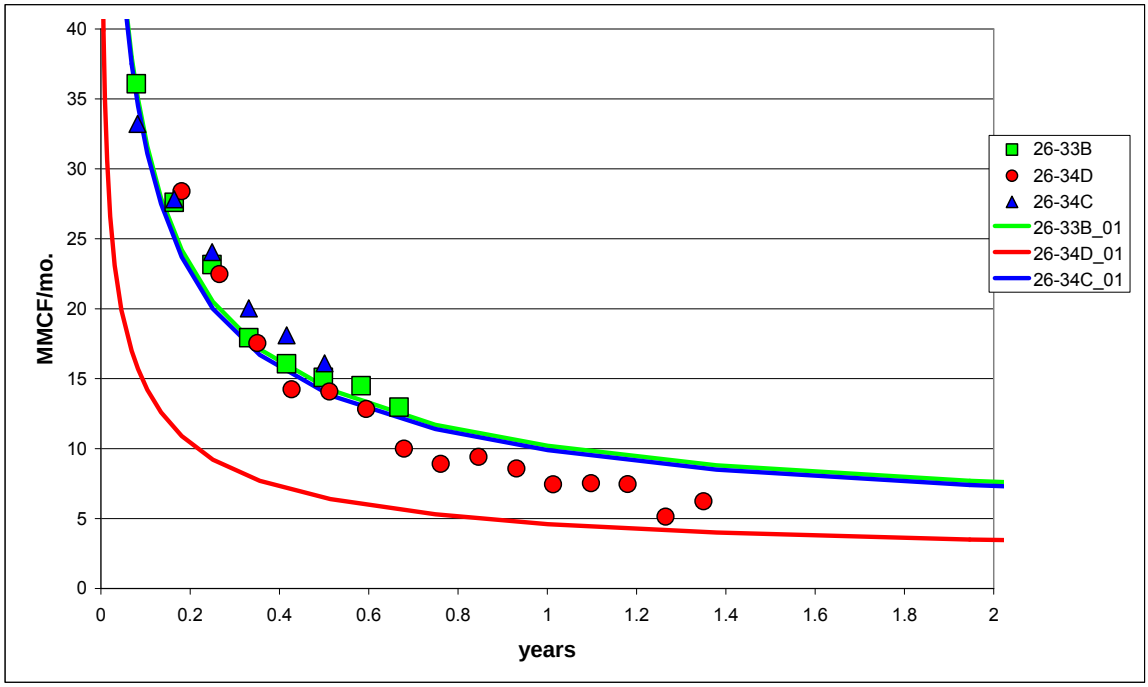

Figure 22. Overlay of Simulated Production Rate Curves for wells 26-33B, 26-34D, and 26-34C

Table 9. Parameters from Gas Well Calibration That Provided the Best Fit for One Realization

Unit	Permeability (kx)	Permeability (ky, kz)	k increase[b]	Porosity
LWFsd	0.2×10^{-17}	0.2×10^{-18}		0.06
HFnsd	0.8×10^{-16}	0.8×10^{-17}	40	0.06
HFfsd	0.8×10^{-17}	0.8×10^{-18}	4	0.06
HFshl	0.8×10^{-17}	0.8×10^{-18}	4	0.06
shale [a]	0.1×10^{-19}	0.1×10^{-19}		0.06

[a] shale properties provided for comparison (not adjusted for calibration)
[b] k increase is permeability multiplier over LWFsd

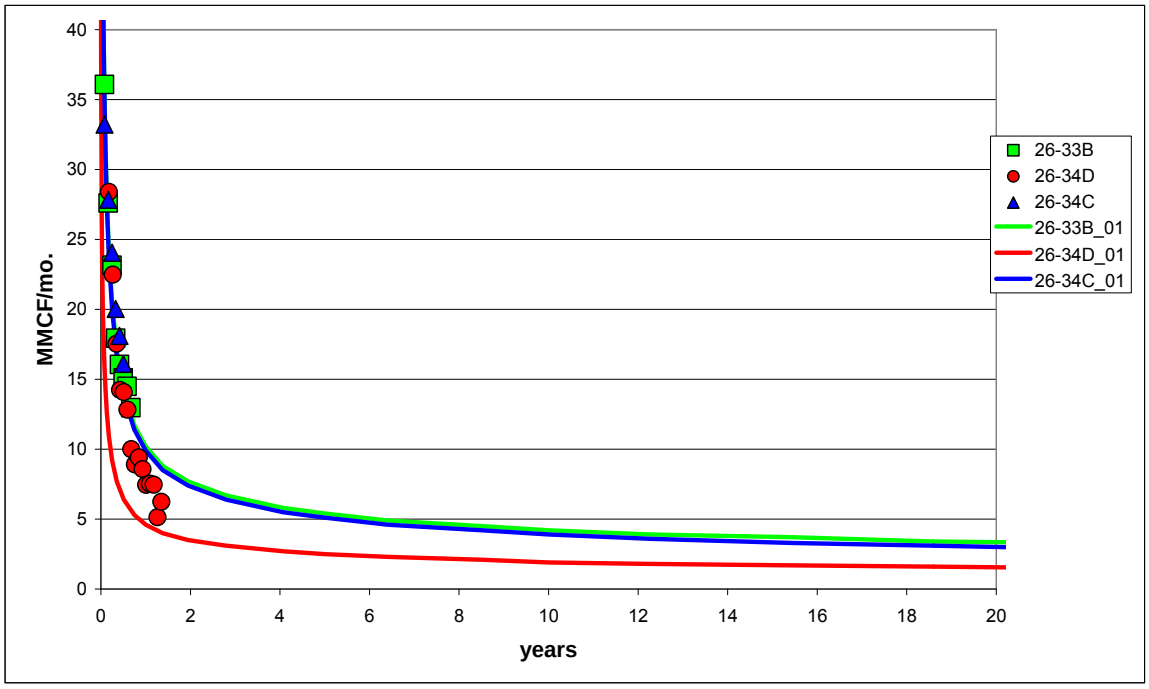

Figure 23. Overlay of Simulated Production Rate Curves for wells 26-33B, 26-34D, and 26-34C (Extended to 20 Years)

The gas well calibrated LWFsd permeability was 0.40 of the reentry well LWFsd calibrated permeability, and the porosity was 0.06 instead of 0.05. Near the well, hydrofracturing increased the sandstone permeability 40× and the shale permeability 800× (4× that of the unfractured sandstone). Far from the well (between the outer and inner hydrofracture ellipsoids), hydrofracturing increased the sandstone permeability 4×, and the shale was assumed to be not fractured.

The simulated production rates of the two wells with more sandstone matched the observed data well; however, the simulated production rates from the well with less sandstone underpredicted the observed rates. This likely is the result of more of the smaller sandstones being selected to be perforated and hydrofractured in this well than passed the criteria for the simulated hydrofracturing. Because of the limited production history, a better method than matching simulated and actual production rates for these wells is to compare the simulated and industry expected total production over the life of a well. With a simulated production life of 25 years,

wells 26-33B and 26-34C would produce about 1.44 and 1.34 BCF, respectively, given the parameters of the calibrated model. The low simulated-production rate well 26-34D would produce about 0.66 BCF. Given the recent development of hydrofracturing technology, there are no wells that have produced for an entire life cycle of 20–25 years. However, these simulated estimates are in line with industry expectations for the wells to produce about a BCF. It is likely that the two high percentage sandstone wells will produce less and the low percentage sandstone well will produce more than was simulated. In actual practice, the sands selected to be hydrofractured are not held to a rigorous cutoff thickness. Wells with less sand will have additional thinner sands targeted and wells with abundant sands may have some sands that meet the 40 ft thick criteria not targeted.

5.0 Rulison Simulation Results

The primary benefit of a numerical model is that past, current, and future scenarios can be tested. The Rulison model was initialized to conditions following the detonation and used to simulate the reentry well production testing, the subsequent pressure recovery after testing ended, migration of contamination from the detonation zone to its current extent (primarily by diffusion), and the effects on the flow system of the recently installed gas wells. The Rulison Path Forward document (DOE 2010) puts forth a logical approach to future gas development in the vicinity of the Rulison test. The model was used to simulate the enactment of the Path Forward drilling plan for one potential time schedule, providing a visual representation with quantifiable results of how the flow system and potential contaminant migration would be affected. Model animations provide a tool to inform any interested party about the Rulison test, the logic behind the Path Forward, and natural gas drilling in the Piceance Basin in general.

The Rulison model simulations are a composite of two separate primary simulations, which are in turn composed of separate simulations as needed to improve use of computation time and assignment of well production rates. The first step after model construction was to simulate the post-detonation events up until the gas wells in the model domain were installed, to 2010. The second step simulated production from the existing gas wells and staged additions of future gas wells for 25 years as suggested in the Path Forward document.

5.1 Simulations from Post-Detonation to 2010 Conditions

The initial modeling simulated conditions from post-detonation, September 10, 1969, up until the gas wells within the model domain began production, about January 1, 2010 (Table 10). Figures 24 through 30 (designated X, for plot of mass fraction THO gas, P for pressure) are vertical sections (y38 on Figure 6) that show the progression of conditions throughout the simulation. Pressure is shown on the concentration plots as black contours to reference with the color pressure plots. The demarcations for Lot 11 are for the east-west boundaries and extend beyond the lot north and south (y increases to the north).

Table 10. Key Steps in Simulating Post-detonation to 2010

Date	Days Since Detonation	Process	Figure
09/10/1969	0	Initial diffusion after the detonation	24
10/04/1970	389	Begin reentry well testing, test 1	25
10/07/1970	392	Production test 1 ends	
10/26/1970	411	Production test 2 begins	
11/04/1970	419	Production test 2 ends	
12/01/1970	447	Production test 3 begin	
12/20/1970	466	production test 3 ends	26
02/02/1971	510	Production test 4 begins	
04/24/1971	591	Test 4 ends, begin pressure recovery	27
09/27/1971	747	Last pressure reading	28
01/01/2010		Simulation ended	30

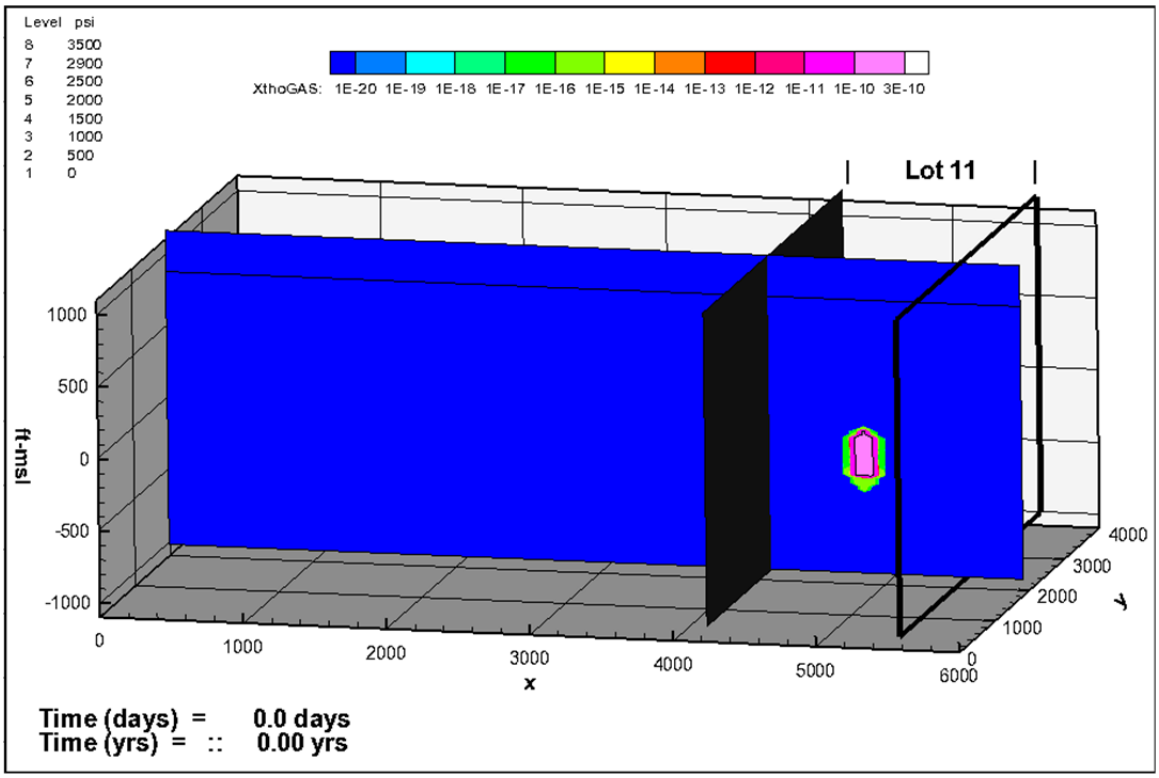

Figure 24X. Initialized Mass Fraction of THO in the Gas Phase (Xthogas) After the Detonation

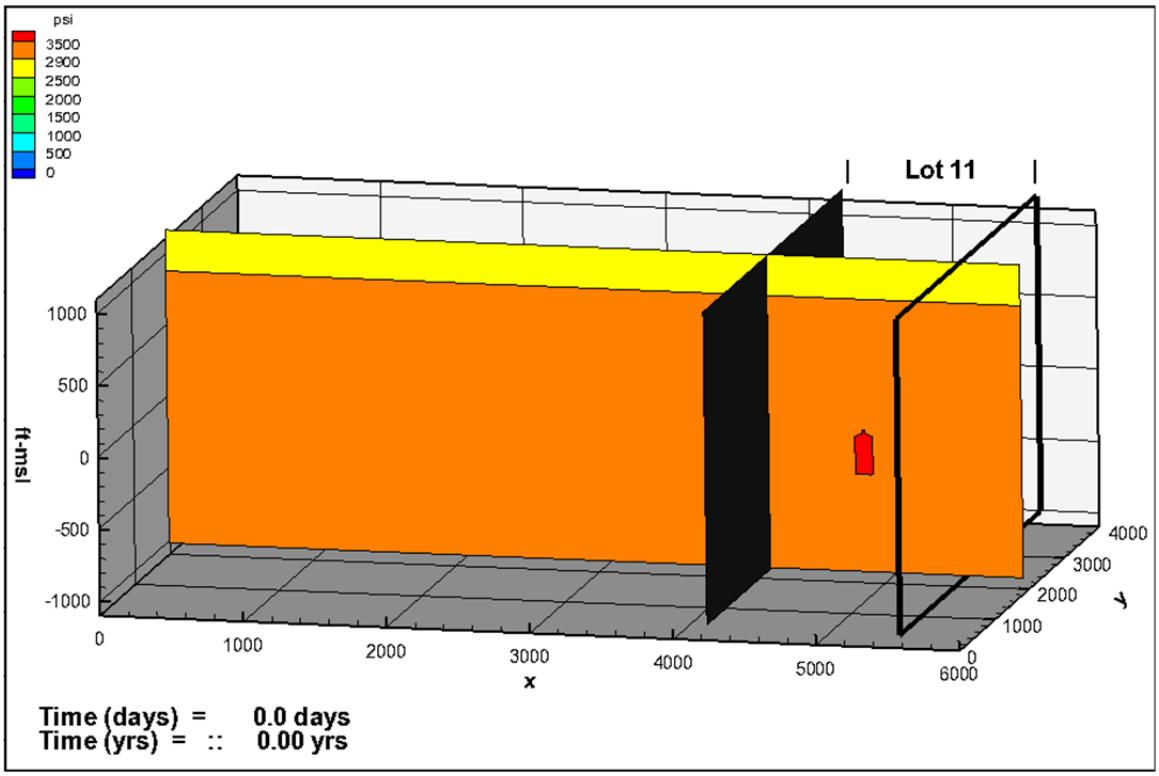

Figure 24P. Initialized Pressure Distribution After the Detonation

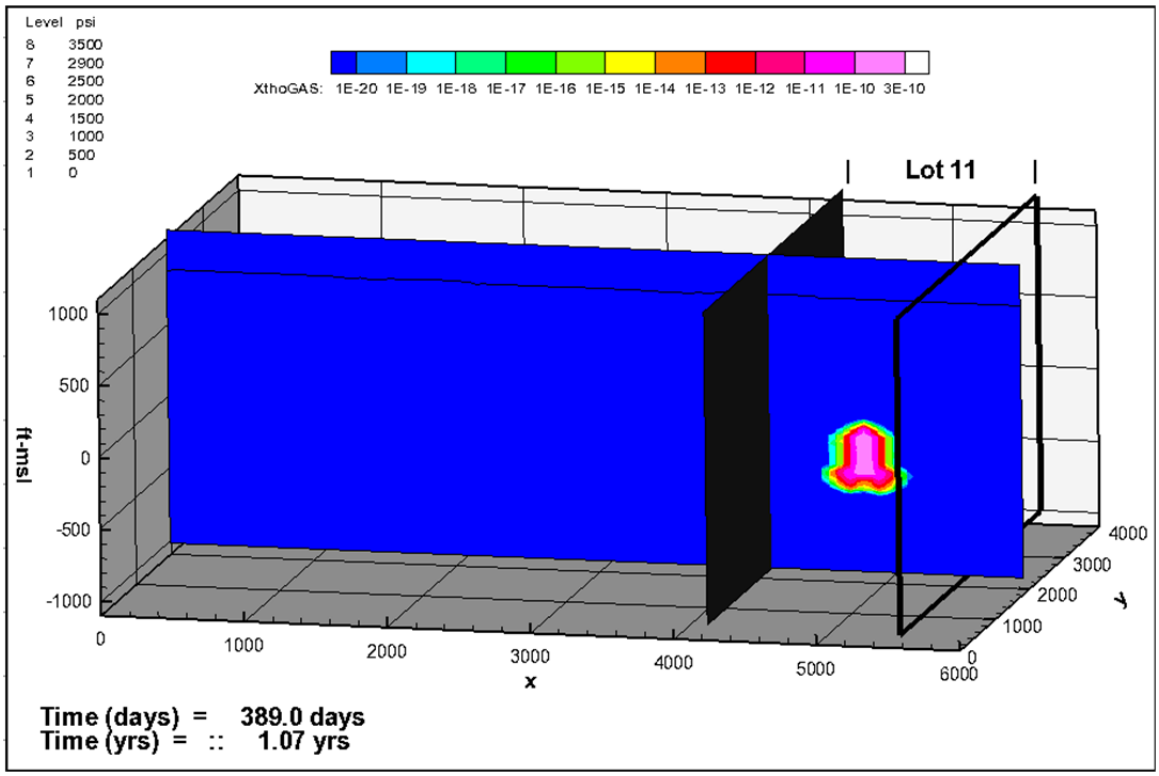

Figure 25X. Mass Fraction of THO Gas Beginning of Production Testing

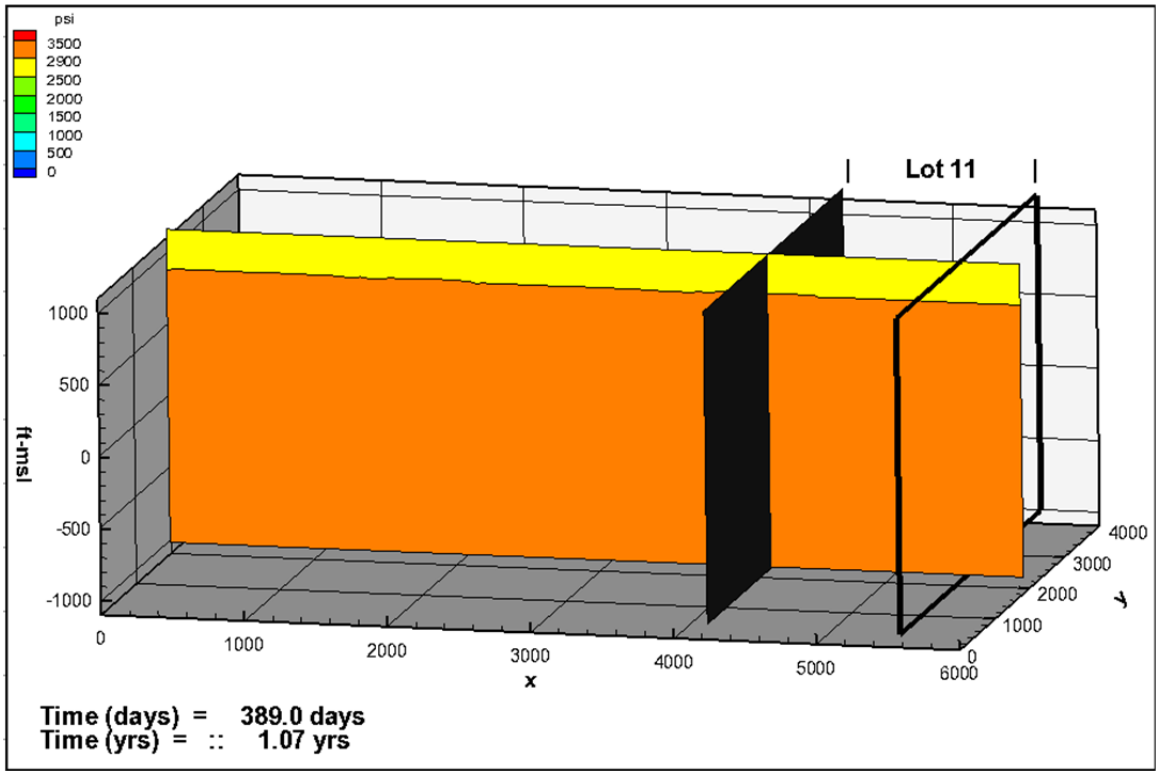

Figure 25P. Pressure Distribution at Beginning of Production Testing

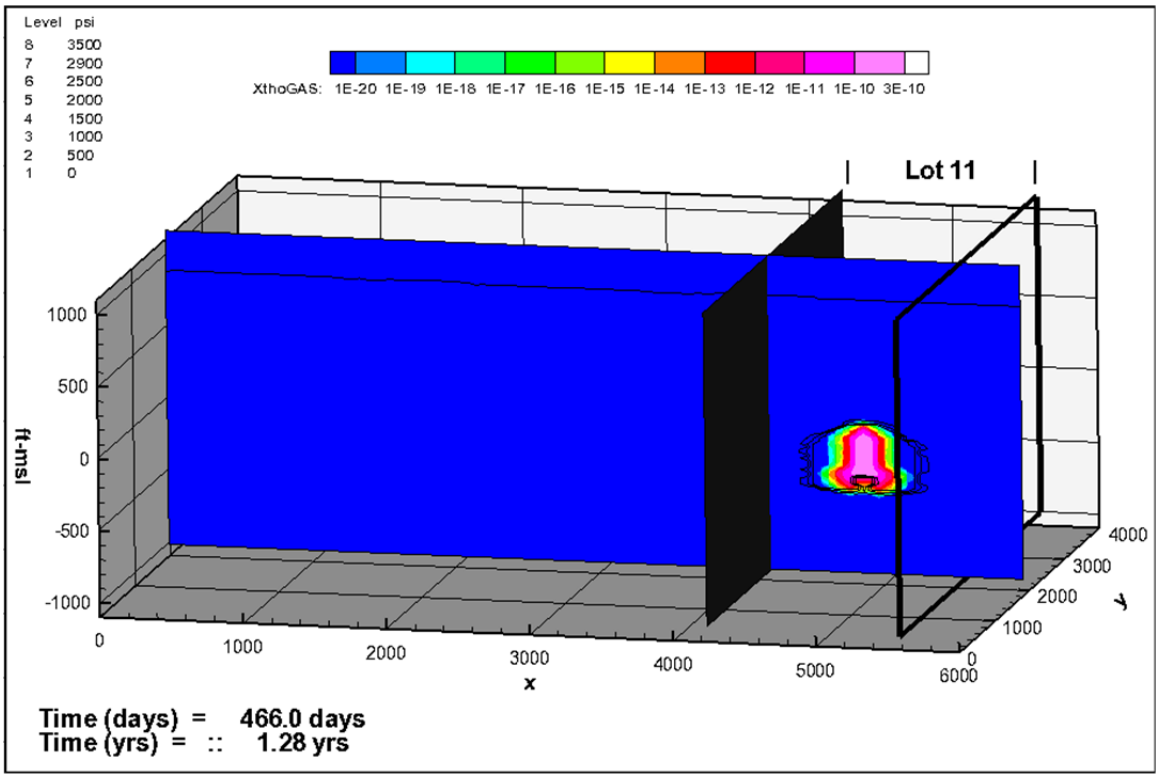

Figure 26X. Mass Fraction of THO After Third Production Test

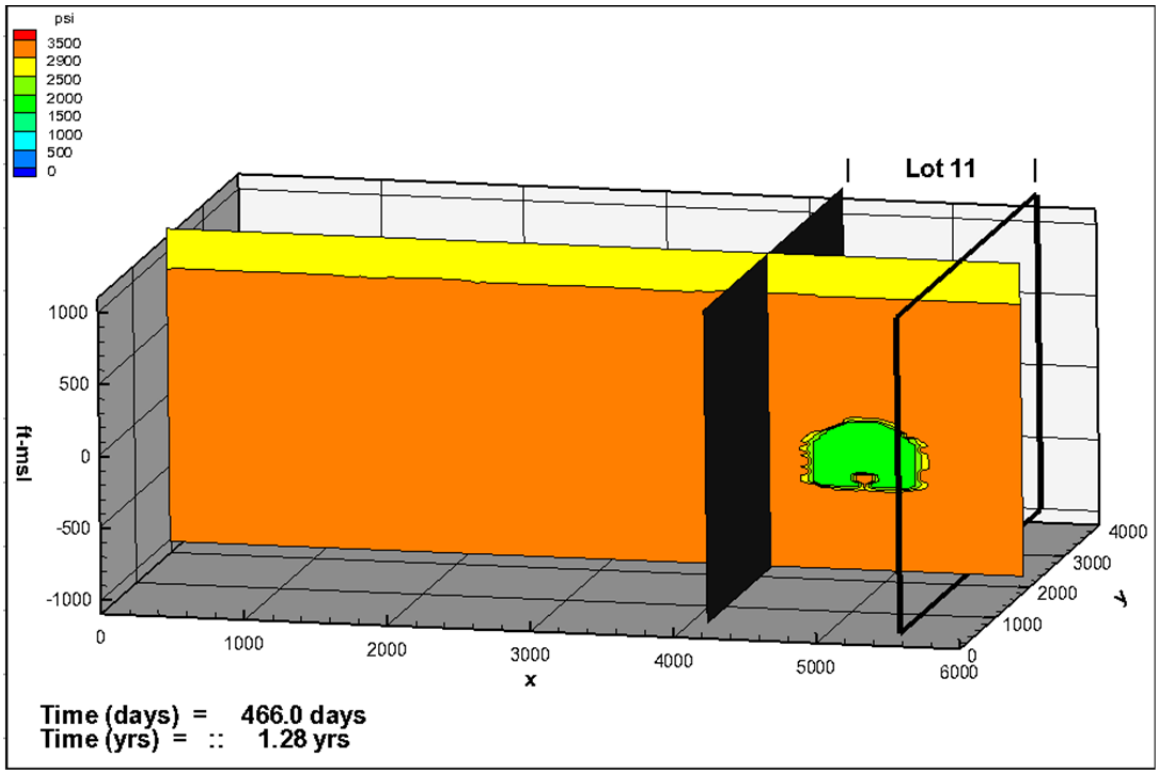

Figure 26P. Pressure Distribution After Third Production Test

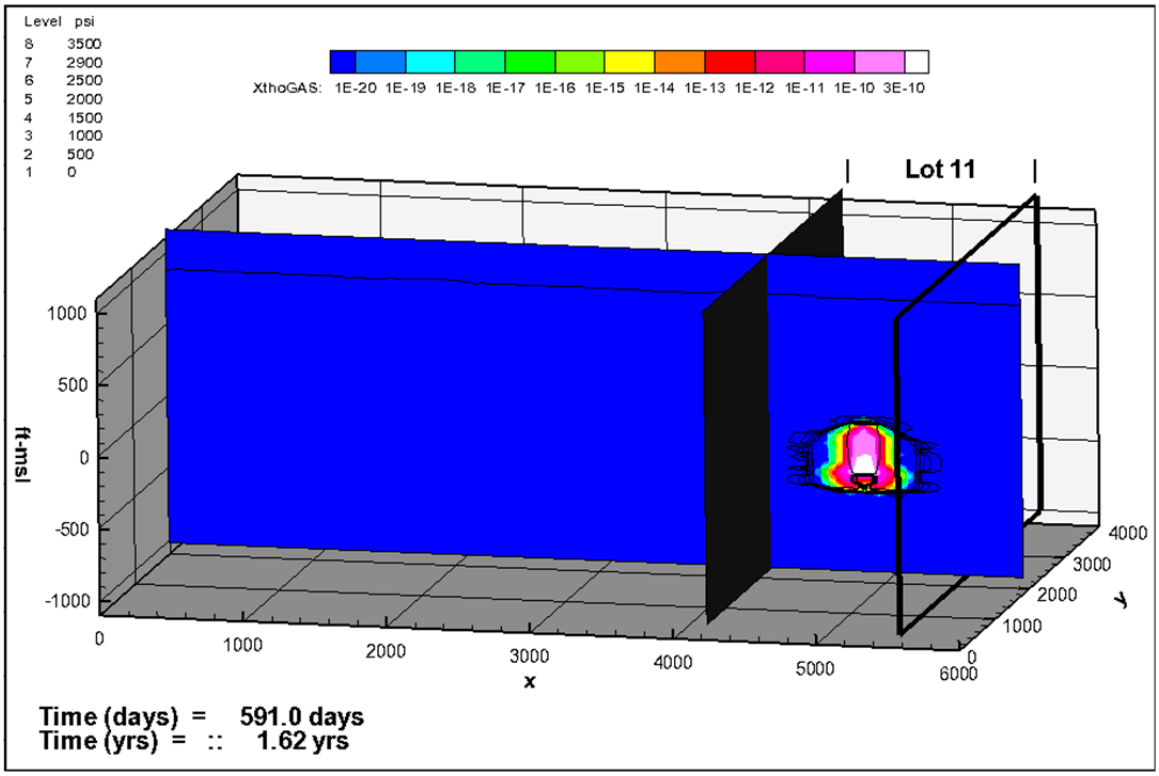

Figure 27X. Mass Fraction of THO After Fourth Production Test (End of Testing)

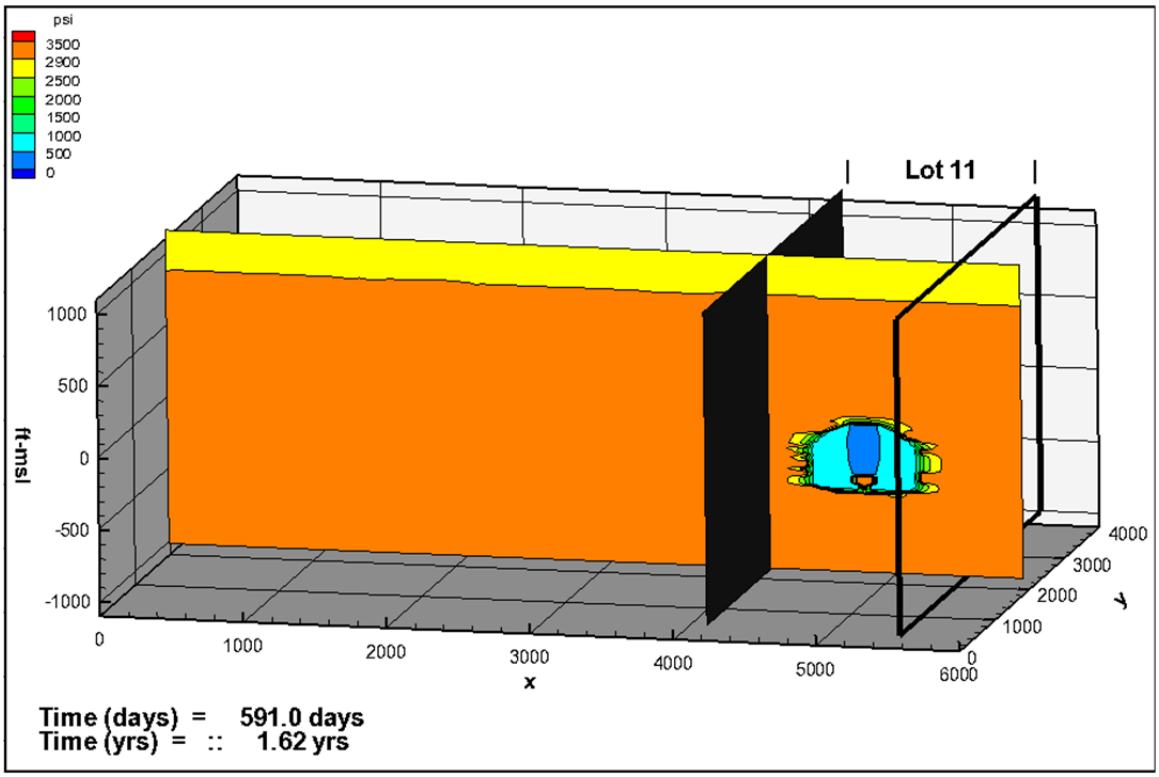

Figure 27P. Pressure Distribution After Fourth Production Test (End of Testing)

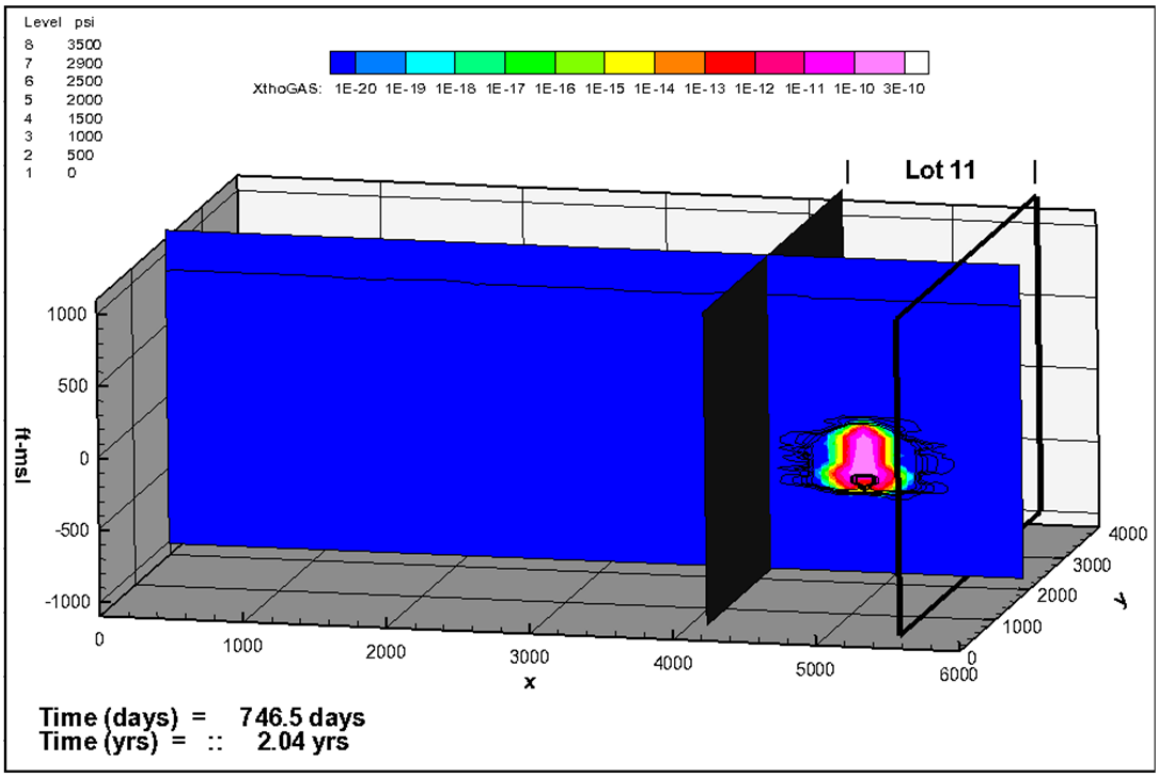

Figure 28X. Mass Fraction of THO After Last Pressure Reading

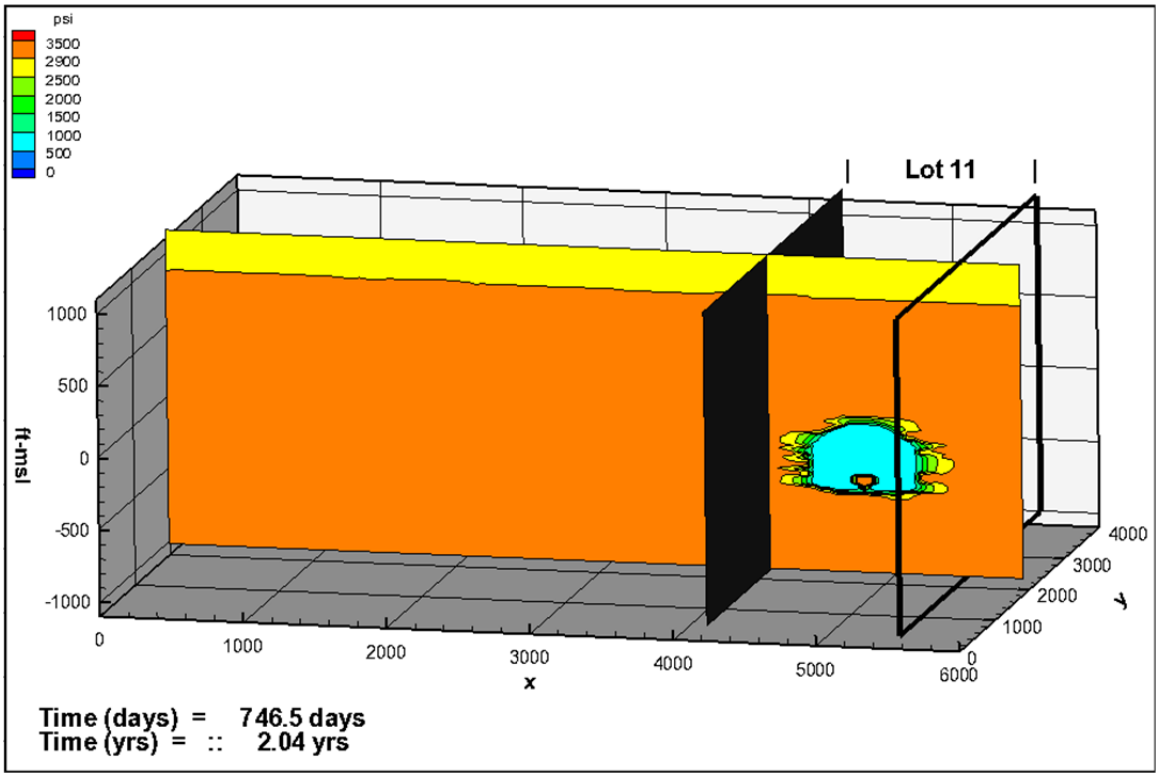

Figure 28P. Pressure Distribution After Last Pressure Reading

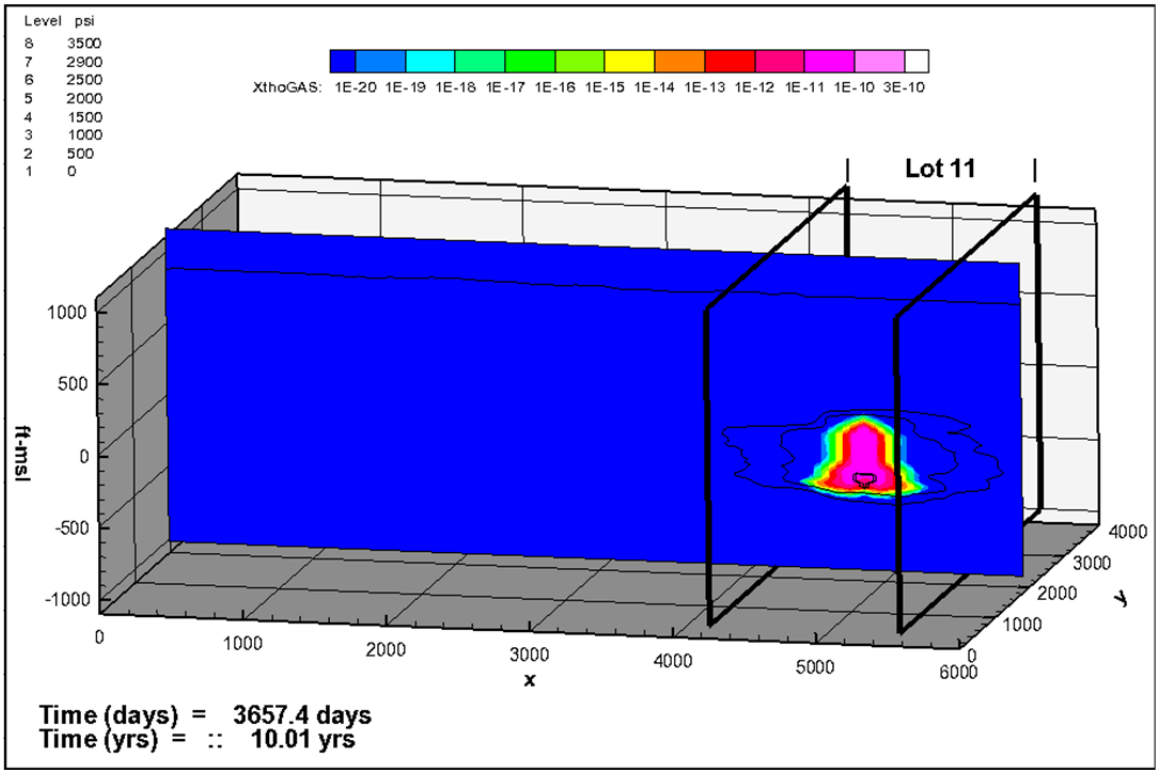

Figure 29X. Mass Fraction of THO 10 Years After Detonation

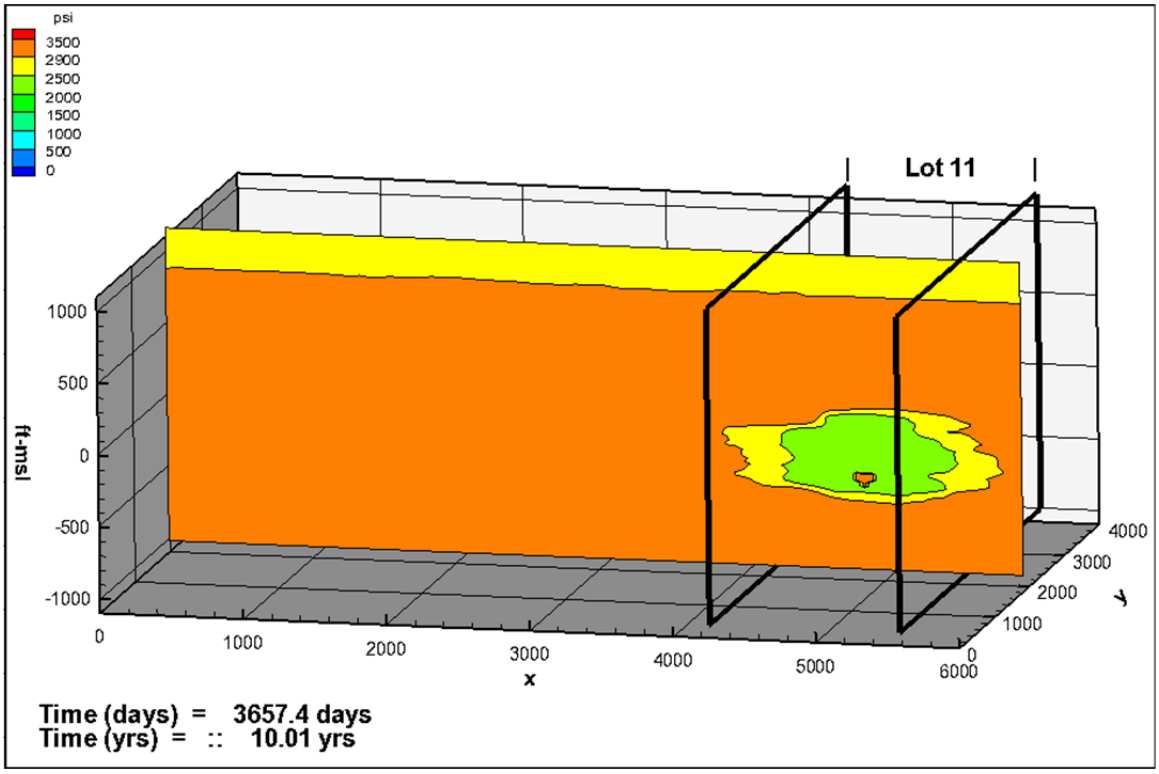

Figure 29P. Pressure Distribution 10 Years After Detonation

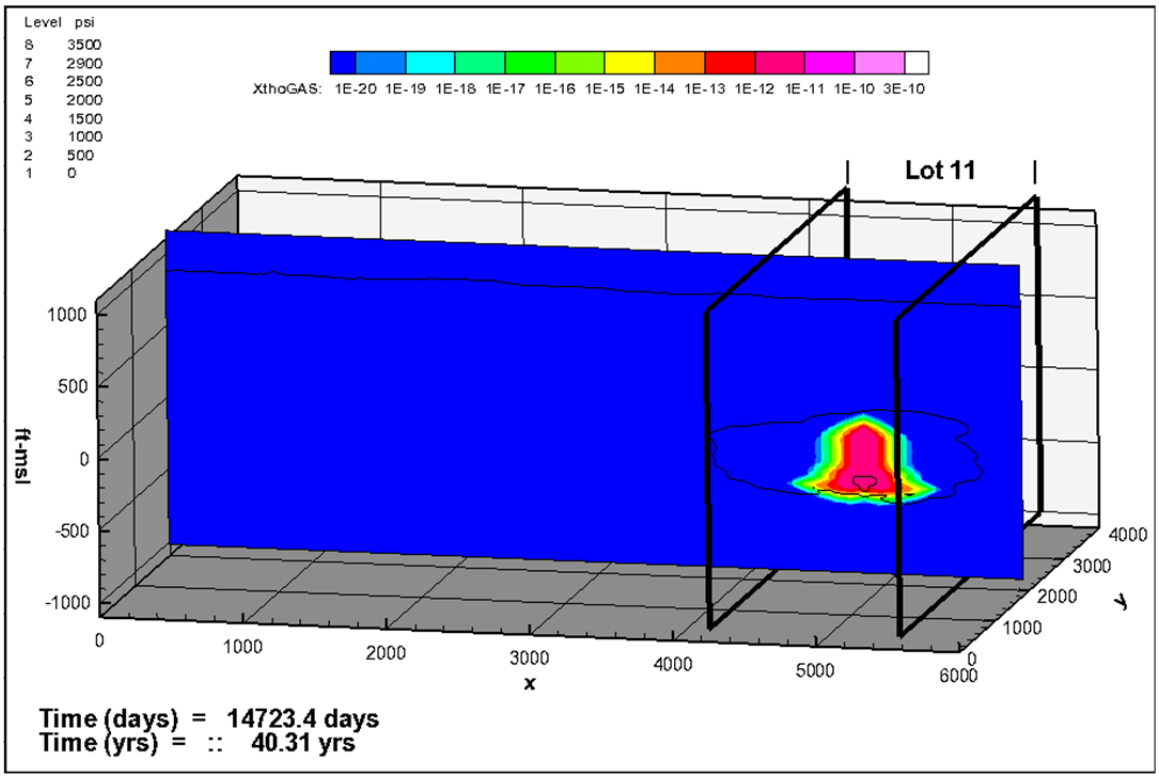

Figure 30X. Mass Fraction of THO in 2010

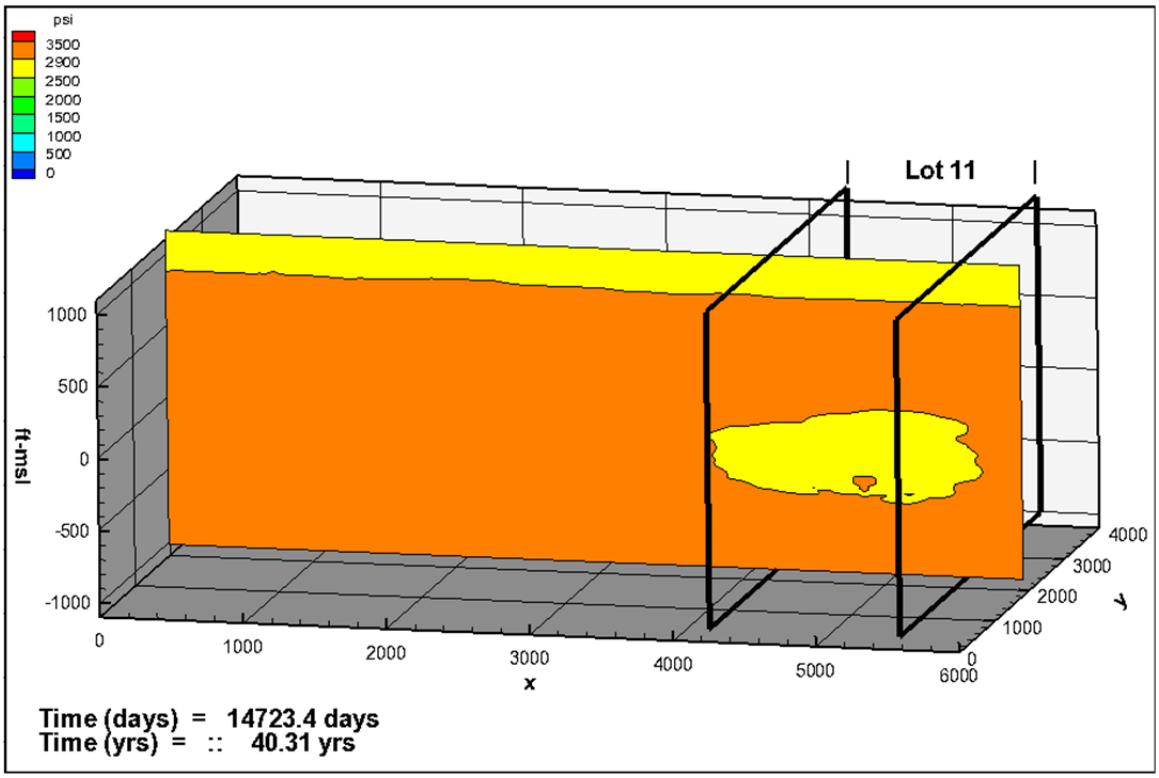

Figure 30P. Pressure Distribution in 2010

The Figure 24 montage shows the initial (10 seconds into the initial simulation) concentration of tritium as mass fraction of THO in the gas phase and the initial pressure distribution.

Figure 25 shows the conditions just before production begins. Key points are the migration of THO from the chimney into the nuclear fractured region, aided by the higher pressure that was initialized in the chimney, and that the pressure has equilibrated with the formation pressure.

Figure 26 shows the conditions after the third production test. Production testing reduced pressures to about 1,500 psi in the detonation zone, creating an inward pressure gradient. The inward gradient did not retrieve much of the tritiated water that had migrated away from the detonation zone by diffusion. Much of the tritium that diffuses outward as tritiated water vapor, partitions into the low mobility aqueous phase in the formation surrounding the detonation zone. The liquid and vapor have the same mole fraction of tritiated water, but the liquid contains far more molecules and therefore most of the tritium. This tritium is difficult to remove by gas extraction only and in an environment where the liquid is much less mobile than the gas, it acts as a persistent source in the same way that the tritiated liquid water in the detonation zone is a persistent source.

Figure 27 shows the conditions after the fourth and last production test. Production reduced pressures to about 250 psi in the chimney and to less than 1,000 psi in the nuclear fractured region. The low pressures caused the evolution of THO from the aqueous phase into the gas phase, significantly increasing the concentration in the gas phase (Figure 27X). The lower pressures also decreased the temperature in the chimney (Figures 31 and 32), which counteracts the THO partitioning into the gas phase. Figure 33 shows the equilibrated temperature distribution 40 years after the detonation and 38.4 years after the production testing ended. The temperature of the melt glass at the base of the chimney is constant at 255 °C to simulate a radioactive heat source and to promote partitioning of THO into the mobile gas phase. Observed actual tritium concentrations decreased throughout the production testing, suggesting that the amount of simulated initial tritium is likely overestimated and that this aspect of the model design is conservative.

Figure 28 shows the conditions after the last actual pressure measurement was taken. Pressures in the chimney have recovered to about 800 psi, and the pressure drop has noticeably extended into the sandstones adjacent to the detonation zone.

Figure 29 shows the conditions 10 years after the detonation. The extent of the contamination has continued to spread but has not reached the lot boundary. The highest concentration contour in the chimney has decreased an order of magnitude. Pressures in the detonation zone have recovered to over 2,000 psi as the pressure sink that resulted from the production testing has spread to the adjacent formation beyond the lot boundary, though at only a very slight pressure differential.

Figure 30 shows the conditions about 40 years after the detonation (2010). The extent of the contamination has continued to spread but still does not reach the lot boundary, and the highest concentration in the chimney has decreased nearly another order of magnitude. Pressures in the detonation zone have recovered to nearly those of the formation prior to the production testing. The key finding from the initial set of simulations is that even with an elongated nuclear fracture region, contamination remains within the institutional control boundary.

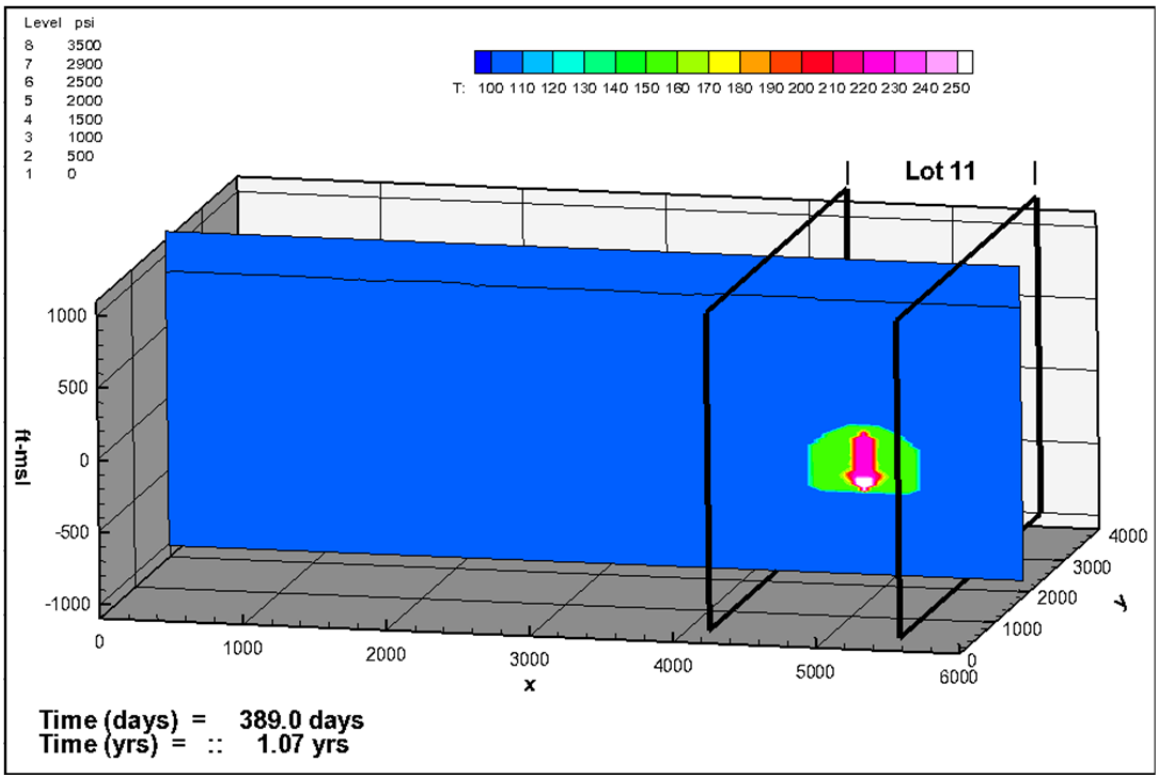

Figure 31. Temperature Distribution Prior to Production Testing

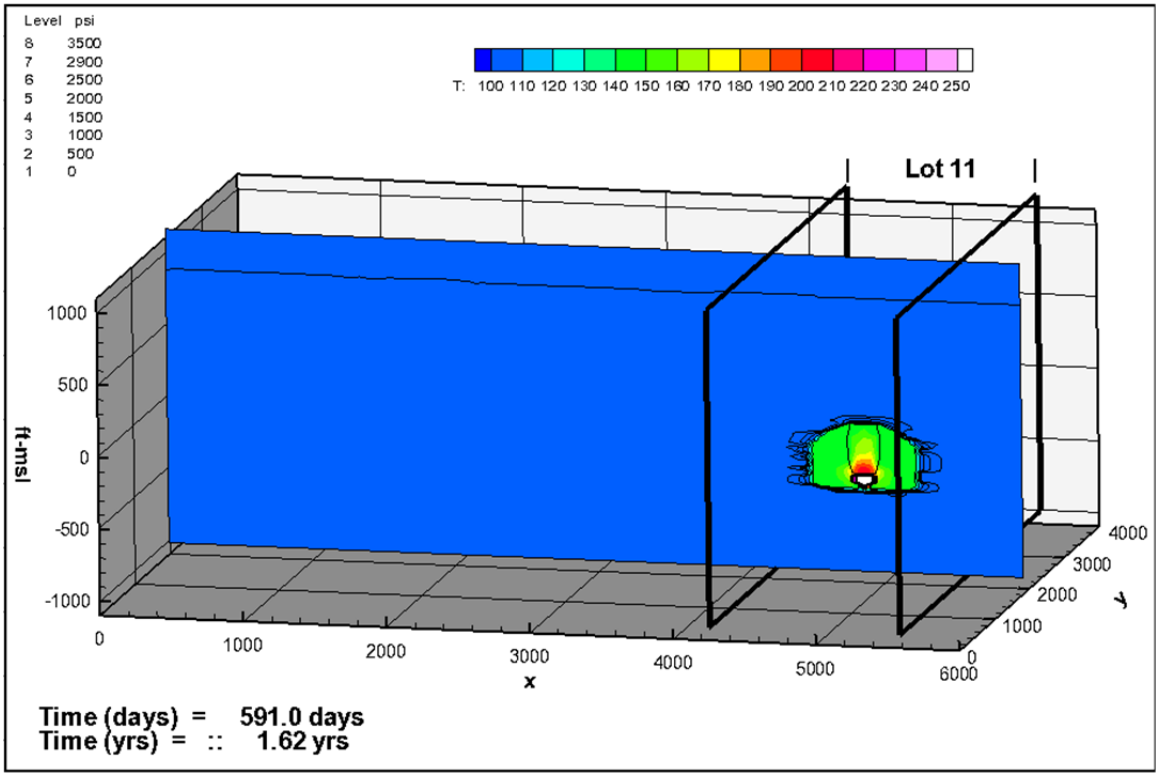

Figure 32. Temperature Distribution at the End of the Fourth Production Test

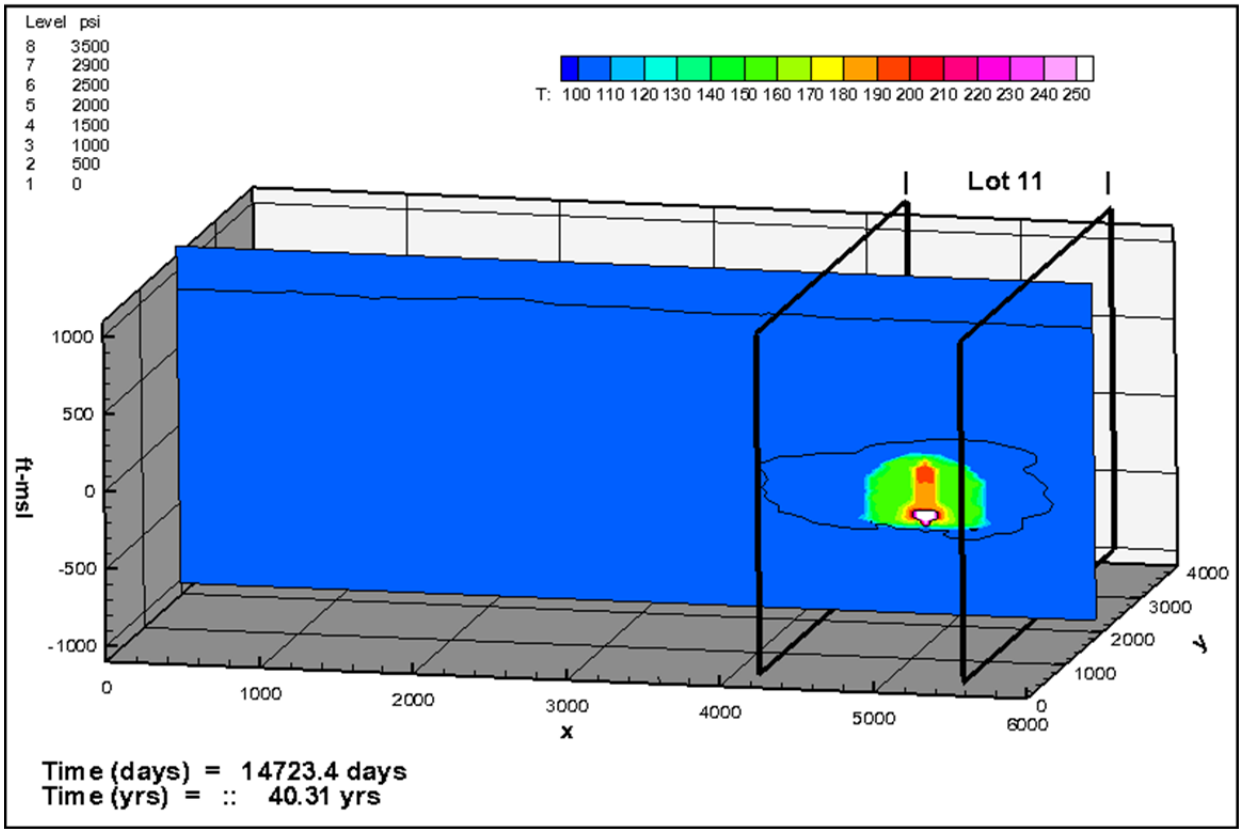

Figure 33. Temperature Distribution Before Gas Well Production (2010)

5.2 Simulation of the Rulison Path Forward

The Rulison Path Forward recommends that wells encroaching on the site be drilled in a conservative, staged approach to minimize the risk of encountering contamination. Drill a set of wells, monitor, drill the next set closer, and so forth. The model was used to simulate this approach for one potential well installation timeline (Table 11) to evaluate potential effects on the institutional control boundary of Lot 11. The simulation continues from the 2010 condition simulation (prior to gas wells within the model domain) and begins with the onset of production from the wells recently installed by Noble Energy in 2010. The simulation assumes that all seven wells began production on January 1, 2010, to simplify the process, though the wells actually began producing at different times between June 2009 and August 2010. Figures 34 through 40 (designated X, for plot of mass fraction THO gas, P for pressure) are vertical sections through the model (locations on Figure 6). Pressure is shown on the concentration plots as black contours to reference with the color pressure plots. Some figures show multiple sections to highlight effects that cannot be seen on a single plane.

Table 11. Milestones in the Rulison Path Forward Simulation

Date	Years Since Gas Production	Process	Figure
2010	0	Noble wells begin production	30
2011	1	1 year into production	34
2015	5	0.5 mile wells begin production	35
2020	10	North/south wells inside 0.5 mile begin	36
2025	15	Adjacent wells begin production	37
2030	20	5 years into adjacent well production	38
2035	25	Noble wells end production	39
2045	35	End simulation	40

The north/south (N/S) wells are inside the half-mile radius but located perpendicular to the east-west natural fracture trend of the formation.

The Figure 34 montage shows the concentration of tritium as mass fraction of THO in the gas phase and the pressure distribution 1 year after production began in the existing gas wells (2011). The concentration distribution is not noticeably different from the distribution from 1 year earlier (Figure 30X), as would be expected in that the producing wells are 0.75 mile from the detonation zone. The effects of production on the pressure distribution around the wells (the effects on only one well can be seen) are as expected.

Figure 35 shows the simulated conditions 5 years into production of the existing wells (2015), just before the theoretical wells located just outside the one-half-mile radius west of the site (one-half-mile wells) begin production (2015). An additional slice (x17) is shown to provide a perpendicular view through the model to allow the effects of more than one well to be seen. It shows that the simulated extent of the pressure effects are primarily east-west and limited (though present) north-south. North/south pressure interaction between the existing wells that began production in 2010 has not been observed. Pressure interaction has been more frequent for wells aligned east/west. The concentration distribution is little changed since 2011.

Figure 36 shows the simulated conditions in 2020, 10 years into production of the existing wells and 5 years into production of the one-half-mile wells. The theoretical wells north and south of the site inside the one-half -mile radius (north/south [N/S] wells) begin production at this time. The concentration distribution is little changed since 2015. Two slices are shown (y38 and y41) so that the effects due to each set of wells can be seen. A window is blanked in y38 to allow the portion of y41 with a one-half-mile well to be seen. This is necessary because the y38 slice cuts between wells along the line of one-half -mile wells. Wells east and west of each other are typically offset to limit inter-well communication.

Figure 37 shows the simulated conditions in 2025, 15 years into production of the existing wells, 10 years into production of the one-half-mile wells, and 5 years into production of the N/S wells. The theoretical wells in the most vulnerable location west of and adjacent to the site (adjacent wells) begin production at this time. The concentration distribution is little changed since 2020, though the extent of the highest concentration is decreasing. Three slices are shown (y38, y69, and x46) to see the effects of multiple wells on the pressure distribution. The top right portion of y38 is blanked to allow the pressure response of the N/S well on y69 to be seen.

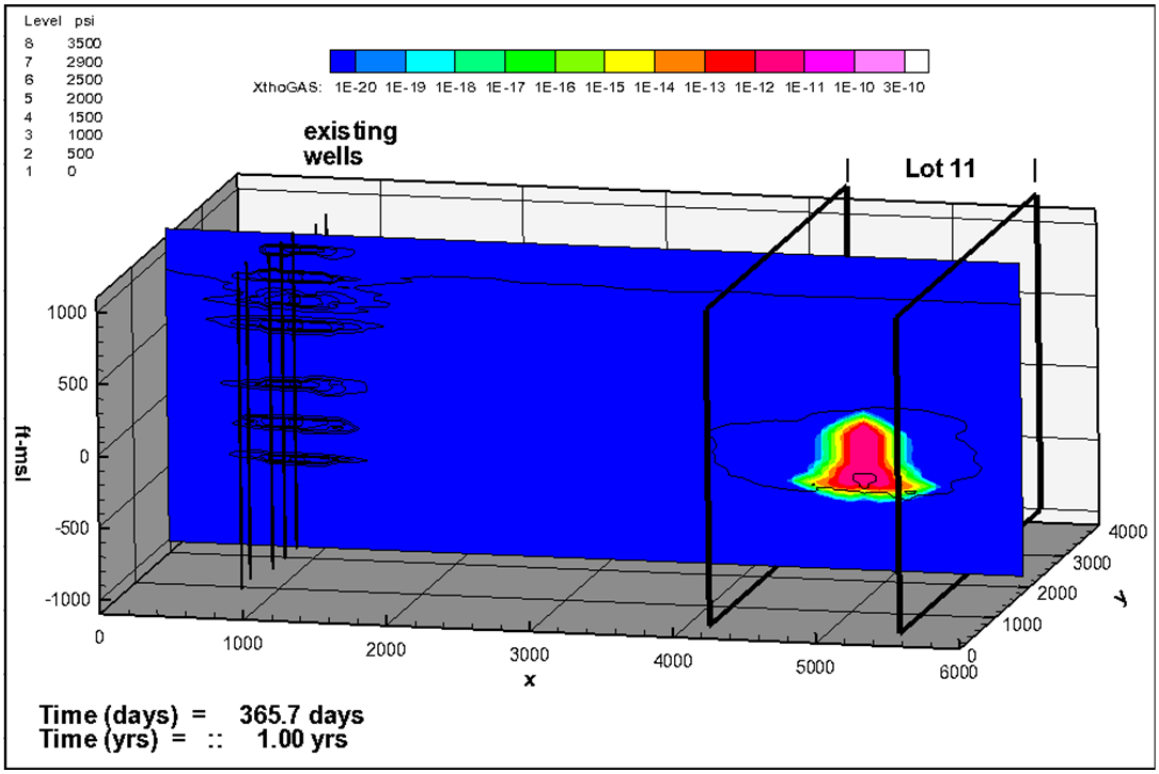

Figure 34X. Mass Fraction of THO in 2011 (y38)

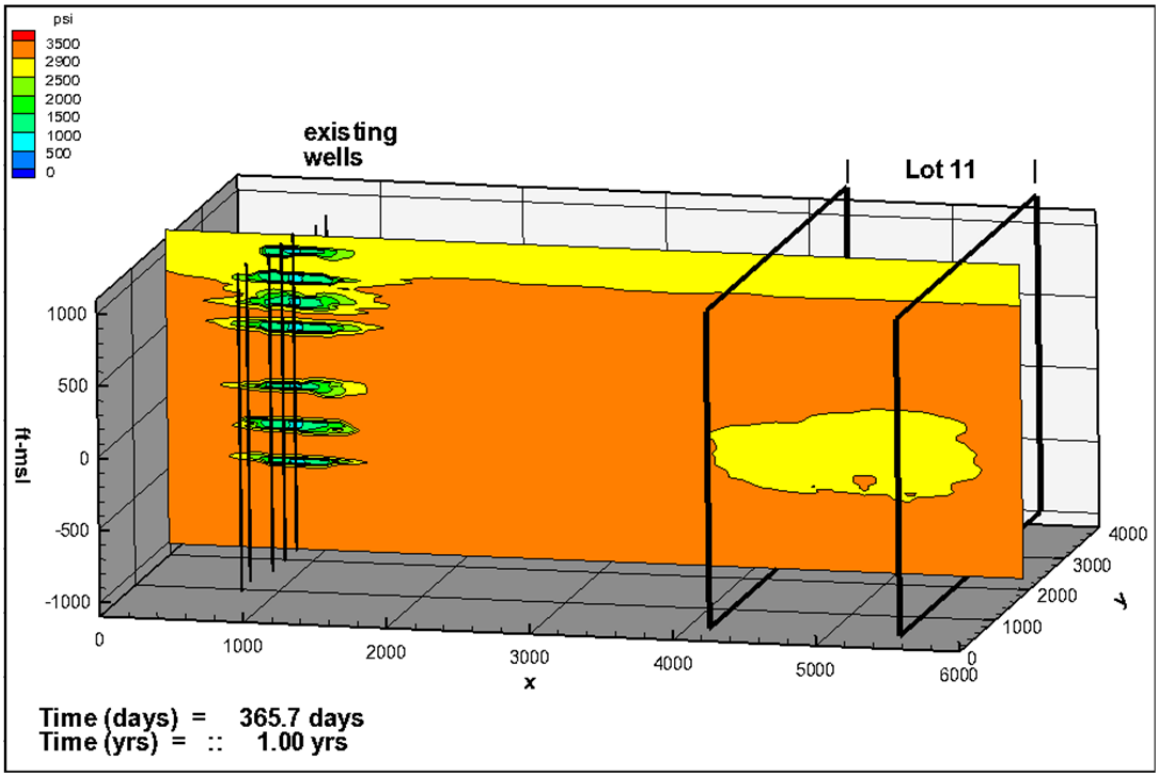

Figure 34P. Pressure Distribution in 2011

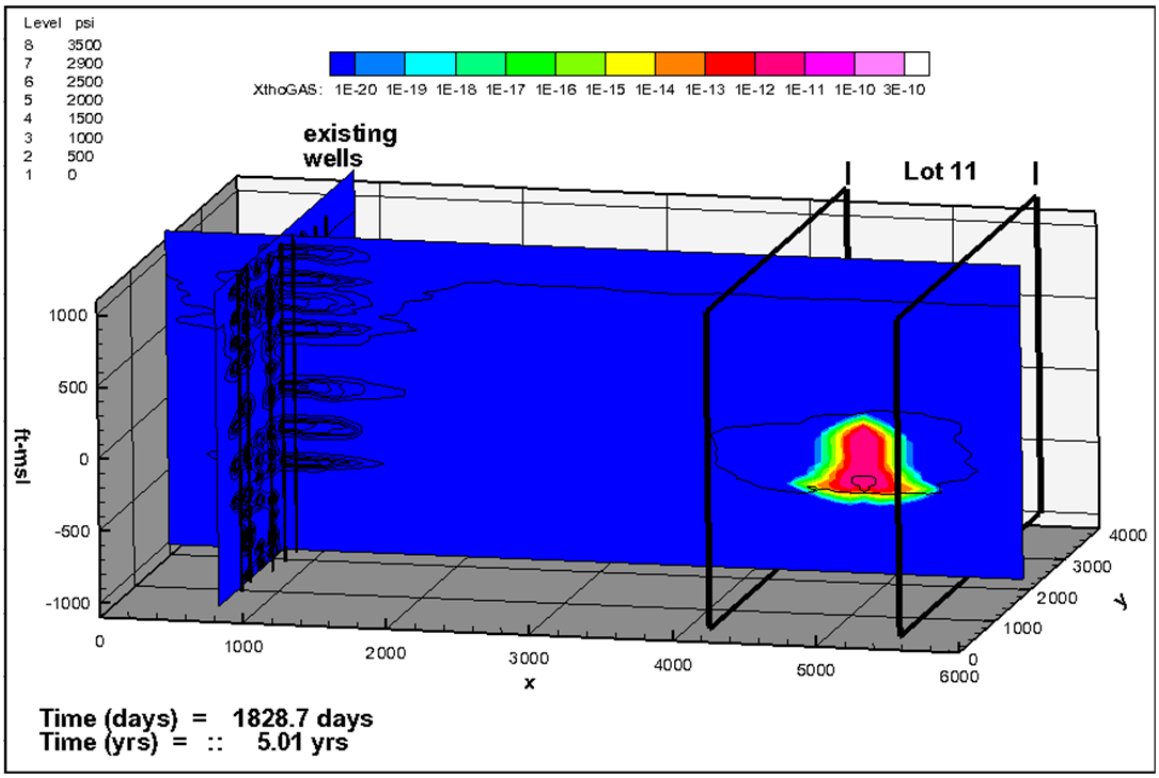

Figure 35X. Mass Fraction of THO in 2015 (y38, x17)

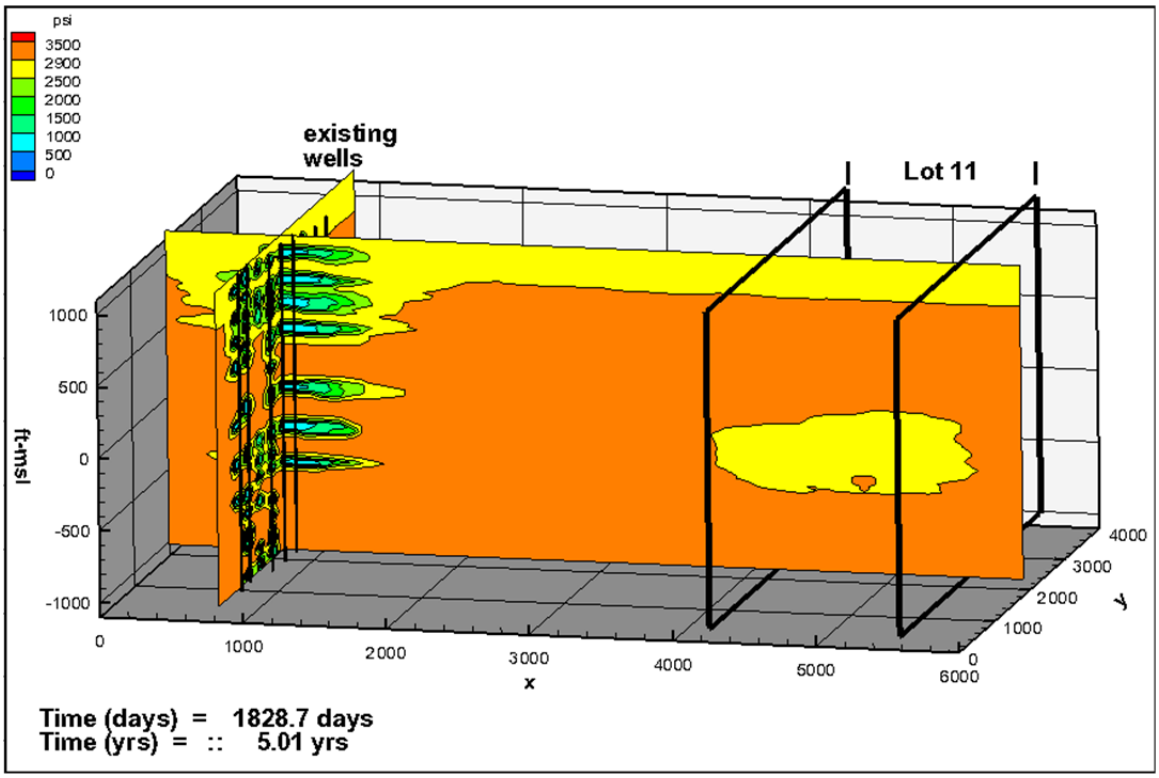

Figure 35P. Pressure Distribution in 2015

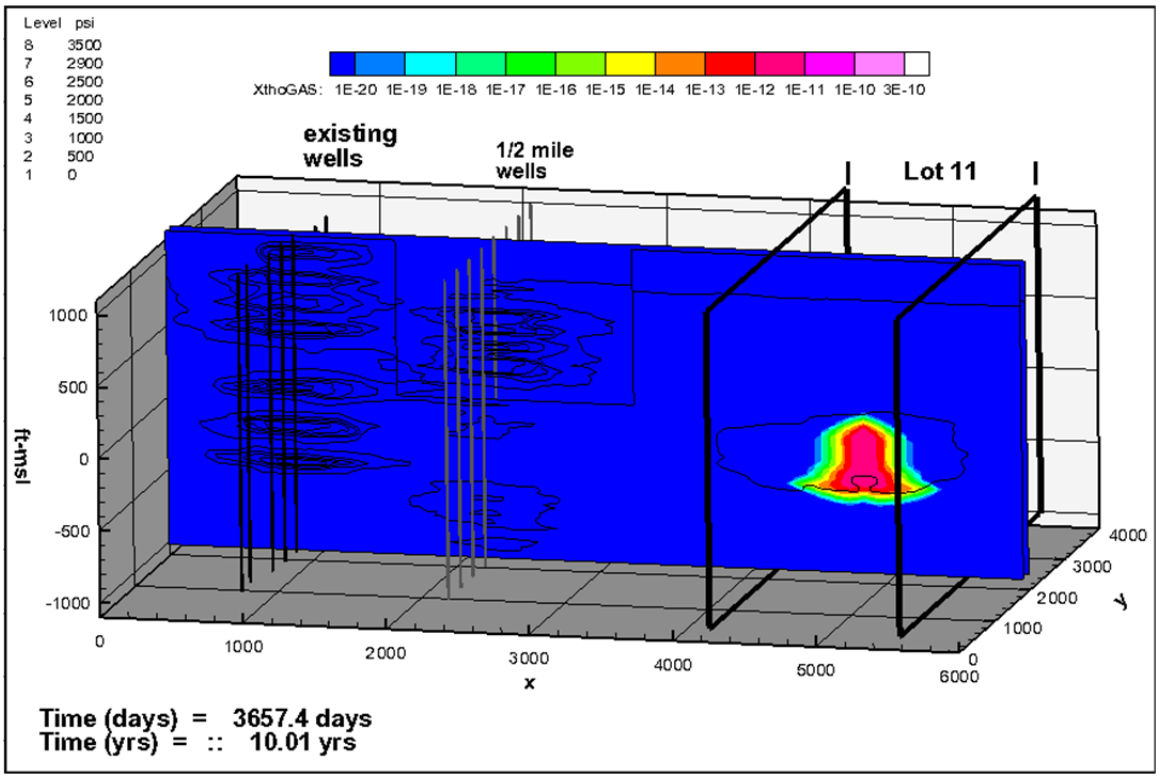

Figure 36X. Mass Fraction of THO in 2020 (y38 with Cutout, y41)

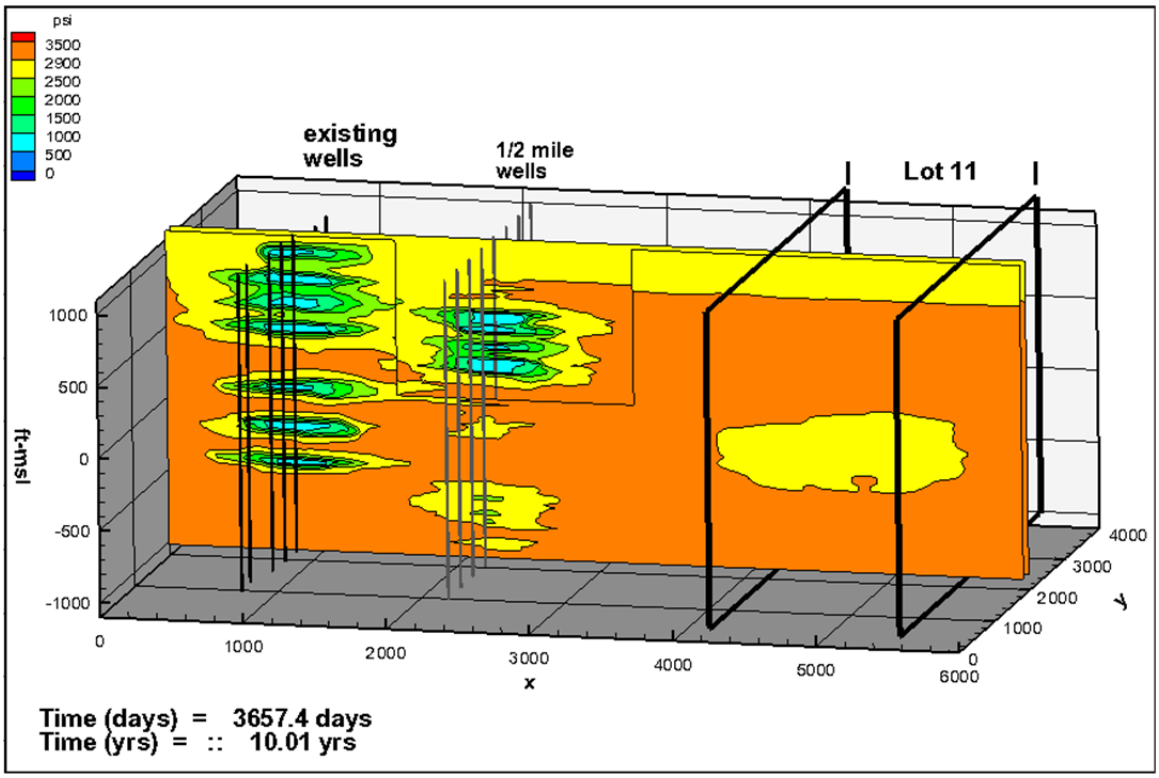

Figure 36P. Pressure Distribution in 2020

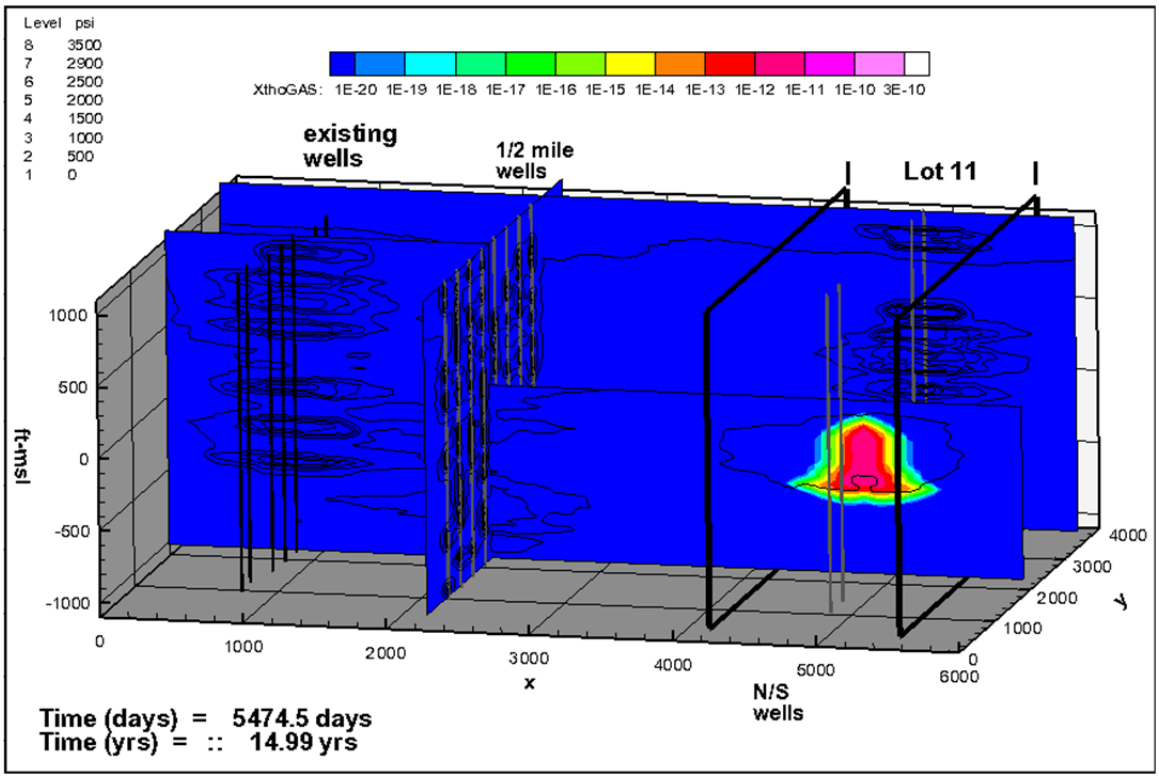

Figure 37X. Mass Fraction of THO in 2025 (y38 with Cutout, y69, x46)

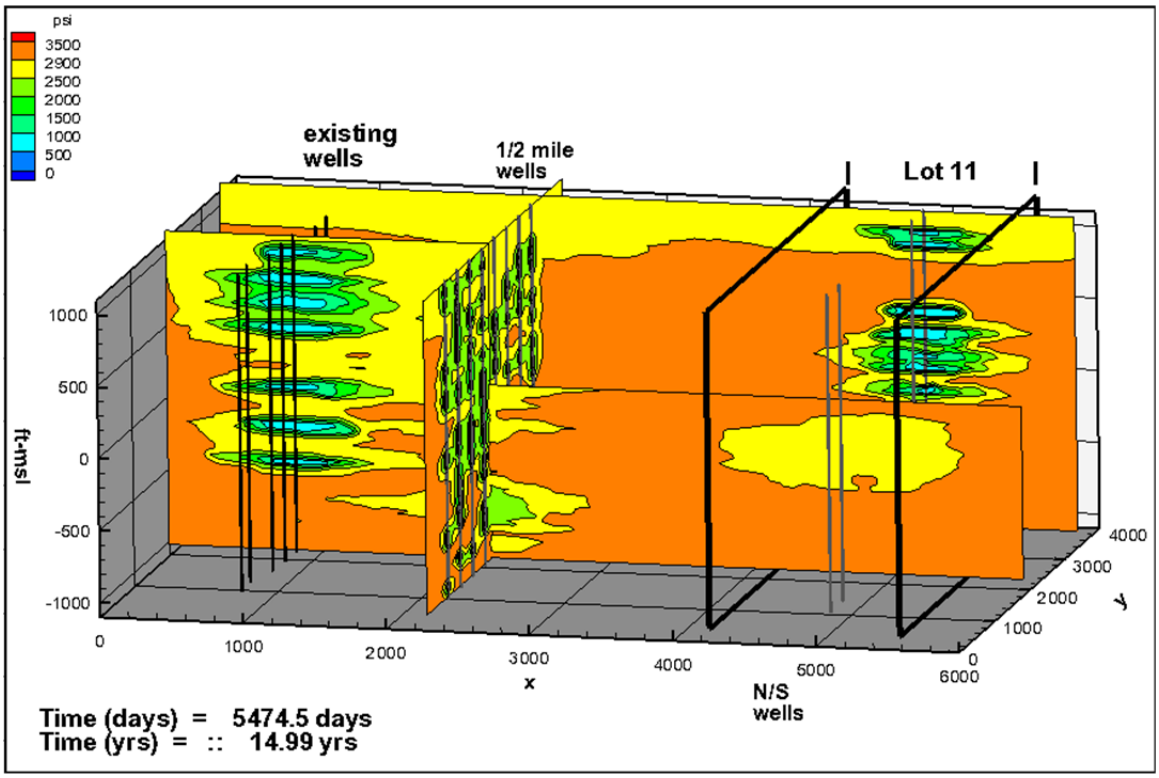

Figure 37P. Pressure Distribution in 2025

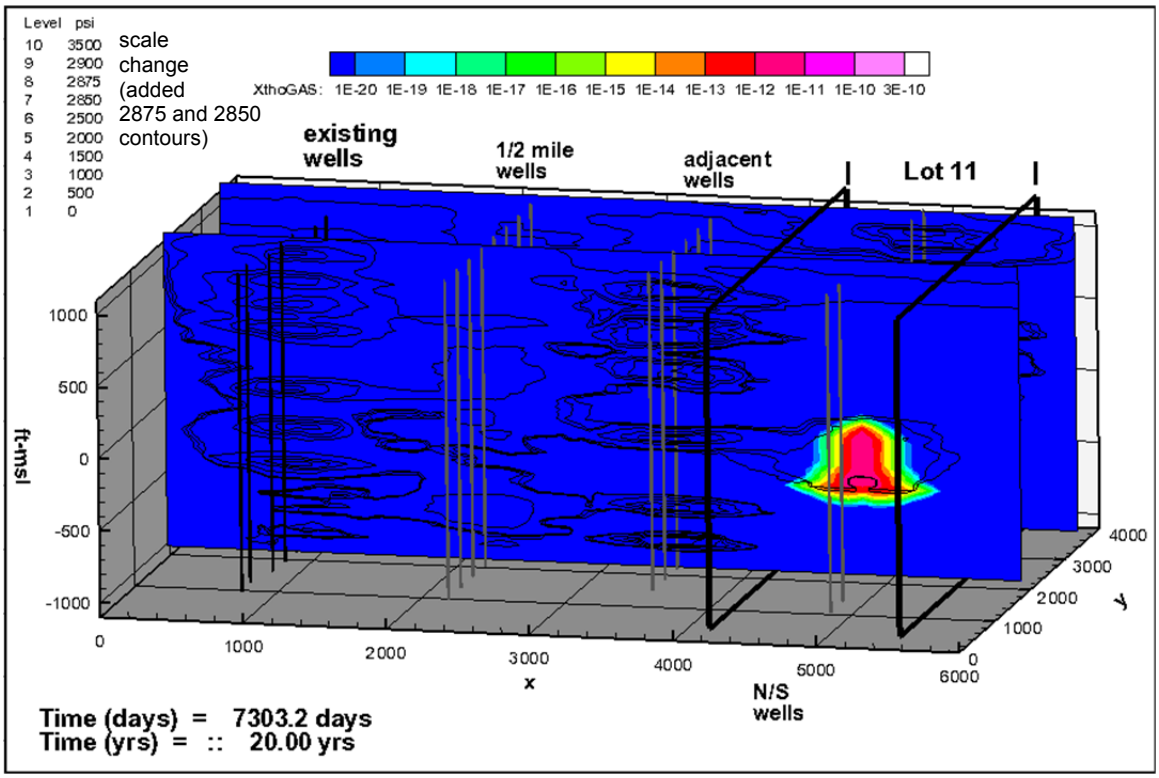

Figure 38X. Mass Fraction of THO in 2030 (y38, x69)

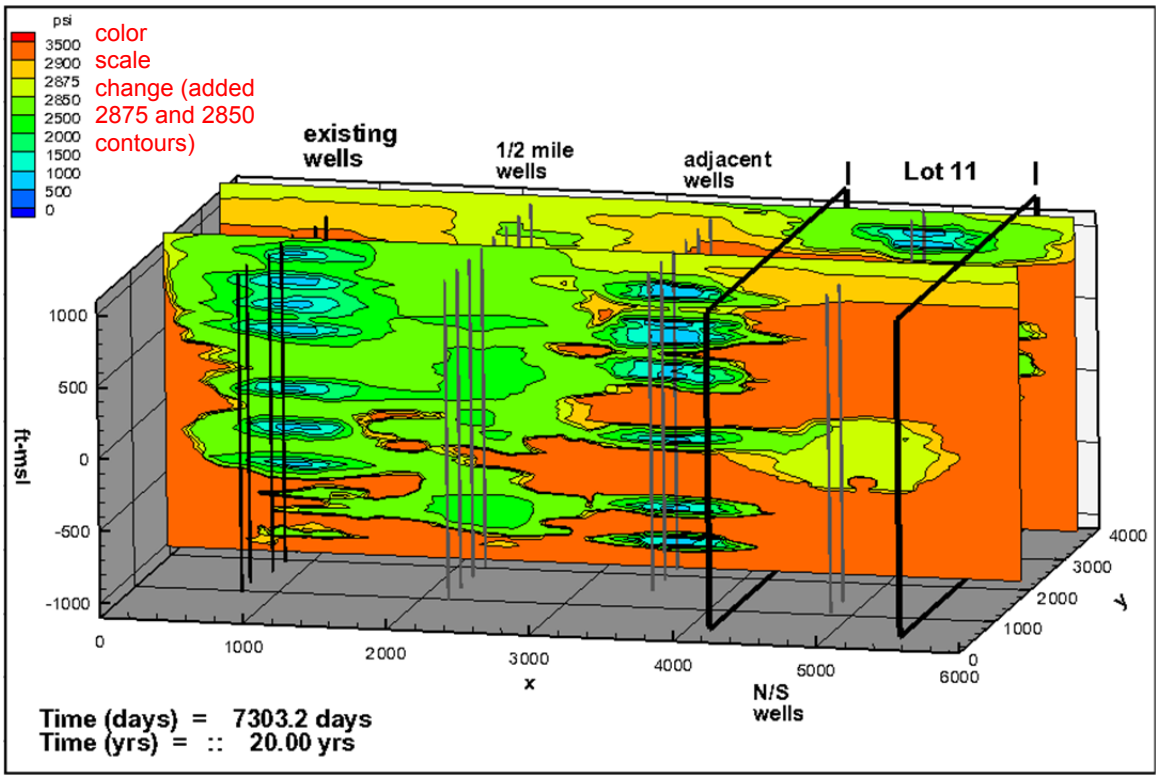

Figure 38P. Pressure Distribution in 2030

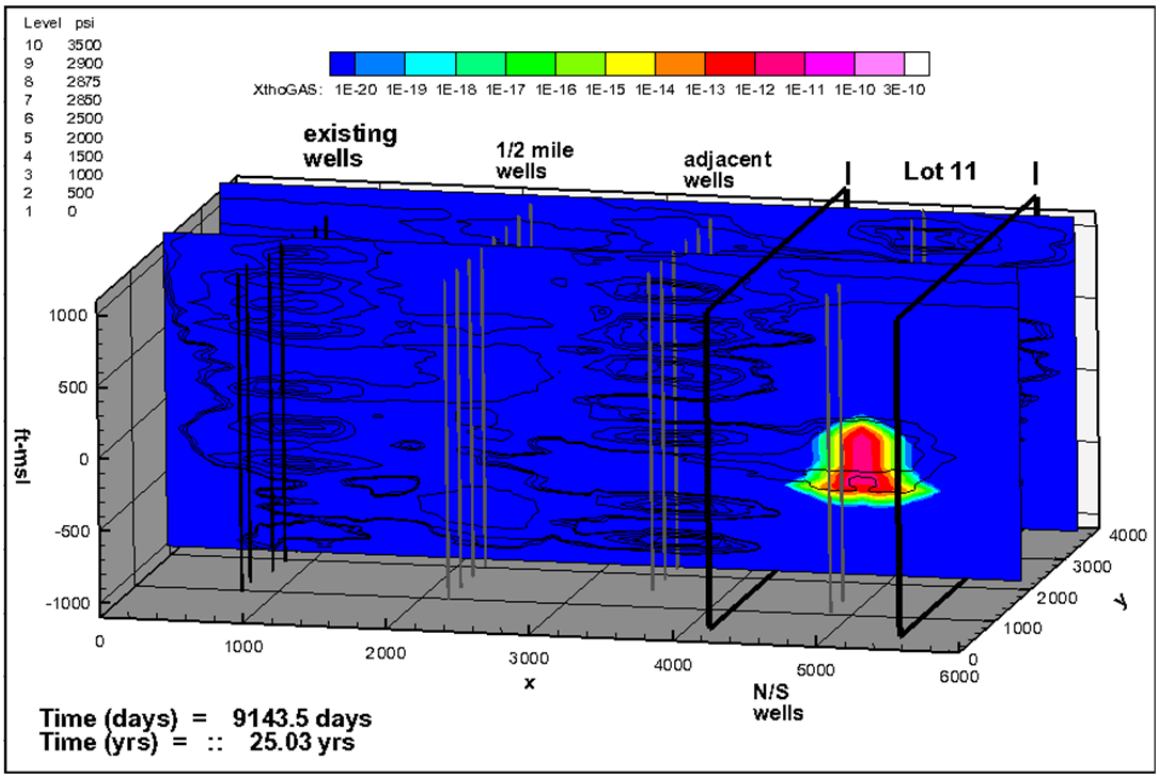

Figure 39X. Mass Fraction of THO in 2035 (y38, y69)

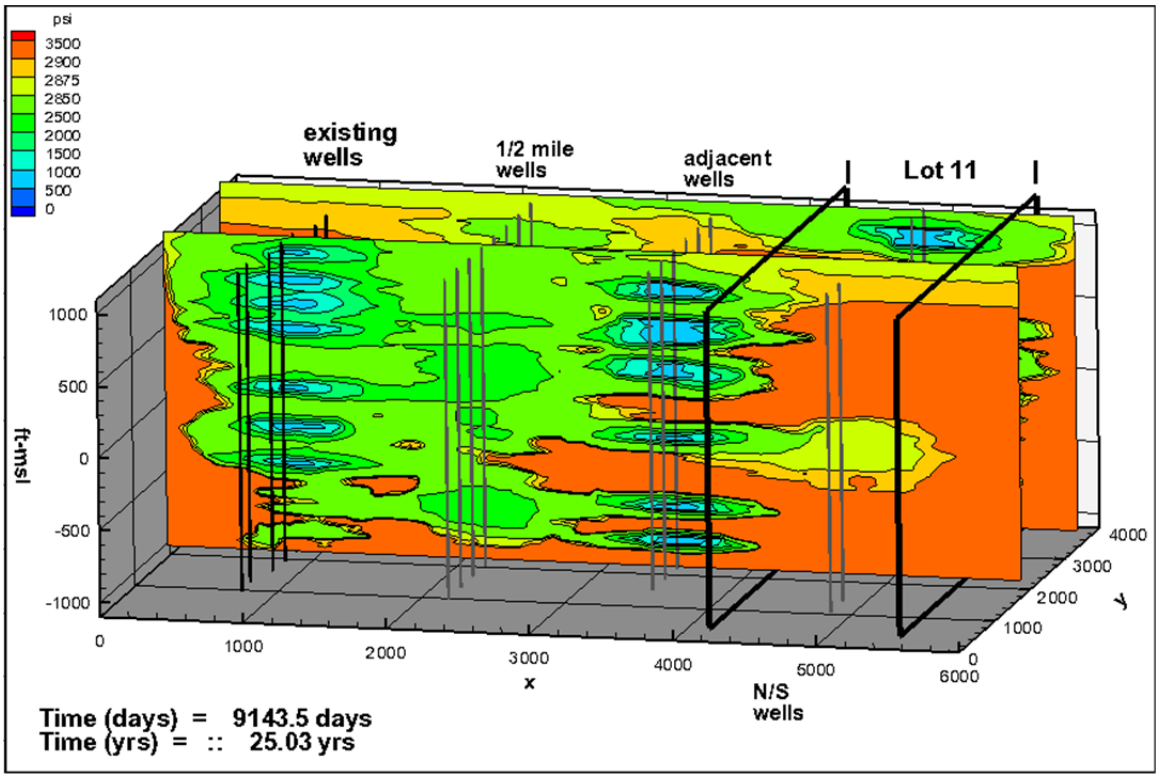

Figure 39P. Pressure Distribution in 2035

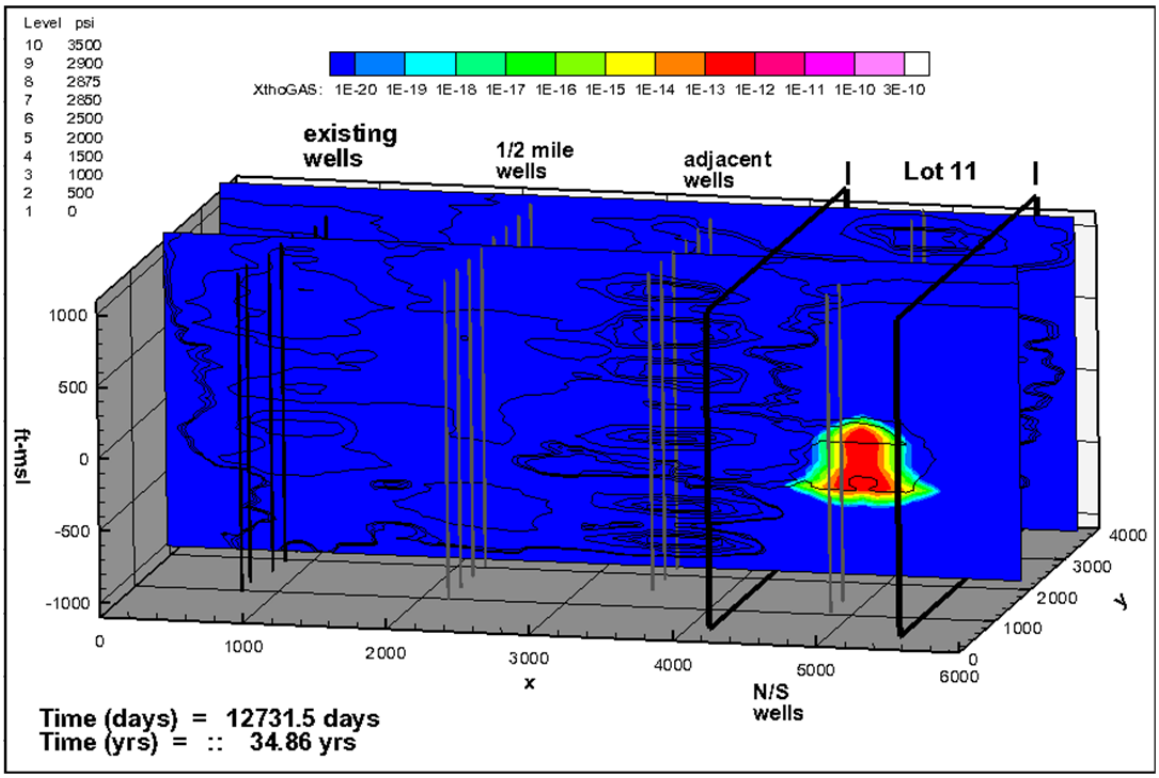

Figure 40X. Mass Fraction of THO in 2045 (y38, y69)

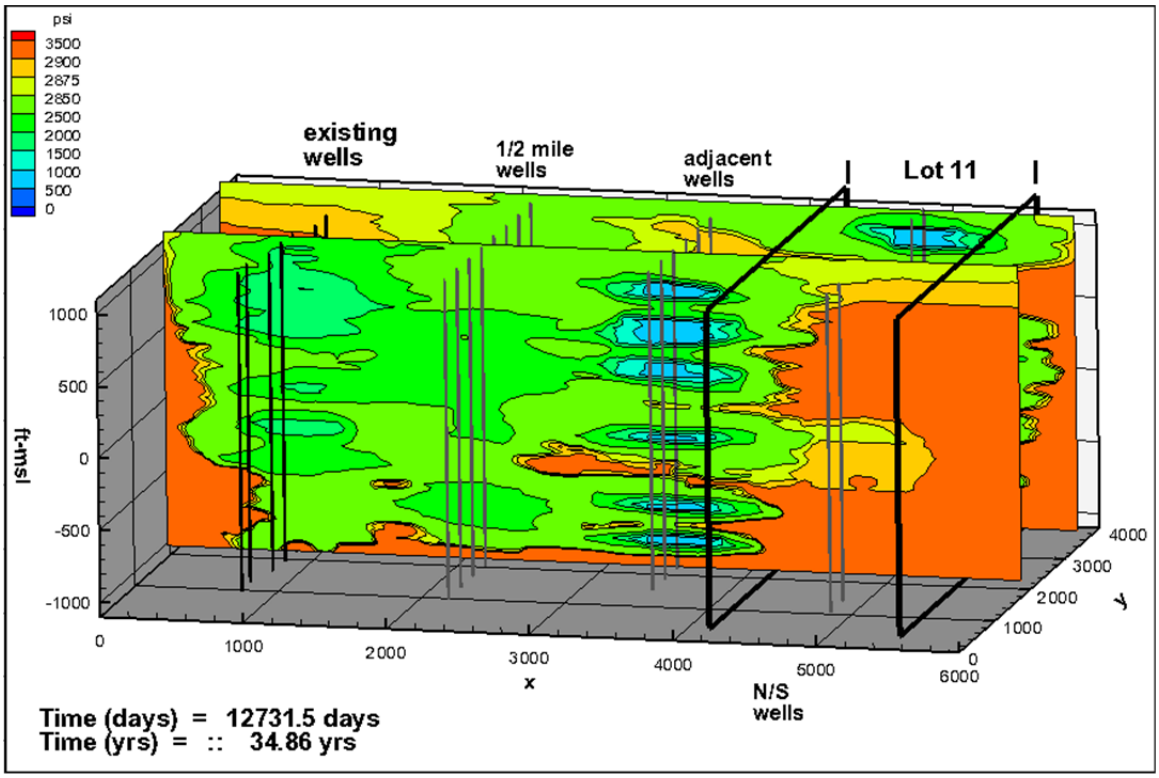

Figure 40P. Pressure Distribution in 2045

Figure 38 shows the simulated conditions in 2030, 20 years into production of the existing wells, 15 years into production of the one-half-mile wells, 10 years into production of the N/S wells, and 5 years into production of the adjacent wells. Two slices are shown (y38 and y69) to see the effects of multiple wells on the pressure distribution (the one-half-mile wells are out of the plane). The concentration distribution is little changed since 2025 and is not being affected by the nearby well production. However, an obvious connection exists between the pressure drawdown at the well immediately west of the site and the remnant lower pressure region of the detonation zone (Figure 38P). Two additional contours (2,850 and 2,875 psi) were added to these and subsequent plots to highlight this effect. The additional contours cause the green colors to be much expanded from previous plots (a visual effect only). The green now represents about 2,800 psi (2,500 psi previously), which is not much different from the unaffected formation pressures of 2,900–3,000 psi. These small differences are well within the natural range of pressures seen among the different sandstone reservoirs of the formation and would likely not be detectable. The small pressure gradient is not sufficient to affect transport in the simulation given the retarding effects of the partitioning of tritiated water from the gas phase to the aqueous phase. However, if the local equilibrium assumption is violated in the unlikely event that gas were to migrate through a preferential pathway where a significant portion of the gas does not come into contact with water, the pressure connection between a producing well and the detonation zone could potentially allow transport of a small amount of tritiated water vapor to this well.

Figure 39 shows the simulated conditions in 2035, 25 years into production of the existing wells (production ends at this time), 20 years into production of the one-half-mile wells (out of the plane), 15 years into production of the N/S wells, and 10 years into production of the adjacent wells. The concentration distribution is little changed since 2030 and is not being affected by the nearby well production. The connection between the pressure drawdown at the well immediately west of the site and the remnant lower pressure region of the detonation zone (Figure 39P) persists, though pressures in the lower part of the detonation zone continue to recover.

Figure 40 shows the simulated conditions in 2045 (end of the simulation), 10 years after production from the existing wells ended, 30 years into production of the one-half-mile wells, 25 years into production of the N/S wells, and 20 years into production of the adjacent wells. The concentration distribution is little changed since 2035, though the highest concentration color contour has decreased an order of magnitude since the beginning of the simulation. The concentration distribution still is not affected by the nearby well production. The connection between the pressure drawdown at the well immediately west of the site and the remnant lower pressure region of the detonation zone (Figure 39P) has increased, though pressures in the lower part of the detonation zone continued to recover. The recovery of pressures at the existing wells, off production for 10 years in the simulation, can be seen by comparing Figure 40P with Figure 39P. The one-half-mile wells (producing for 30 years at this time) show lower pressures than the existing wells that have been off production for 10 years because they are out of the plane, and there is limited north-south communication between the wells.

Figure 41 shows the simulated conditions in 2045 with pressures below 2,250 psi blanked. Pressures above 2,250 psi are greater than the lowest pressure measured by drill stem testing of the productive interval in the exploratory well prior to the detonation. This shows limited communication between the one-half-mile wells (the section cuts between wells) and limited communication between perforated intervals in the adjacent wells. The vertical communication between the upper perforation interval of existing well 26-33B (at the top of the lower two-thirds

of the Williams Fork Formation immediately below the upper one-third of the Williams Fork) suggests the model properties of the upper one-third of the Williams Fork could be adjusted.

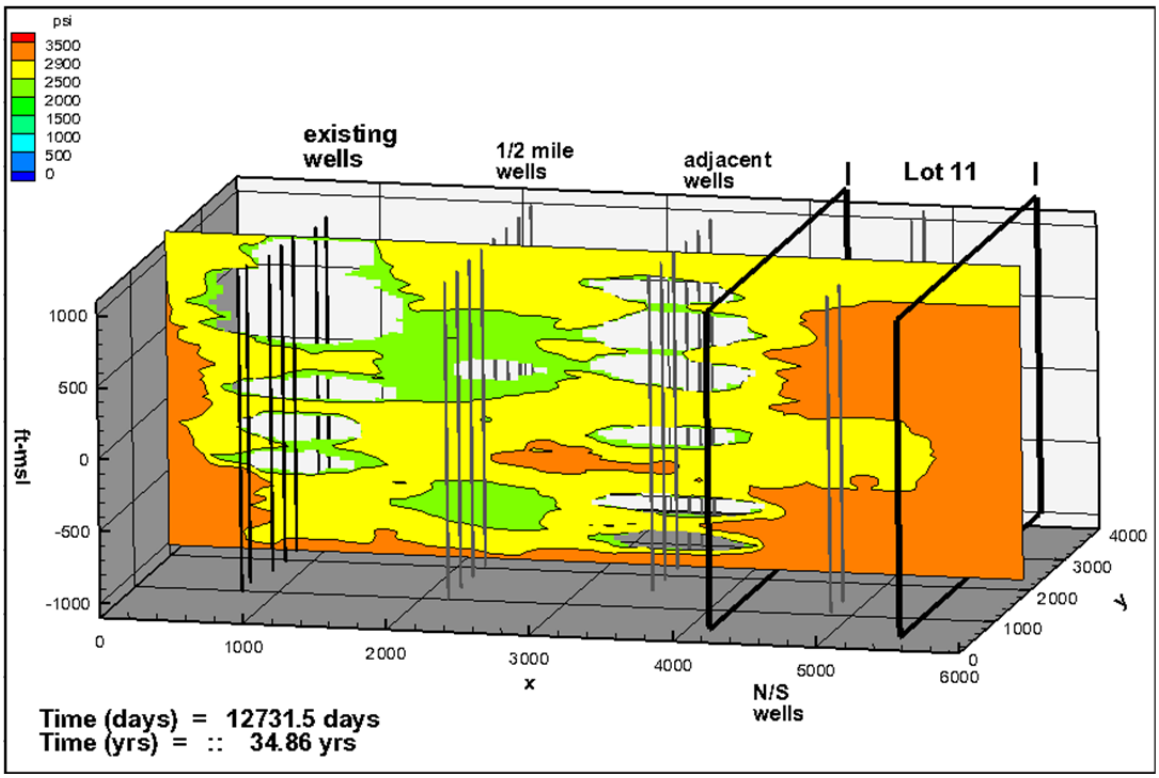

Figure 41. Pressure Distribution in 2045 with Pressures Below 2,250 psi Blanked

A plot of the temperature distribution (Figure 42) at the end of the simulation (2045) shows that the temperature within the detonation zone did not materially change during the gas well simulation. This was caused by the constant temperature source of the melt glass. The plot also shows the decrease in temperature at production wells in response to the lower pressures during production.

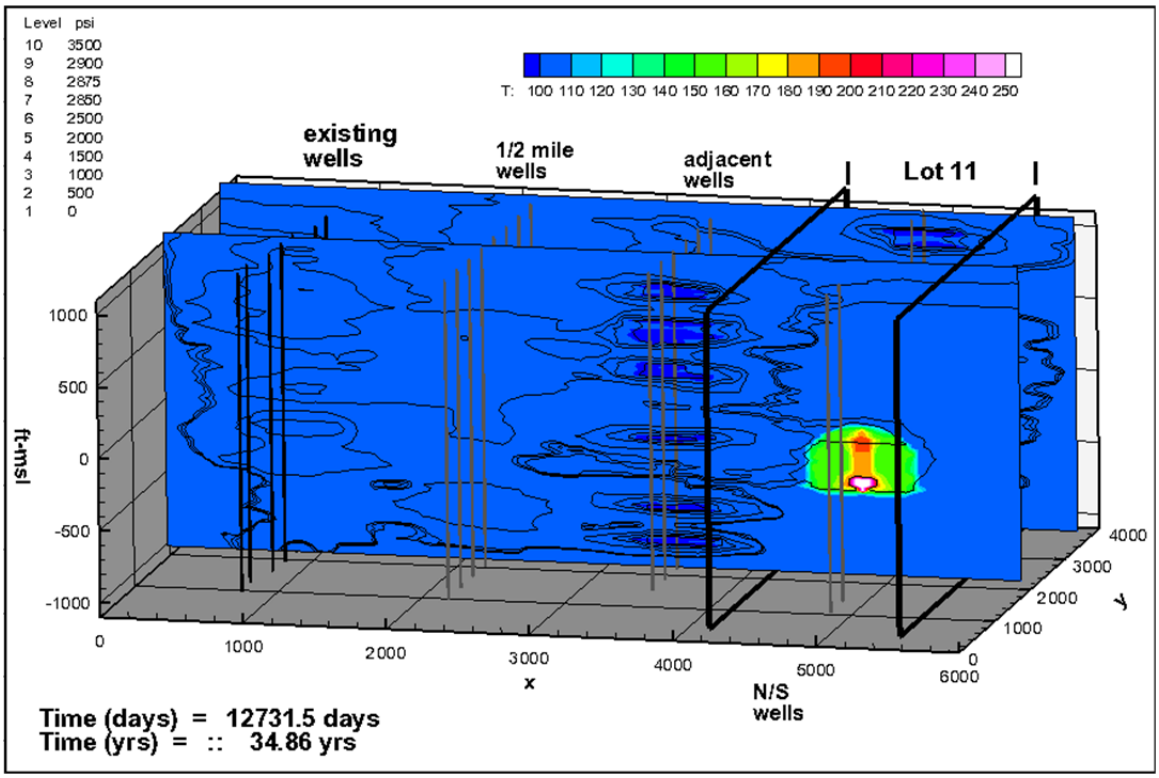

Figure 42. Temperature Distribution at the end of the Simulation Time (2045)

6.0 Summary and Conclusions

The primary objective of this study was to enlarge the model domain so that drilling activity, both present and future (Rulison Path Forward), could be simulated and the potential effects on the Rulison site could be evaluated. The model simulated the production from existing wells (installed in 2010) and theoretical future wells installed in a staged approach. The model was calibrated to both the historical production and pressure data from the reentry well and to the production data from the recently installed gas wells. Attempts were made to be more conservative than previous models by elongating the detonation zone (both the chimney and surrounding nuclear fractured region) in the direction of the natural fracture trend in the area.

This study confirmed the results of the previous Rulison modeling in that it predicts that contamination, in the form of tritiated water, is contained within the institutional control boundary of Lot 11. This is based on a conceptual model that assumes the fractured formation can be simulated using an equivalent porous media approach. The frequency, connectivity, and limited permeability extent of individual fractures perform as a pore matrix within a representative elementary volume the size of the individual model elements.

The finding that THO did not migrate from the detonation zone was fully expected considering the retarding effects of THO vapor coming into contact with liquid water. However, the possibility that production from nearby gas wells will reduce pressure in the formation enough to make a connection with the detonation zone was confirmed, at least for a few perforated intervals in a simulated well in the most vulnerable location adjacent to the detonation zone. The induced

pressure gradient was less than observed natural pressure variations in different sandstones in the same well and was not sufficient to induce contaminant migration or alter the shape of the contaminant distribution within the detonation zone. However, the pressure connection between a simulated gas production and the detonation zone should not be completely discounted.

The figures in this text and animations on the accompanying DVD provide simulation results that simplify the concept of the Rulison Path Forward and gas production in the Piceance Basin in general.

7.0 References

Many of the documents are available on the LM website:
http://www.lm.doe.gov/Rulison/Documents.aspx

AEC (U.S. Atomic Energy Commission), 1973. *Project Rulison: Managers Report*, NVO-71, PNE-R-63, Nevada Operations Office, Las Vegas, Nevada.

Austral Oil Company, 1977. *Project Rulison Well Plugging and Site Abandonment Final Report*, NVO-187, Nevada Operations Office, Las Vegas, Nevada.

Bowen, S.M., D.L. Finnegan, J.L. Thompson, C.M. Miller, P.L. Baca, L.F. Olivas, C.G. Geoffrion, D.K. Smith, W.Goishi, B.K. Esser, J.W. Meadows, N. Namboodiri, and J.F. Wild, 2001. *Nevada Test Site Radionuclide Inventory, 1951–1992*, LA-13859-MS, Los Alamos National Laboratory, Los Alamos, New Mexico, September.

Byrnes, A.P., and R.M. Cluff, 2009. *Analysis of Critical Permeability, Capillary Pressure and Electrical Properties for Mesaverde Tight Gas Sandstones from Western U.S. Basins*, U.S. DOE Contract Number: DE-PS26-04NT42072.

CER Geonuclear, 1975. *Project Rio Blanco Radioactivity and the Environment: RB-AR-2 Addendum*, PNE-RB-63 Addendum, October 1975.

Cooper, C.A., M. Ye, and J. Chapman, 2007. *Tritium Transport at the Rulison Site, a Nuclear-Stimulated Low-Permeability Natural Gas Reservoir*, Desert Research Institute Report No. 45224.

Cooper, C.A., M. Ye, J. Chapman, and R. Hodges, 2009. *Addendum: Tritium Transport at the Rulison Site, a Nuclear-stimulated Low-permeability Natural Gas Reservoir*, Desert Research Institute.

Cooper, C.A., J. Chapman, and R. Hodges, 2010. *Update of Tritium Transport Calculations for the Rulison Site: Report of Activities and Results During 2009 - 2010*, Desert Research Institute Letter Report, 28 pp.

Corey, A.T., 1954. *The Interrelation Between Gas and Oil Relative Permeabilities*, NNA.19900720.0036, Producers Monthly, 38–41, November.

DeGolyer and MacNaughton Co., 1971. Report on Interpretation of Test Data for Project Rulison in the Rulison Field, Garfield County, Colorado. Prepared for Austral Oil Company, Inc.

DOE (U.S. Department of Energy), 2000. *United States Nuclear Tests July 1945 through September 1992*, NV-209 Rev. 15, Nevada Operations Office, Las Vegas, Nevada.

DOE (U.S. Department of Energy), 2010. *Final Rulison Path Forward*, LMS/RUL/SO4617, Office of Legacy Management, Grand Junction, Colorado, June.

Frank, G.W., 1971. The nuclear stimulation of a natural gas reservoir – Project Rulison. World Petroleum Congress, 8(3), 355-363.

Frink, R.O. and J.A. Wethington, Jr., 1971. Tritium Exchange Between Hydrocarbons and Steam, Transactions of the American Nuclear Society, 12(2): 467-468, October.

Green, G.N., 1996. *The Digital Geologic Map of Colorado in ARC/INFO Format,* USGS Open File Report 92-0507, U.S. Geological Survey.

Lucas, L.L., and M.P. Unterweger, 2000. "Comprehensive Review and Critical Evaluation of the Half-Life of Tritium," *Journal of Research of the National Institute of Standards and Technology*, 105(4), July-August.

Montan, D.N., 1971. Project Rulison Gas Flow Analysis, Nuclear Explosives Technology.

Mualem, Y., 1976. "A New Model for Predicting the Hydraulic Conductivity of Unsaturated Porous Media", *Water Resour. Res.*, 12(3): 513–522.

Narasimhan, T.N., P.A. Witherspoon, and A.L. Edwards, 1978. "Numerical Model for Saturated-Unsaturated Flow in Deformable Porous media, Part 2: The Algorithm," *Water Resour. Res.*, 14(2): 255–261.

Nork, W.E., and P.R. Fenske, 1970. *Radioactivity in Water—Project Rulison*, NVO-1229-131.

Pruess, K., C. Oldenburg, and G. Moridis, 1999. *TOUGH2 User's Guide, Version 2.0*, LBNL-43134.

Reynolds, M., 1971. *Project Rulison—Summary of Results and Analyses*, presented at the American Nuclear Society winter meeting, Miami, Florida.

Smiles, D.E., W.R. Gardner, and R.K. Shulz, 1995. "Diffusion of Tritium in Arid Disposal Sites," *Water Resour. Res.*, 31(6): 1483–1488.

Smith, C.F., 1971. *Gas Analysis Results for Project Rulison Production Testing Samples*, UCRL-ID-51153, Lawrence Livermore National Laboratory, Livermore, California.

Sokol, D., 1970. *Ground Water Safety Evaluation—Project Gasbuggy*, PNE-1009, prepared by Teledyne Isotopes, Palo Alto, California, for the U.S. Atomic Energy Commission, Nevada Operations Office, Las Vegas, Nevada, September.

Toman, J., 1974. *Project Rio Blanco: Project Scientist's Summary Report of Production Test Data and Preliminary Analysis of Top Chimney/Cavity*, UCRL-76280, Lawrence Livermore Laboratory, Livermore, California.

Van Genuchten, M.Th., 1980. "A Closed-Form Equation for Predicting the Hydraulic Conductivity of Unsaturated Soils," NNA.19911009.0008, *Soil Sci. Soc.*, 44: 892–898.

Yurewicz, D.A., K.M. Bohacs, J.D. Yeakel, and K. Kronmueller, 2003. "Source Rock Analysis and Hydrocarbon Generation, Mesaverde Group and Mancos Shale, Northern Piceance Basin, Colorado," in Peterson, K.M., T.M. Olson, and D.S. Anderson, eds., *Piceance Basin 2003 Guidebook: Rocky Mountain Association of Geologists*, pp 130–153.

Zhang, K., Y.S. Wu, and K. Pruess, 2008. *User's Guide for TOUGH2-MP—A Massively Parallel Version of the TOUGH2 Code*, LBNL-315E.

This page intentionally left blank

Appendix A

Summary of Reports on Projects Rio Blanco and Rulison from 2001 Through 2010

This page intentionally left blank

Introduction

The U.S. Department of Energy (DOE) and its predecessor agencies conducted a program in the 1960s and 1970s that evaluated technology for the nuclear stimulation of low-permeability natural gas reservoirs. The objective of the program was to produce natural gas from formations not conducive to production by conventional means such as hydraulic fracturing. As a result, all of the tests were conducted in low-permeability formations contained within natural gas reservoirs. These conditions precluded contact of the test radionuclides with mobile, potable water, and hence the risk of human exposure was considered very low to non-existent. At the conclusion of each project, surface facilities were removed, wells were plugged and abandoned, and drilling restrictions were instituted for the subsurface region immediately around the nuclear cavities.

In the 1990s, DOE began a thorough environmental restoration program to remediate and close facilities that supported nuclear testing. The three gas-stimulation test sites (Projects Rio Blanco, Rulison, and Gasbuggy) are included in the program now under the direction of the Office of Legacy Management. Although the land surfaces at the sites had previously been cleaned and closed, additional testing and analysis is being conducted to assure that the closures meet current environmental standards. Similarly, the disposition of the subsurface regions impacted by the tests is being re-evaluated. Of particular concern for the subsurface is an assessment of the drilling intrusion restrictions in place to determine if they are sufficiently protective of human health and the environment. This concern arises from a lack of documentation on the rationale used to establish the restricted regions. Standard oil and gas reservoir evaluations are poorly suited to analyze the problem as they focus on flow of fluids in the subsurface, whereas the question here is one of transport of radionuclides. Significant advances in understanding contaminant transport in the subsurface have been made in the decades since the drilling restrictions were initially established.

Projects Rulison and Rio Blanco are located in west-central Colorado. At Rulison, a 40-kiloton nuclear device was detonated 2,568 m below the land surface in the Williams Fork Formation on September 10, 1969. At Rio Blanco, three 33-kiloton nuclear explosives were simultaneously detonated in a single emplacement well in the Mesaverde Group and Fort Union Formation, at depths of 1,780, 1,899, and 2,039 m below land surface on May 17, 1973. The objective of these previous modeling efforts was to estimate lateral distances that tritium released from the detonations may have traveled in the subsurface and evaluate the possible effect of postulated natural-gas development on radionuclide migration. Of the radionuclides present in the gas phase, tritium dominates in terms of quantity of radioactivity in the long term and contribution to possible whole body exposure. Other radionuclides were considered in the analysis, but the majority occur in relatively immobile forms (such as nuclear melt glass).

The models only replicated subsurface processes and did not account for additional factors such as mixing and dilution in a nearby hypothetical gas production well, nor did they account for exposure scenarios (e.g., transmission and dilution in a pipeline, inhalation routes from gas use) required to assess either exposure limits or doses.

2001 Preliminary Report Pertaining to Rio Blanco, DRI Pub. 45186; also DOE/NV/13609-15

The first report in the series is an outline of an approach toward the development of models for both the Rio Blanco and Rulison sites, followed by a very preliminary set of simulations of gas, water, and tritium transport following the three simultaneous 33-kiloton nuclear detonations in 1973 at the Rio Blanco site. A preliminary conceptual flow and transport model was developed that recognized that the gas 'reservoir' is actually in rock of very low matrix permeability and that the dominant permeable pathway for fluids is through a network of fractures created by regional tectonism. The gas-in-place is basin-centered, meaning that much of it is located downdip from water-saturated regions in the formation(s), there are few obvious gas-water contacts, and there are no obvious trapping mechanisms, as gas is present mostly in lenticular reservoirs from tens to hundreds of meters in length.

The intrinsic permeability of the formation was estimated prior to the test as being between 8×10^{-18} to 10^{-15} m^2. This is an average value that considers flow through both the sandstone and shale, and flow through both fractures and matrix (although fractures probably dominated flow). The degree of heterogeneity was largely unknown, except that the formation contains both sand and shale lenses (i.e., the actual values of permeability of the individual units was not known). Post-test drilling indicated that there was no connectivity among the three cavities. The initial tritium radioactivity release from the three simultaneous detonations was estimated as 3,000 Ci (curies), with 40 percent of the radioactivity trapped in the melt. Details of the rock matrix and fractures were largely unknown, and thus ignored in the model, and instead gas and liquid water were assumed to flow through a fracture network that was modeled as an equivalent porous medium.

Two-dimensional flow and transport was modeled through a single formation, the Upper Cretaceous Mesaverde Group, with an intrinsic permeability of 3×10^{-17} m^2 and a porosity of 0.105. Although the upper device was detonated in the Ohio Creek Member of the Upper Cretaceous Fort Union Formation, the member status of the lower two devices was unknown. Results of the simulations are not discussed here as they were entirely superseded by the results presented in the 2005 Rio Blanco report.

2004 Letter Report Documenting Rulison Results

A letter report was prepared in 2004 describing a small study to investigate the gross behavior of tritium transport away from a chimney created by the Rulison nuclear detonation. This report set the tone for the 2007 report. A conceptual model was developed, in which the detonation occurred in the Williams Fork Formation, the chimney was modeled with the same properties as the nuclear-stimulated fractures (chimney properties were unknown), and a hydraulic fracture zone was included outward from the production well, which was located 457 m (1,500 ft) from the emplacement hole. The results showed that for a period of 35 years following the detonation, molecular diffusion controlled tritium transport (a natural horizontal or vertical gas-phase gradient, if present, was unknown) traveled about 125 m from the detonation (or working) point, but never extended beyond the drilling exclusion zone. A period of gas production from the hypothetical well resulted in minimal tritium migration, which also did not reach the exclusion boundary. The results are considered obsolete, as the intrinsic permeability of the nuclear-stimulated zone of fractures (modeled as an equivalent porous medium) was overestimated by two orders of magnitude and the permeability of the hydraulic (production) fractures was overestimated by a factor of two (as compared with the 2007 report). Most importantly, the 2007 report presented the results of Monte Carlo simulations through 500 separate random permeability and porosity fields.

2005 Report on Rio Blanco, DRI Pub. No. 45215; also DOE/NV/13609-45

The geologic model was improved over the 2001 letter report such that it included the Mesaverde Group and overlying Fort Union Formation. The upper device was detonated in the lower part of the Fort Union Formation, while the middle and lower devices were detonated in the Mesaverde Group (now Formation). Both formations are low-permeability shale (permeability ~10^{-17} m^2), with lenses of slightly higher permeability sandstone spread throughout. The length of some of these lenses is as great as 1,000 m. The formations are hydrostatically pressured; horizontally, the pressure gradient(s) were not well known, as production tests were not run to completion due to the length of time required to reach quasi-steady state.

The geologic model was incorporated into a conceptual flow and transport model that included transport of radionuclides (tritiated water and krypton gas) in a two-phase (gas and liquid) system. The conceptual flow and transport model was developed into a numerical model. Radionuclides released from the cavity were transported in both liquid and gas phases, and were allowed to partition between phases in accordance with Henry's law. Two types of simulations were conducted: one that investigated flow away from the three nuclear cavities in a regional pressure field, and the other that investigated flow from only the middle cavity/chimney toward a producing gas well. The permeability and porosity, however, were that of the Fort Union Formation (the formation in which the upper detonation occurred) as its permeability is higher, and this would be a more 'conservative' simulation (i.e., transport would be exaggerated). The reason that flow was only investigated from the middle chimney is that symmetry could be assumed in the model as fluid flow and tritium transport would be identical in the other two chimneys, which allowed the upper and lower horizontal boundaries between the detonations to be streamlines dividing flow between the upper and middle detonations, and middle and lower detonations, respectively. In addition, a few simulations were conducted that included discrete

fractures in the vicinity of the cavities. Results showed fractures to be important when flow-controlling fractures were spaced greater than 20 m apart. For a greater fracture density, flow through fractures and flow through matrix gas resulted in nearly identical concentrations, indicating that inclusion of discrete fractures in this model may be unnecessary. The reason is that matrix diffusion of tritium in the gas phase acts to make the concentration field more uniform between fractures and matrix. There is an extensive discussion of these simulations in the report.

Two types of models were developed: Type 1, in which methane gas and liquid water with a single radionuclide mixed in both phases migrated within the natural gas reservoir in response to chemical gradients (i.e., liquid and gas diffusion), slight regional pressure gradients, and radionuclide decay. In these simulations, transport was modeled away from all three cavity/chimneys. A second type of model was run (Type 2) in which flow and transport was through a narrow interval, 120 m high (discussed in previous paragraph), away from a single cavity/chimney toward a producing gas well located outside the current drilling exclusion boundary. Drilling is currently prohibited within 183 m (600 ft) of the emplacement well. The well was located 291 m away from the center of the cavity/chimney, such that hydraulic fractures from the production well were assumed to reach the exclusion boundary. The Type 2 simulations were also used to conduct uncertainty analysis using the Monte Carlo method to address parametric uncertainty of porosity and intrinsic permeability.

The Type 1 simulations show that for various combinations of intrinsic permeability and slight regional pressure gradient, the leading edge of the tritium mass fraction (i.e., concentration) field never extends beyond 100 m from the center of the three cavity/chimneys (Figure 1). These results, however, did not address the impact of a hypothetical nearby gas-producing well. To address this scenario, three-dimensional Type 2 simulations were required.

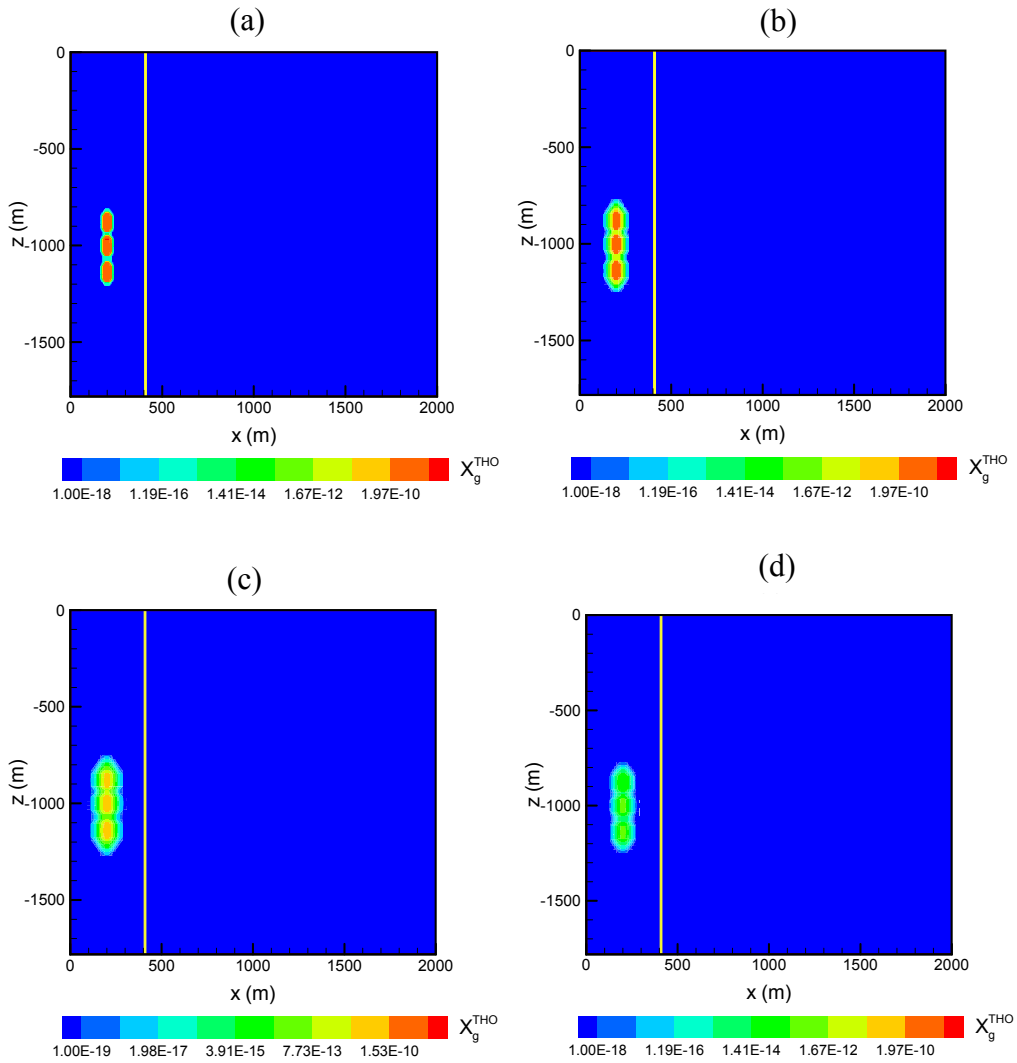

Figure 1. Results of a two-dimensional simulation showing mass fraction of tritiated water vapor, X_g^{THO} from the three detonations. The times are (a) 1 month, (b) 20 yr, (c) 100 yr, and (d) 250 yr. The vertical line located at x = 404 m shows the location of the drilling exclusion boundary with respect to the location of the detonations.

The three-dimensional Type 2 simulations modeled flow and transport away from a single cavity/chimney toward a production well (Figure 2). The reservoir properties were those of the Fort Union Formation, as intrinsic permeability is about an order of magnitude greater than for the Mesaverde Group. Several simulations were conducted that investigated sensitivity of permeability, production rate, initial and residual liquid saturation, and tortuosity. For example, a one order-of-magnitude increase in intrinsic permeability had little effect on the transport of tritium, as the Péclet number for gas transport (a ratio between diffusive and advective flow) was much less than one (the highest gas velocities were never greater than 10^{-8} m s^{-1}). The value of initial and residual liquid (and hence gas) saturation had an effect of diffusing tritium in the gas phase, but the distances varied only by several tens of meters or so. High gas saturation resulted in more spreading and mixing of tritium in the gas phase, and it allowed the center of the tritium 'plume' to diffuse more rapidly than for cases where initial gas saturation was low. The choice of tortuosity model had the greatest effect on transport; a relative permeability based model resulted

in radionuclide transport distances approximately 100 m greater than for a saturation-dependent (Millington-Quirk) model. As little research has been conducted on tortuosity in two-phase systems in the past 45 years, a lack of understanding of tortuosity may be the greatest limitation in the models.

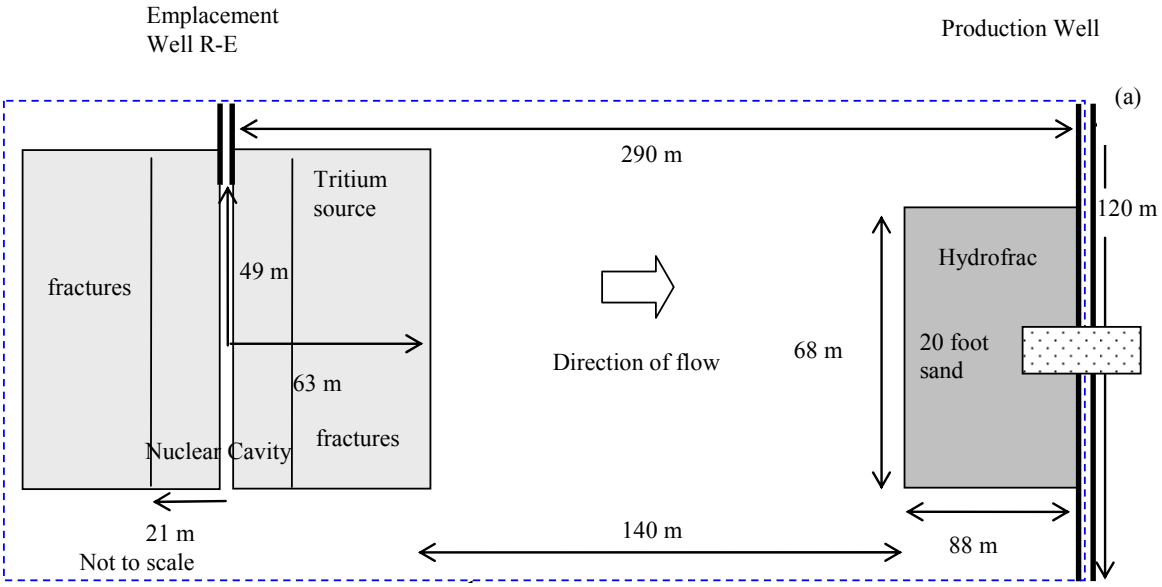

Figure 2. Model formulation for gas flow and tritium transport to a production well

Based on the Type 2 simulations with gas production, uncertainty of tritium transport in the gas reservoir was assessed using the Monte Carlo method. Permeability and porosity of the Fort Union Formation were considered as random parameters due to their heterogeneity in the site. Distributions of and the correlation between the two variables were identified based on their onsite core measurements from two boreholes, assuming that the measurements were representative. Five hundred realizations of correlated random fields of the two parameters were generated and used to construct the TOUGH2 input files. Except for these two random parameters, other model parameters remained the same as those of the Type 1 simulations with reference parameters. The stabilization of the statistics of quantities of interest obtained from the 500 realizations was examined empirically and the results suggested that 500 realizations were sufficient to yield meaningful statistics used to quantify tritium transport uncertainty. The 50th percentile represented the prediction of tritium transport in an average sense, while the 5th and 95th percentiles quantify associated predictive uncertainty caused by the uncertain values of permeability and porosity due to their heterogeneity at the site. The 5th and 95th percentiles were considered superior to the mean and variance of the mass fractions for uncertainty assessment in this project, since there is no evidence that the simulated mass fractions followed normal distributions. Whereas the 50th percentile tritium plume did not approach the production well during the entire simulation period, the 95th percentile tritium plume approached, but did not reach, the production well during and after the production period (Figure 3). The breakthrough curves of the 95th percentile of tritium mass fraction at the production well indicated that the tritium concentration could be several orders of magnitude higher than the mass fraction of deterministic Type 2 simulations, suggesting that the uncertainty was not negligible. Nonetheless, the peak mass fraction at the production well was close to the environmental background value. Additional uncertainties remain that could not be quantified by the Monte

Carlo analysis either due to lack of data (e.g., the lateral gradient) or because they are a conceptual component (e.g., location of production well, presence of multiple wells).

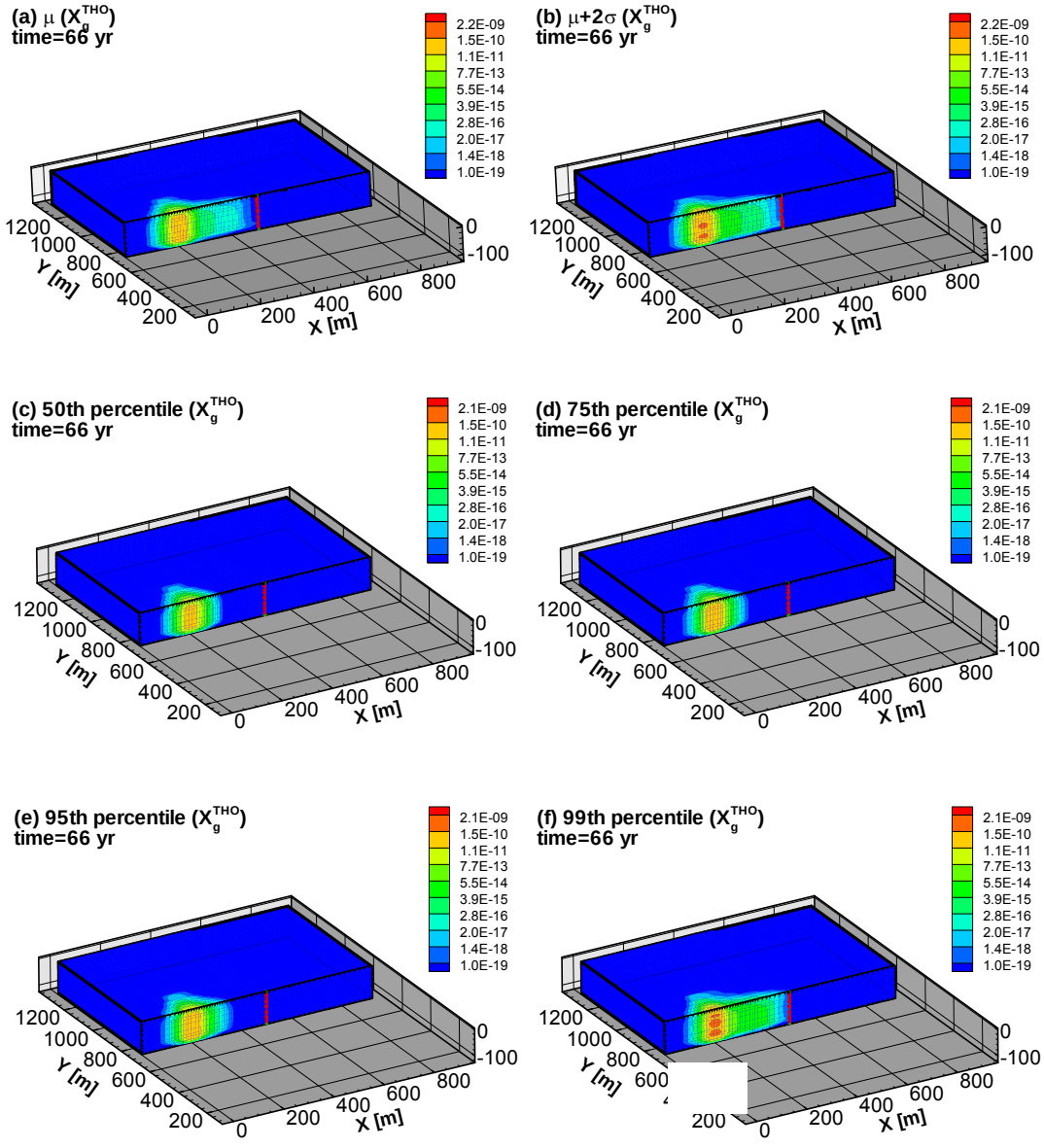

Figure 3. (a) Mean (μ), (b) upper bound of the 95 percent confidence interval (μ+2σ), (c) 50th percentile, (d) 75th percentile, (e) 95th percentile, and (f) 99th percentile of mass fraction of tritium in gas phase at 66 years after the detonation (one year after the end of gas production).

2007 Report on Rulison, DRI Pub. No. 45224; also DOE/NV/13609-54 and Ye et al., 2009, Reservoir Evaluation & Engineering, 12(6), pp. 974–984; doi 10.2118/114920-PA.

The objectives of this work were to calculate the nature and extent of tritium contamination in the subsurface from the Rulison test from the time of the test through the year 2007, and to evaluate tritium migration under natural-gas production conditions to a hypothetical gas production well in the most vulnerable location outside the DOE drilling restriction. The natural-gas production scenario involves a hypothetical production well located 258 m horizontally away from the detonation point, outside the edge of the current drilling exclusion area. The production interval in the hypothetical well is at the same elevation as the nuclear chimney created by the detonation, in order to evaluate the location most vulnerable to tritium migration. The basic idea is similar to that of the Rio Blanco model, but the manner in which the model was implemented was more complex than that of the Rio Blanco model. The most important difference is that permeability and porosity were treated as spatially variable, such that the permeability fields were completely heterogeneous, in contrast to the Rio Blanco work in which permeability and porosity were uniform throughout each computer simulation. Other differences between these simulations and those of the Rio Blanco site are that the range of permeability and porosity was different, as was the distance from the detonation point to the hypothetical producing natural gas well.

A three-dimensional geologic model was developed of the local Williams Fork Formation at the Rulison site that includes a sequence of sandstone and shale lenses conditioned on observations at two site wells. The dominant flow and transport direction is east-west, in agreement with the direction of regional fractures in the area. The average sandstone lens length is approximately 161 m and mean thickness is 7.5 m. The sandstone lenses are characterized by very low intrinsic permeability in core measurements (on the order of 10^{-18} m^2), while reservoir tests indicated higher permeabilities (up to 10^{-16} m^2) presumably as a result of fractures encountered at the field scale. Porosity of Williams Fork sandstone units was to be between 0.01 and 0.1. Shale units are considered barriers to flow, with intrinsic permeability of 10^{-20} m^2.

A conceptual flow and transport model for the area around the emplacement well was developed to investigate the rates of tritium transport in the subsurface away from the chimney. As was the case for Rio Blanco, tritium is transported as the tritiated water molecule ^3HHO in both the gas and aqueous phases from the nuclear chimney (located in Lot 11) radially outward under a chemical concentration gradient for 38 years (the time from the nuclear test until 2007). At this time the hypothetical gas production well was placed in the model 258 m directly to the west, in Lot 12, and gas production was simulated for 30 years. During this time, transport was enhanced by the pressure gradient created by the production well.

The geologic and conceptual models were implemented in the numerical simulator TOUGH2, and an equivalent porous medium approximation was used to model the fractured environment. Permeability and porosity distributions were developed based upon a statistical analysis of core data. Distributions were also developed for fracture permeability and hydraulic fracture (fractures surrounding the hypothetical gas production well that are induced to enhance flow around the well bore) length based on a multiple of the core permeability data, and literature values, respectively. Five hundred realizations were solved in TOUGH2, each representing one equally likely combination of sandstone-shale geometry and parameter values. Each model

realization was simulated to determine the most likely length and time scales of tritium transport away from the chimney.

The simulator allows for partitioning between phases as well as radioactive decay. Results show that for the first 38 years following detonation of the nuclear device, tritium transport is controlled by gas diffusion and radioactive decay. The shape of the tritium plume is not dependent on the permeability field, as diffusion is controlled by tortuosity, which is in turn controlled by gas saturation and porosity. Based on the 50th percentile of the 500 Monte Carlo simulations, the maximum travel distance of tritium was approximately 80 m from the nuclear detonation point during the 38-year period of diffusion. This is essentially the distance fractured by the nuclear detonation.

Production from the hypothetical gas well begins 38 years after the nuclear detonation (in the year 2007). Results of the Monte Carlo simulations suggest that tritiated water vapor above background concentrations will not reach the production well at the 95th percentile (Figure 4). The peak mass fraction of tritium (mass of tritiated water in the gas phase to mass of the gas phase per unit volume) in the gas phase at the 95th percentile is 1.01×10^{-21} g^{THO} g_{gas}^{-1}, as compared to the background mass fraction of tritium prior to nuclear testing, estimated at 10^{-20} (mass of tritiated water vapor to mass of gas, estimated from the background atomic ratio of 10^{-18} atoms of tritium to atoms of hydrogen). Breakthrough at the production well above background concentration was observed at the 99th percentile, with a peak mass fraction of 2.33×10^{-19} g^{THO} g_{gas}^{-1}, occurring 68 years after the nuclear test. Partitioning of tritium between the gas and liquid phases resulted in liquid phase mass fractions approximately two times higher than those in the gas phase.

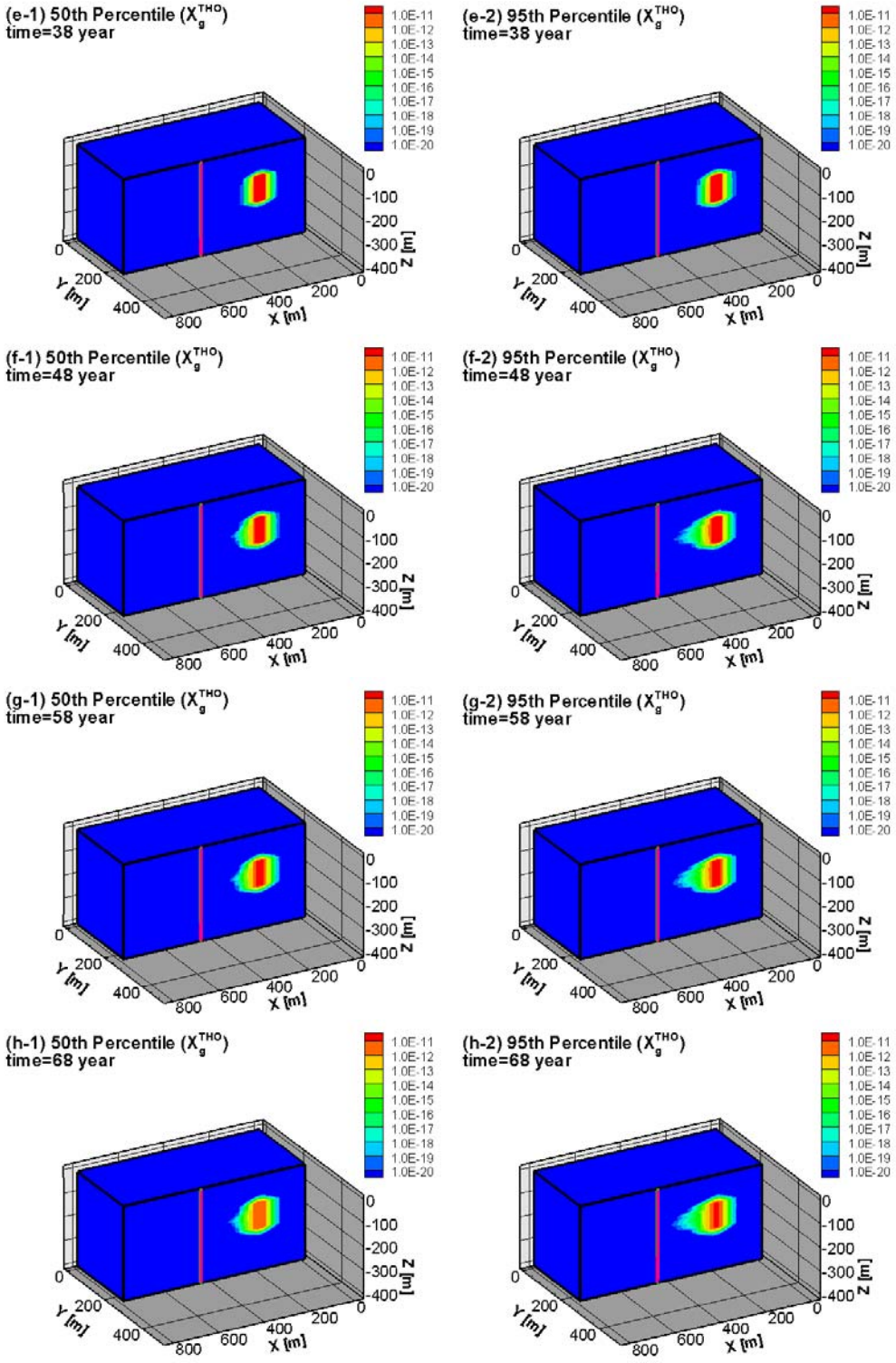

Figure 4. Results of Monte Carlo simulations showing the mass fraction of tritiated water vapor at the 50th (left column) and 95th (right column) percentiles for at the start of gas production (38 years after the nuclear detonation) through the end of gas production (68 years after the detonation). The top of the simulation is 2,368 m below the land surface.

2008 Addendum on Rulison

The results of the 2007 report discussed above suggested that there was less than five percent probability of tritium reaching a hypothetical gas production well located 258 m from the detonation point. Reviews of the model results indicated concerns with the value of the partitioning coefficient controlling the distribution of tritiated water between liquid and vapor phases, the assignment of effective porosity to hydraulically generated fractures surrounding the hypothetical production well, and the treatment of molecular diffusion in the partially saturated reservoir. These concerns were addressed in the 2008 addendum through additional computer simulations that tested the impact of these model features on the degree to which tritium is transported away from the detonation point.

Independent evaluation of the partitioning coefficient identified that the value used in Cooper et al. (2007) was inappropriate for the subsurface temperatures present in the gas reservoir at Rulison. A more correct value leads to no transport of tritium above background to the production well because tritiated water is strongly favored in the immobile aqueous phase (Figure 5).

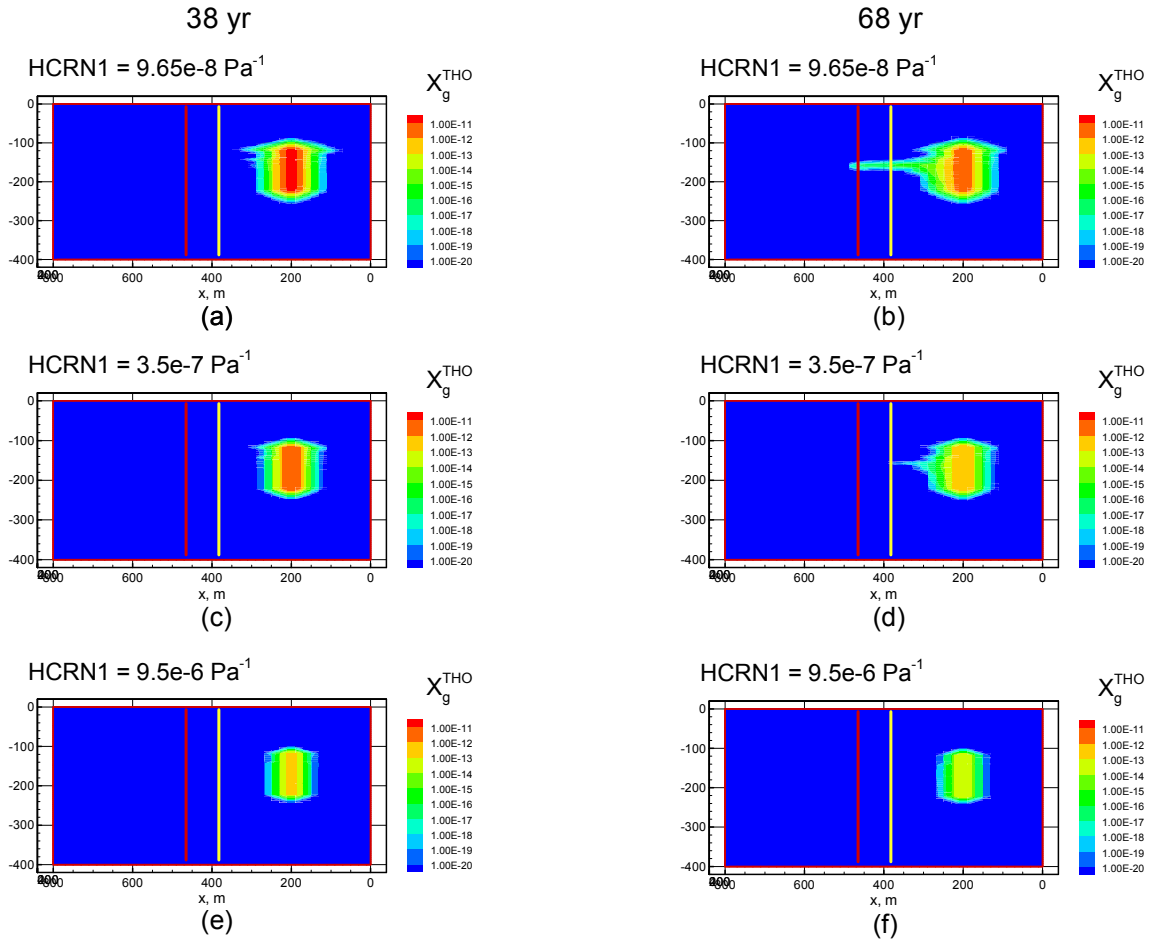

Figure 5. Results of three simulations in which the inverse Henry's law constant was changed. The three simulations used realization 10, which represents gas-phase tritium concentration at the 99th percentile in Cooper et al. (2007). The left-hand column shows the field of X_g^{THO} 38 years after the nuclear detonation while the right-hand column shows X_g^{THO} at 68 years. The first row, (a) and (b), shows the X_g^{THO} field for an inverse Henry's law constant appropriate for a temperature of 312 °C, while the second row shows the results for exactly the same simulation but with the inverse Henry's law constant equivalent to a temperature of 230 °C. The third row is the same as the first two, but for an inverse Henry's law constant appropriate for a reservoir temperature of 101 °C. The yellow vertical line in each figure depicts the location of the lot 11/12 boundary while the red vertical line shows the location of the gas production well.

Another limitation of the 2007 model was that the hydraulic fractures around the production well were assumed to have a porosity of 10 percent. This was changed in the 2008 Addendum to assume that the hydraulic fractures increased intrinsic permeability, but not porosity. This resulted in porosity values in the hydraulically fractured zone to be the same as the native formation. Reduction of this porosity to that of the host sandstone increases the velocity of the gas phase and accompanying tritiated water vapor (Figure 6).

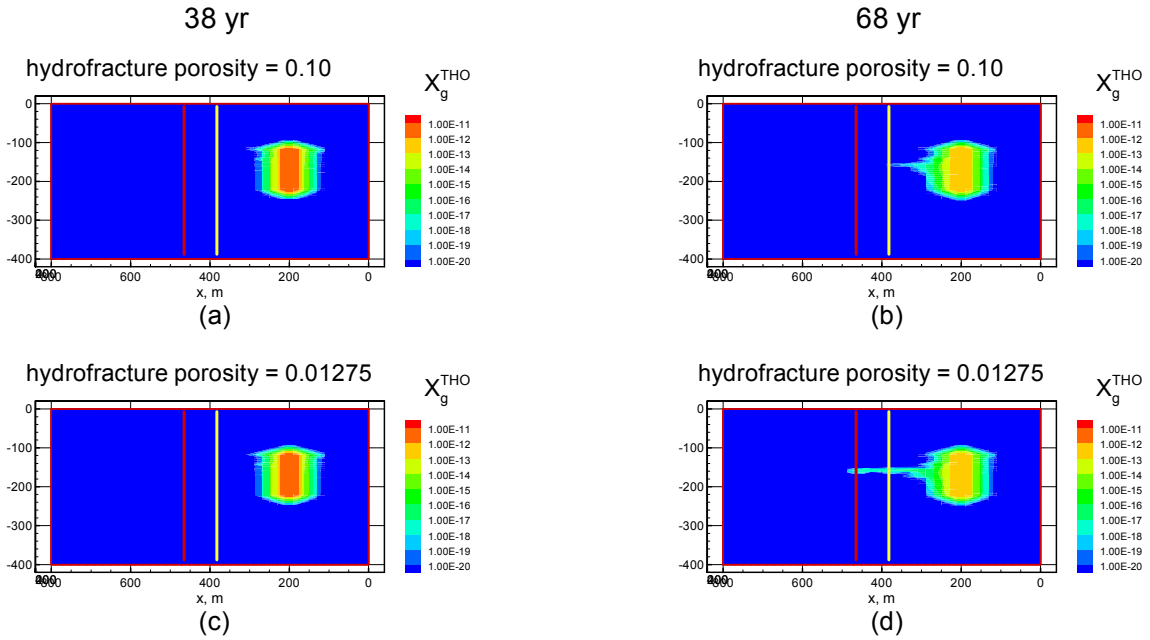

Figure 6. Results of two simulations that compare the effect of different hydraulic fracture porosity, based upon realization 10, and using partitioning for 230 °C. The upper row shows gas-phase tritium mass fraction toward a production well in which the EPM hydraulic fracture porosity is 0.10, while the lower row shows the same mass fraction field with a hydraulic fracture porosity equivalent to that of the native sandstone, in this case 0.01275. The yellow vertical line in each figure depicts the location of the lot 11/12 boundary while the red vertical line shows the location of the gas production well.

With respect to tritium diffusion, application of a tortuosity value that was constant and greater than the Millington-Quirk saturation-dependent model used previously resulted in greater diffusive spreading of the tritium plume. Both the hydraulic fracture porosity and diffusivity changes favored enhanced tritium transport away from the nuclear chimney, but their combined effects were overwhelmed by the effect of the partitioning coefficient, such that the new simulations predict *less* tritium transport than presented in Cooper et al. (2007). Only when partitioning was assumed to occur under the elevated temperature conditions that may be present in the bottom of the nuclear cavity, was transport observed at concentrations higher than that in Cooper et al. (2007) Figure 7 and Table 1. These conditions were not representative of the subsurface in the upper nuclear chimney or the surrounding formation. All of the additional simulations and sensitivity tests were performed with only the top ten of the 500 equally probable realizations considered by Cooper et al. (2007). Each of the 500 realizations presents an equally likely distribution of sandstone and shale; their porosity, permeability, and the length of the hydraulic fractured zone were selected from ranges possible for the formations. Focusing on only the ten realizations with the most transport neglected the importance of the sandstone-shale geometry in limiting transport from the nuclear chimney. Only in those few realizations with well-connected sandstone between the nuclear chimney and the production well was there any opportunity for transport. For those low probability cases, the new simulations showed that the tritiated water partitioning coefficient is the next dominant factor to control transport. Although low porosity and liquid water contents of the hydraulic fracture zone and small tortuosity values had the potential to increase tritium transport away from the chimney, they were much less

important than the configuration of the sandstone-shale geometry and partitioning of tritiated water between phases.

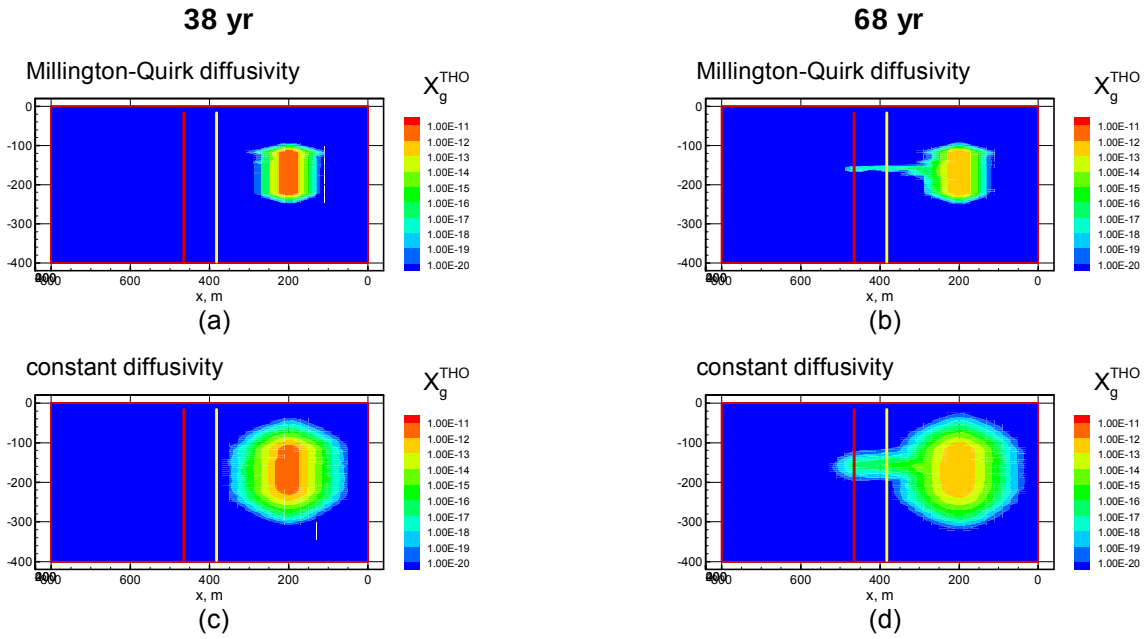

Figure 7. Results of two simulations in which the diffusivity model is compared. Realization 10, which was at the 98th percentile in breakthrough in the 2007 report was used for both simulations. The left-hand column shows the mass fraction of tritiated water vapor X_g^{THO} 38 years after the nuclear detonation while the right-hand column shows X_g^{THO} at 68 years. The first row, (a) and (b), shows the X_g^{THO} field for a simulation in which the Millington-Quirk tortuosity model was used, while the second row shows the results for a similar simulation in which the diffusivity was assumed constant. The yellow vertical line in each figure depicts the location of the lot 11/12 boundary while the red vertical line shows the location of the gas production well.

Table 1. Peak tritium mass fraction in the gas phase (X_g^{THO}) at the production well location for the ten Monte Carlo realizations with the most transport. Peak values occur between 48 and 68 years after the nuclear test. Three model results are shown for each realization: the results from Cooper et al. (2007); results with H_c^{-1} for 101 °C (realistic for most of the chimney except for the lowermost part), lower hydraulic fracture porosity, and constant diffusivity; and results for H_c^{-1} for 230 °C (probably only realistic for the lower part of the chimney where the detonation occurred), lower hydraulic fracture porosity, and constant diffusivity.

NMC	***Cooper et al. (2007)*** $_x$ (X_g^{THO})	H_c^{-1} **=101 °C** $_y$ (X_g^{THO})	H_c^{-1} **=230 °C** (X_g^{THO})
10	2.33×10^{-19}	$\sim 10^{-30}$	9.25×10^{-17}
30	3.38×10^{-19}	$\sim 10^{-35}$	1.79×10^{-20}
80	5.48×10^{-18}	$\sim 10^{-30}$	5.10×10^{-17}
118	6.58×10^{-20}	$\sim 10^{-39}$	8.58×10^{-23}
143	1.08×10^{-19}	$\sim 10^{-37}$	1.53×10^{19}
185	2.77×10^{-19}	$\sim 10^{-27}$	3.95×10^{16}
303	5.64×10^{-20}	$\sim 10^{-30}$	6.83×10^{17}
321	2.16×10^{-18}	$\sim 10^{-37}$	1.07×10^{20}
372	1.48×10^{-17}	$\sim 10^{-30}$	6.99×10^{18}
493	1.09×10^{-19}	$\sim 10^{-36}$	3.62×10^{20}

2010 Letter Report Update on Rulison

In 2010, a second enhancement (beyond the Addendum, discussed above) was made to the 2007 model. In this case, twelve random permeability/porosity fields were generated based upon updated statistics of the sandstone percentage (assumed to be 40 percent as opposed to 49 percent in the 2007 Report and 2008 Addendum). The sandstone porosity and permeability were determined based upon calibration to post-shot production of gas from the chimney. Other model enhancements included the following:

- The tortuosity value was changed to a constant value, 0.047 (derived in the addendum), rather than a parameter that could be as low as 10^{-5} (as was used in the 2007 report)
- Tritium partitioning between the gas and aqueous phases was completely dependent upon temperature
- A single value of sandstone permeability and porosity is used, rather than a distribution, based upon the calibration
- Gas production was simulated using a deliverability approach (production against specified pressure) rather than prescribed flow
- Nuclear fracture and hydraulic fracture continua were simulated as having ellipsoidal shape in the horizontal plane rather than cylindrical, resulting in longer fracture lengths in the east-west direction
- The hydraulic fracture continua simulated fracturing of all rock within 100 m and an outer zone of increased permeability in only sandstone, rather than the single, smaller, increased-permeability zone in only sandstone simulated in the previous model
- Separate capillary pressure and relative permeability curves were used for sandstone, shale, hydraulic fractures, and the nuclear chimney

A plan view of the simulation domain is shown in Figure 8, showing the 'ellipsoidal' fracture fields. The maximum distance of the nuclear-generated (chimney) fractures in the east-west (i.e., *x*-) direction was 100 m from the detonation, while the distance in the *y*-direction was 60 m. In the original model, nuclear-generated fractures extended 80 m in both the *x*- and *y*-directions. With respect to the hydraulic fractures, two different zones were developed (Figure 8). Within the inner zone, it was assumed that both the sandstone and shale units would be fractured, while in the outer zone, it was assumed that the shale would be too plastic to be fractured, such that only the sandstone would be fractured. The result of this is that the intrinsic permeability of the fractures zones was changed. The details are presented in Table 1 of the Addendum.

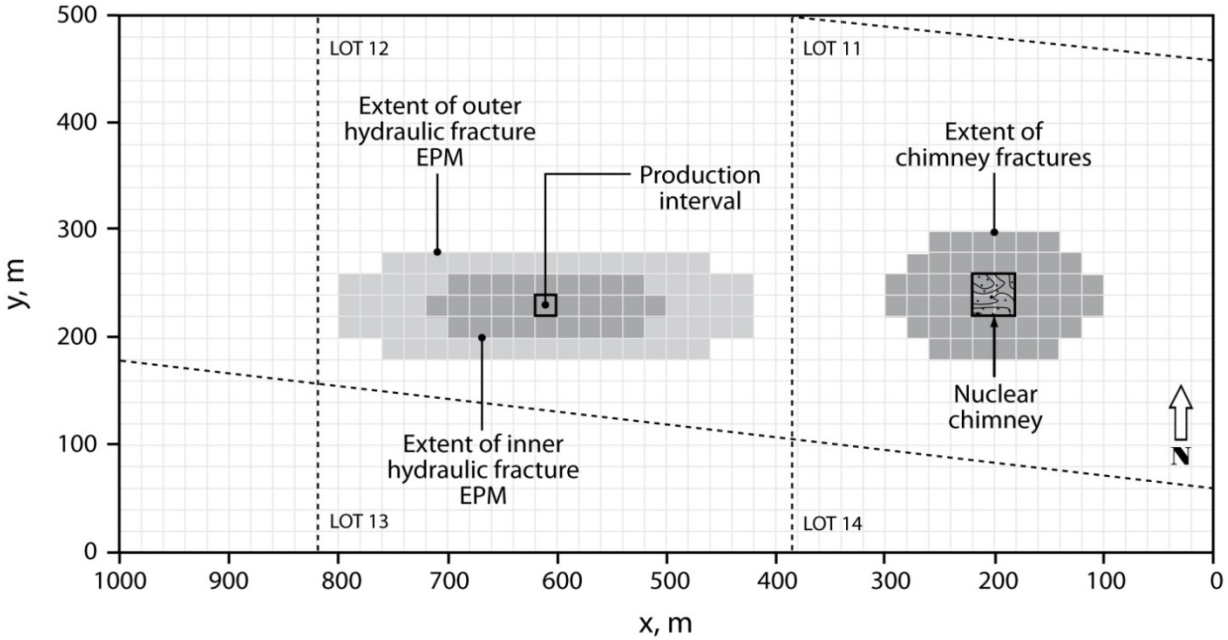

Figure 8. Plan view of the computational domain with nuclear chimney, chimney fractures, and inner and outer ellipsoidal fracture continua. Flow was from the nuclear chimney on the right toward the production well in the center of lot 12.

The model was calibrated against well test conducted subsequent to the nuclear detonation, in 1970 and 1971. The purpose of the calibration was to determine the best fit values for the native sandstone, the nuclear chimney, and the nuclear-generated (or explosion-related) fractures. The model was calibrated by prescribing a known flow rate to the re-entry borehole (the 'well' that was tested) and adjusting the permeabilities until the model pressure response matched that of the measured pressure during the test.

The tritium partitioning coefficient used in the 2007 report was for a temperature higher than that existing anywhere in the reservoir, and as a result, the simulations overpredicted tritium transport (i.e., they were overly conservative). This was changed in the Addendum to include a more realistic value for the reservoir temperature, realizing that the temperature in the cavity was much higher, and required a coefficient that would favor additional tritium in the gas phase. In the 2010 update, the issue was fully resolved by modifying the TOUGH2 program to handle temperature-dependent partitioning everywhere in the simulation domain. This was an important improvement over the manner in which partitioning was handled in the previous reports.

The results of the first 41 years of diffusive transport, prior to the implementation of a producing gas well, are shown in Figure 9. The results show that transport never extends beyond the boundary between lots 11 and 12. Although the simulation is for one permeability/porosity realization, the results are nearly identical for all 12 realizations, as diffusive transport is independent of permeability, and the porosity changes were so small between realizations that the differences in plume character is not discernible between simulations. The reason that the plume is now bell-shaped, in comparison to the results of previous simulations, is due to the higher temperature at the bottom of chimney, where the nuclear device was located, and the temperature is much hotter, favoring tritium partitioning into the gas phase.

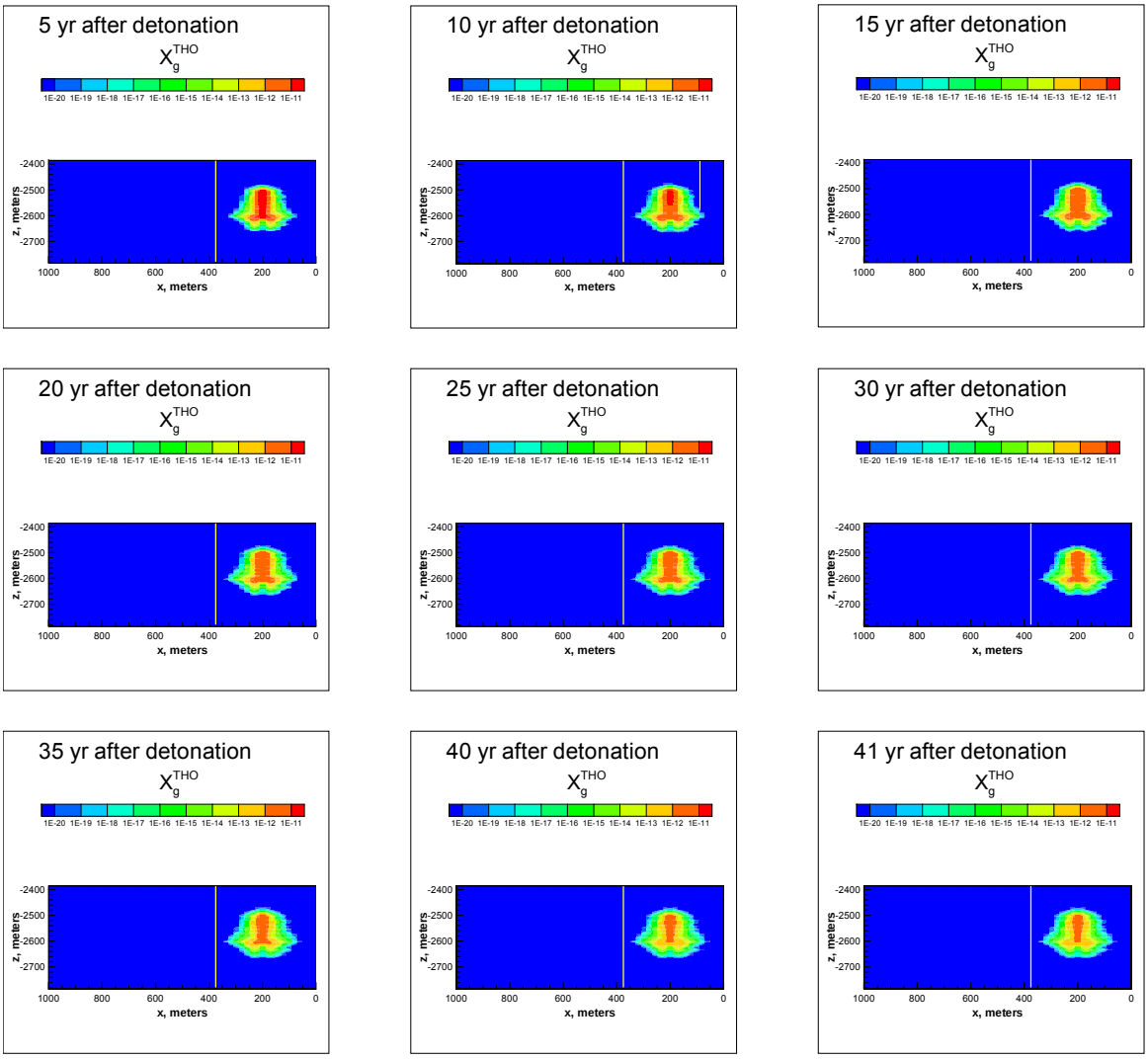

Figure 9. Mass fraction of tritiated water vapor in five-year increments for 41 years following the nuclear detonation for realization 1. Each pane shows a two-dimensional vertical east-west slice that cuts through the detonation point. Corresponding values in picocuries are 4 x 10^{10} picoCuries per liter (liquid water equivalent of condensed vapor) for X_g^{THO} =10^{-10} (the red end of the scale) to 4 pCi l^{-1} for X_g^{THO} =10^{-20} (the blue end of the scale). The vertical axis is depth below land surface, and the vertical yellow line depicts the boundary between lot 11 (to the right of the line) and lot 12.

Simulation results for all 12 permeability/porosity realizations are shown in Figure 10. Each panel in the figure is for the same time, 30 years after the start of gas production from the hypothetical gas well, which is the time of maximum transport. After 30 years, production was assumed to stop which would lead to a relaxation of the drainage gradient toward the well during production. In all twelve simulations, tritium did not extend beyond the boundary between lots 11 and 12, and therefore remained more than 200 m from the production well throughout the simulation. This is consistent with the results of the 2007 report, which showed that tritium would not reach the well in over 95 percent of the simulations.

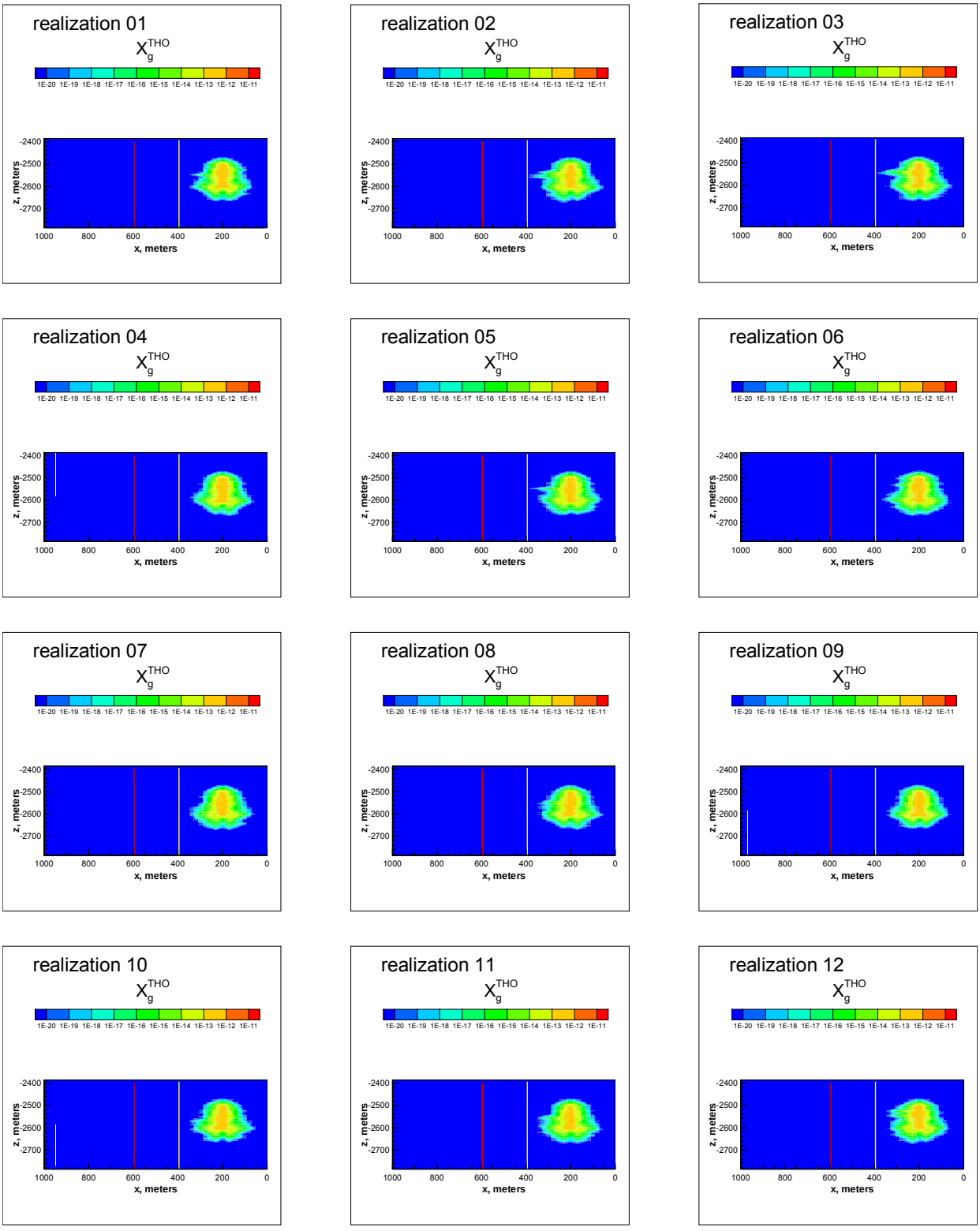

Figure 10. Mass fraction of tritiated water vapor after 30 years of gas production from the well, for all 12 realizations. The vertical axis is depth below land surface. The vertical yellow line is the boundary between lot 11 (to the right of the line) and 12, while the vertical red line shows the location of the hypothetical production well.

TOUGH2 Computer Program

The conceptual model includes flow and transport as coupled processes that must be solved simultaneously to get a realistic understanding of the radionuclide distribution. The TOUGH2 (**T**ransport **o**f **U**nsaturated **G**roundwater and **H**eat) integral finite difference simulator was used to implement the model as it handles three-dimensional, multiphase, multicomponent heat and mass transport through porous media in a fully coupled manner (Pruess et al. 1999). The code fully accounts for the movement of gaseous and liquid phases, their transport of latent and sensible heat, and phase transitions between liquid and vapor occurring under pressure, viscous, capillary, and gravity forces according to Darcy's law. The program provides options for specifying injection or withdrawal of energy (heat) and fluids. The equation of state module that was implemented (EOS7R) is capable of handling four components: water, air, solute and heat. TOUGH2 is a DOE-sponsored code that has been used extensively to study heat and mass flow in geothermal reservoirs, saturated/unsaturated zones, and oil and gas reservoirs. Several changes were made to the TOUGH2 program in order for it to correctly simulate the important processes. The EOS7R module assumes the gas phase to be air and air/water mixtures. This was easily changed to replace air properties with those of methane, which are important in the density and viscosity correlations.

References

Cooper, C.A., and J. Chapman, 2001. Modeling approach for evaluating radionuclide transport in nuclear-stimulated gas reservoirs, DRI Publication no. 45186, also DOE/NV/13609-15, 36 pp.

Cooper, C.A., 2004. Scoping analysis of gas phase transport from the Rulison underground nuclear test, Desert Research Institute Letter Report, also DOE/NV/13609-LTR2004-01, 12 pp.

Cooper, C.A., M. Ye, J. Chapman, and C. Shirley, 2005. Radionuclide migration at the Rio Blanco Site, a nuclear-stimulated low-permeability natural gas reservoir, DRI Publication no. 45215, also DOE/NV/13609-45, 94 pp. plus three appendixes.

Cooper, C.A., M. Ye, J. Chapman, 2007. Tritium transport at the Rulison site, a nuclear-stimulated low-permeability natural gas reservoir, Desert Research Institute publication 45224, and DOE Office of Legacy Management, DOE/NV/13609-54, 102 pp.

Cooper, C.A., M. Ye, and J.B. Chapman, 2008. Addendum: Tritium transport at the Rulison Site, a nuclear-stimulated low-permeability natural gas reservoir, unpublished Desert Research Institute, Reno, Nevada, letter report, 18 pp. plus two appendixes.

Cooper, C.A., J.B. Chapman, Y. Zhang, R. Hodges, and M. Ye, 2010. Update of tritium transport calculations for the Rulison Site: Report of activities and results during 2009–2010, unpublished Desert Research Institute, Reno, Nevada, letter report, 24 pp.

Pruess, K., C. Oldenburg, and G. Moridis, 1999. *TOUGH2 User's Guide, Version 2.0*, LBNL-43134, Berkeley, California.

Ye, M., C.A. Cooper, J.B. Chapman, D. Gillespie, and Y. Zhang, 2009. Geologically based Markov chain model to simulate solute tracers in natural gas reservoirs with uncertain conditions, SPE Reservoir Evaluation & Engineering, 12(6), pp. 974–984, doi 10.2118/114920-PA.

This page intentionally left blank

Appendix B

Method Used to Create Sandstone - Shale Realizations

This page intentionally left blank

Transition-probability based geostatistical model for the Rulison and Rio Blanco Sites

Yong Zhang and David Gillespie

Desert Research Institute

April 8, 2011

In this study, logs from the Rulison emplacement well (R-E), the Rulison exploratory well (R-EX), and six recently drilled Noble Energy gas production wells (BM 26-33b, 26-33c, 26-33d, 26-34a, 26-34b, and 26-34c) are incorporated into TPROGS [Carle et al., 1998] to simulate the distribution of sandstone and shale facies. In comparison to traditional variogram-based geostatistical methods, the transition probability/Markov approach in TPROGS improves consideration of spatial cross-correlations and facilitates the integration of geologic interpretation of facies architecture into the model development process.

The results were used to generate several equally probable facies distribution realizations of the Rulison subsurface (upper and lower Williams Fork Formation) that were used to populate the model mesh. The wells within the Rio Blanco model domain do not reach the lower Williams Fork Formation. The statistics from the well data at Rulison were used with the well data at Rio Blanco to generate several equally probable facies distribution realizations of the Rio Blanco subsurface (Ft Union Formation, and the upper and lower Williams Fork Formation).

1. Upper Williams Fork Formation (UWF)

The average thickness for sandstone, 13.0 ft, is fitted by the measured transition probabilities along the vertical direction (Figure 1). Here the transition probability is defined by the following conditional probability

$$t_{ij}(h) = \Pr\{j \text{ occurs at } x+h \mid i \text{ occurs at } x\} \quad ,$$

where x is a spatial location, h is the lag (separation vector), and i, j denote facies.

In Figure 1, the intersection of the grey line (tangent of transition probability) with lag axes indicates the average thickness of each facies. The shale facies is treated as the background category in TPROGS, since it has a higher proportion than sandstone. The measured average thickness for shale is 16.46 ft.

The volumetric proportion of sandstone and shale is 44.4% and 55.6%, respectively. This is similar to the proportion observed in the UWF at Rio Blanco (which is 43.6% and 56.4% for sandstone and shale, respectively). In Figure 1, the dashed line denotes the proportion of each facies.

Figure 1 also shows that the Markov chain model fits the measured transition probabilities. The good agreement is due to the relatively abundant data along the vertical direction.

For the horizontal direction (Figure 2), the calculation of mean length for each facies contains intrinsic uncertainty, due to the sparse data along this direction (similar to many other sites). The facies distribution along the horizontal direction is assumed to be isotropic, since no data at present shows clearly the anisotropic pattern. The mean length along the horizontal direction is 650 and 823 ft for sandstone and shale, respectively. The 650-ft mean length for sandstone is estimated by the measured transition probabilities along the horizontal direction (Figure 2). It is also on the same order as the one (528-ft) used by Cooper et al. [2007] for the Rulison site. The 823-ft mean length for sandstone is the best-fit result of TPROGS, based on the measured transition probabilities (note that in the horizontal direction, shale can also be treated as the background category).

2. Lower Williams Fork Formation (LWF)

The average thickness for sandstone, 12.4 ft (see Figure 5), is smaller than that in the UWF unit. Similarly, the proportion of sandstone (42.5%, calculated by driller's logs), is relatively smaller than that in UWF. The calculated average thickness for shale is 16.7 ft.

Sandstone is less continuous in the LWF than the sandstone in the UWF. The mean length (along the horizontal direction) for LWF sandstone is 450 ft, which is 70% of the mean length in UWF. A shorter mean length in LWF than UWF is expected, since the LWF was deposited primarily in an alluvial system and the UWF in primarily a marine depositional system. Note again that the 450-ft mean length for sandstone is estimated by the measured transition probabilities (Figure 6), which contain high uncertainty and apparent noise due to the sparse data on the horizontal direction.

The volumetric proportion of sandstone and shale is 42.5% and 57.5%, respectively. Hence the LWF has less sandstone than the UWF.

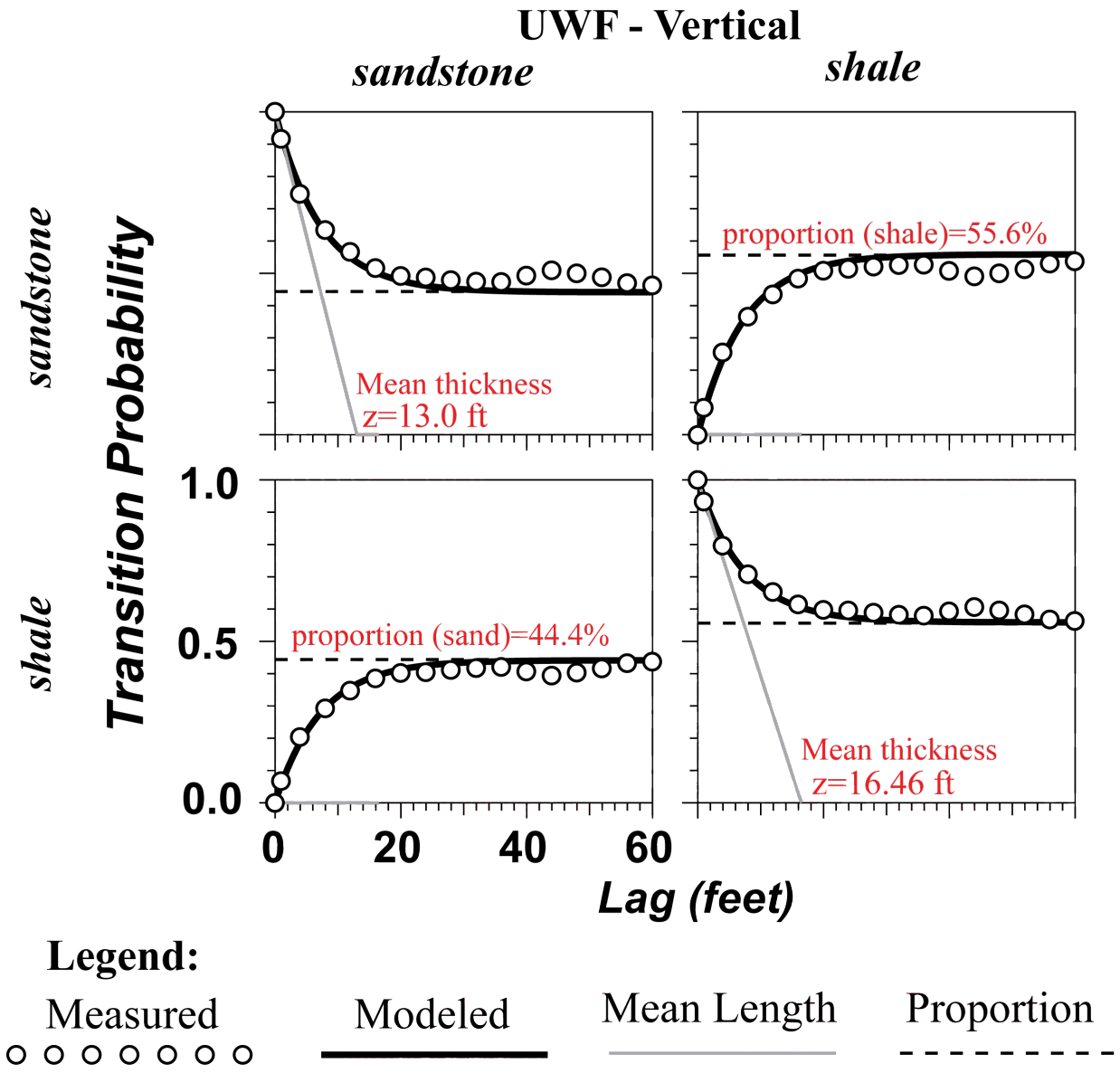

Figure 1. UWF-Vertical: The Markov Chain/Transition probability model along the vertical direction built for UWF, using 6 wells.

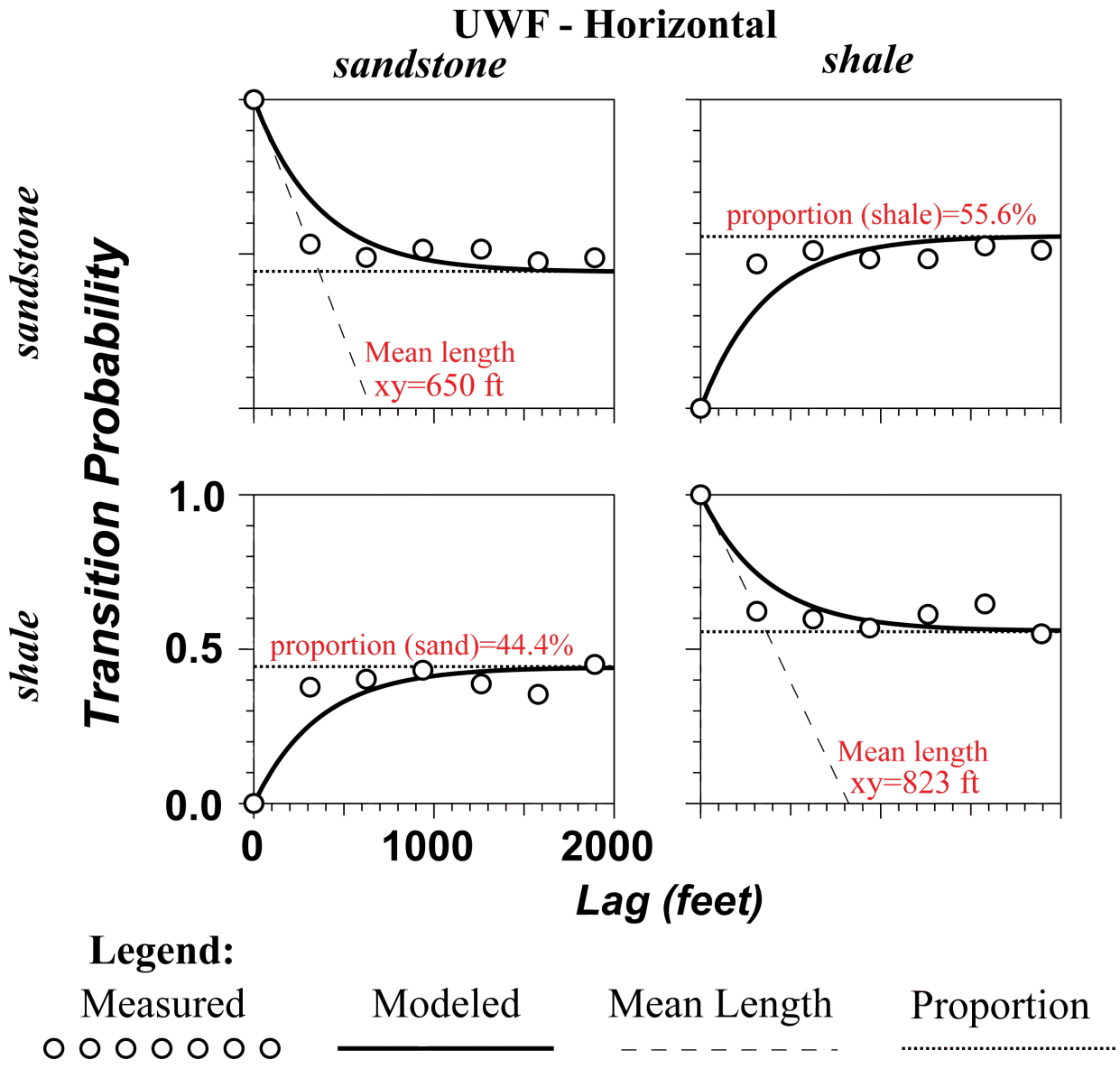

Figure 2. UWF-horizontal: The Markov Chain/Transition probability model along the horizontal direction built for UWF, using 6 wells.

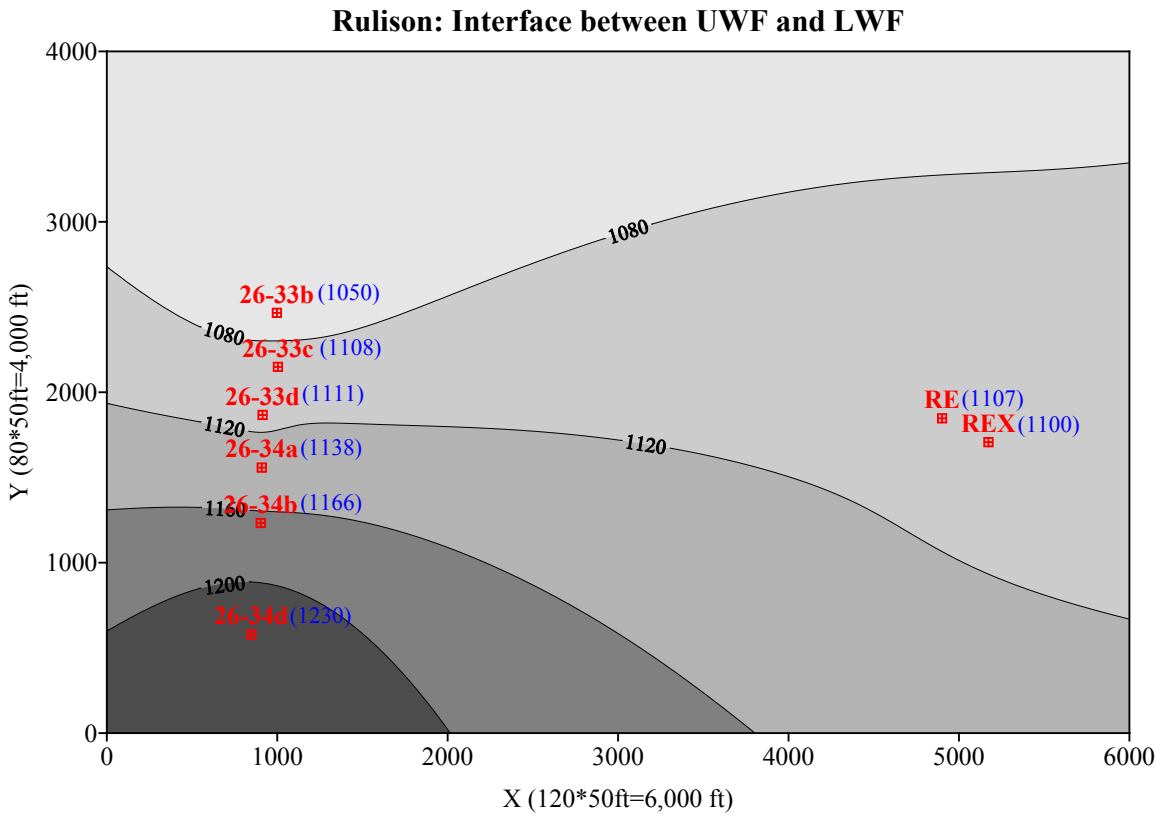

Figure 3. Elevation (feet) of the interface between the UWF and LWF. The contour was generated by interpolating the interface at the 8 wells, using Kriging method. The blue font on the right side of each well denotes the elevation of the interface. Note that the interface for well 26-33 and 26-34 was interpreted by: "*The topmost continuous sandstone unit was picked as the top of the WF. Around 1200 feet there is a silty zone that seem to separate the thicker more continuous units and thinner units below. The top of Gas was picked at the first continuous sandstone unit below the silty zone. The top of the Cameo was selected based on the bottom of the somewhat continuous sandstone units and the top of the discontinuous units below*". The interface for R-E and R-EX was picked as the first continuous sandstone unit below the silty zone.

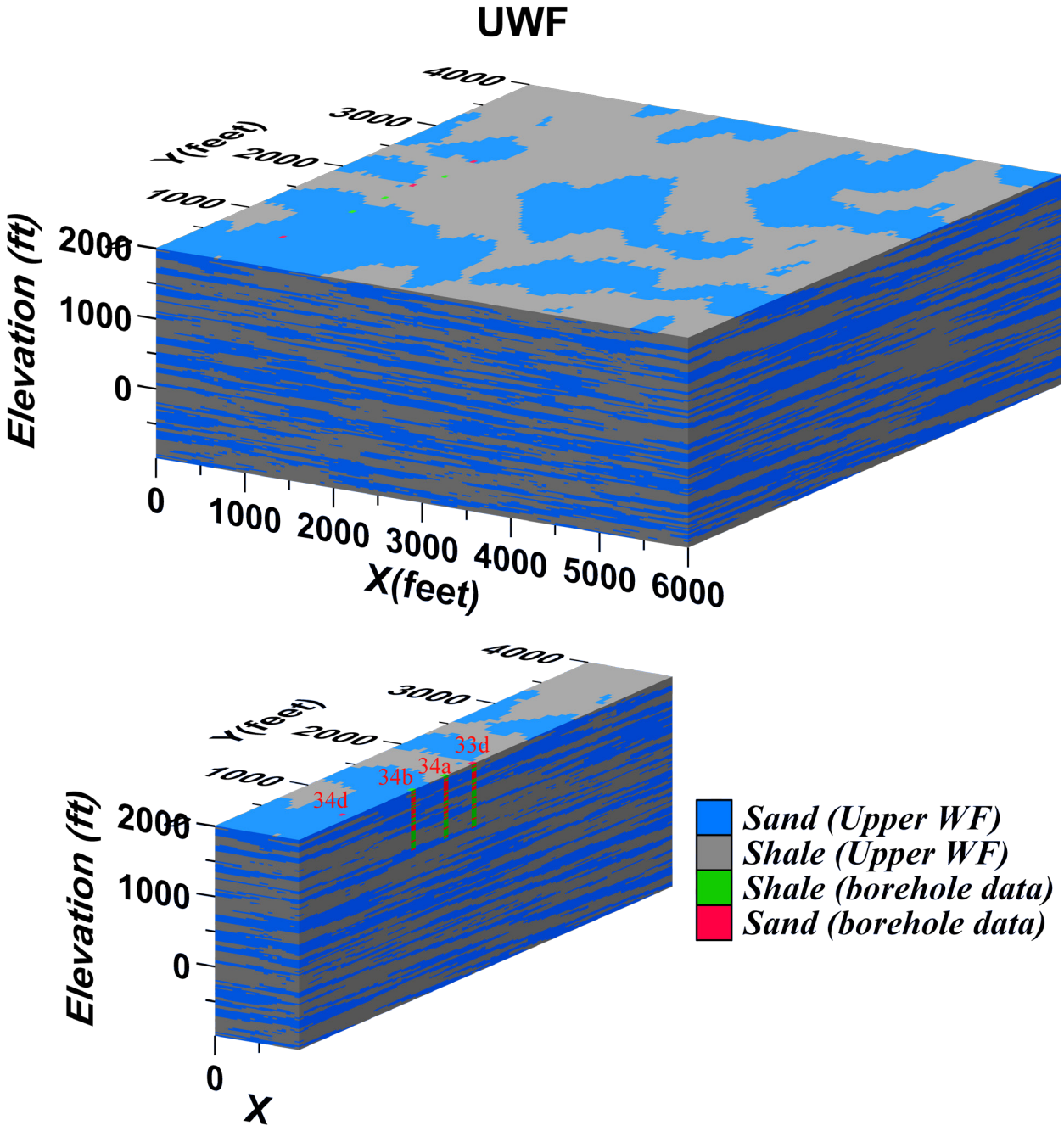

Figure 4. Rulison-UWF facies model (3-d view and an exploded view) built by TPROGS (using the model shown in Figure a 1 and Figure 2).

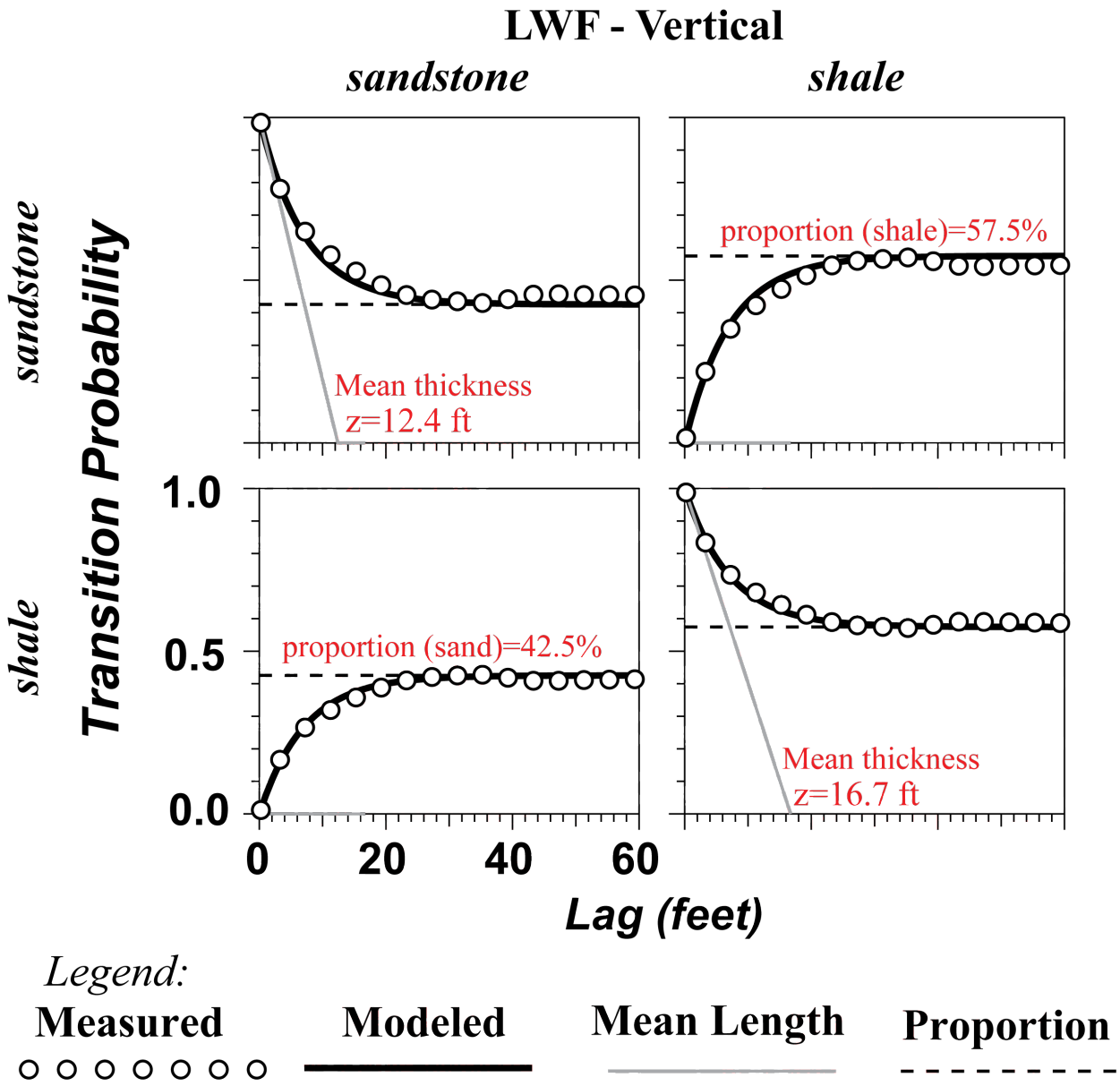

Figure 5. LWF-Vertical: The Markov Chain/Transition probability model along the vertical direction built for LWF, using 8 wells.

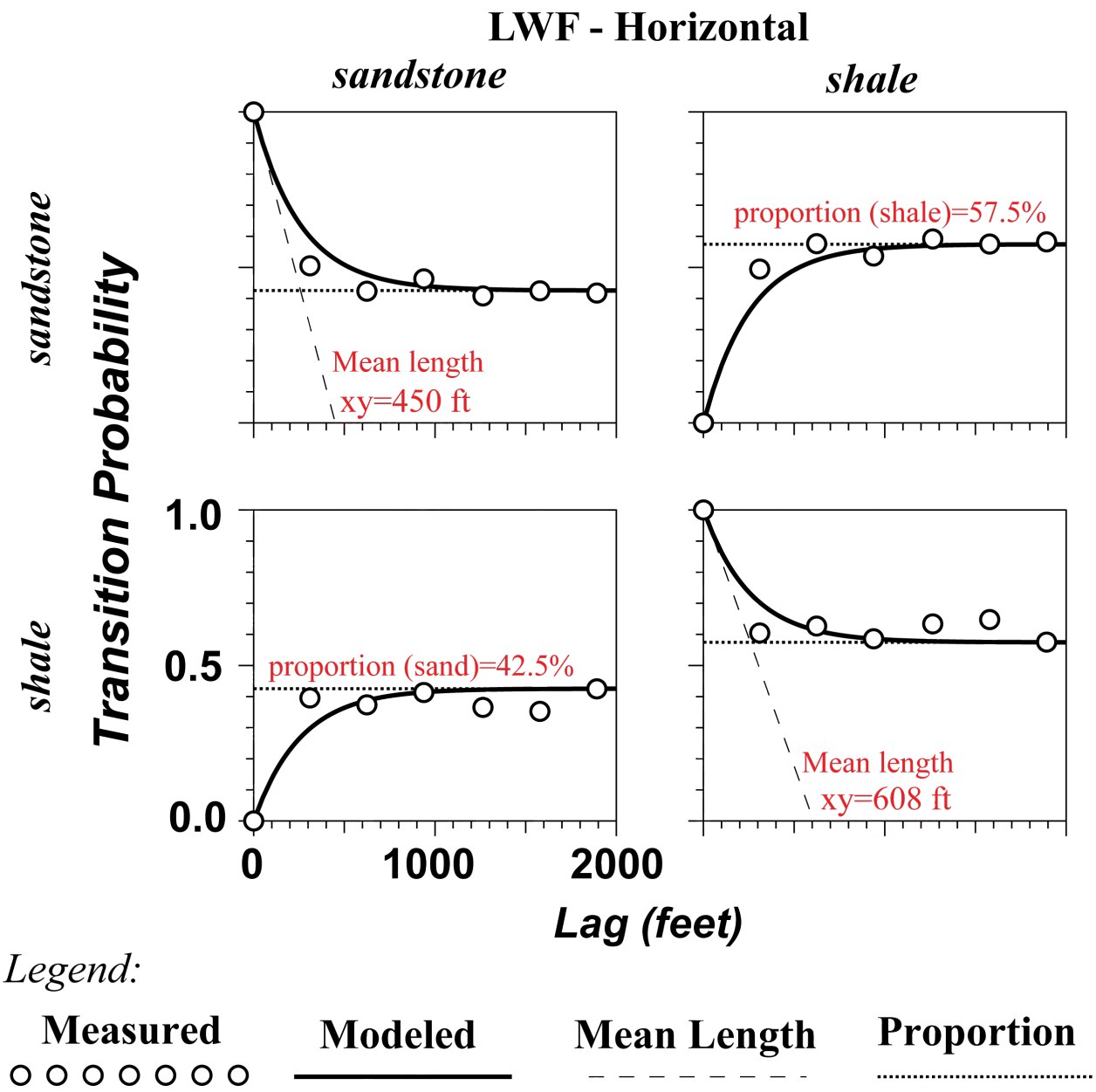

Figure 6. LWF-horizontal: The Markov Chain/Transition probability model along the horizontal direction built for LWF, using 8 wells.

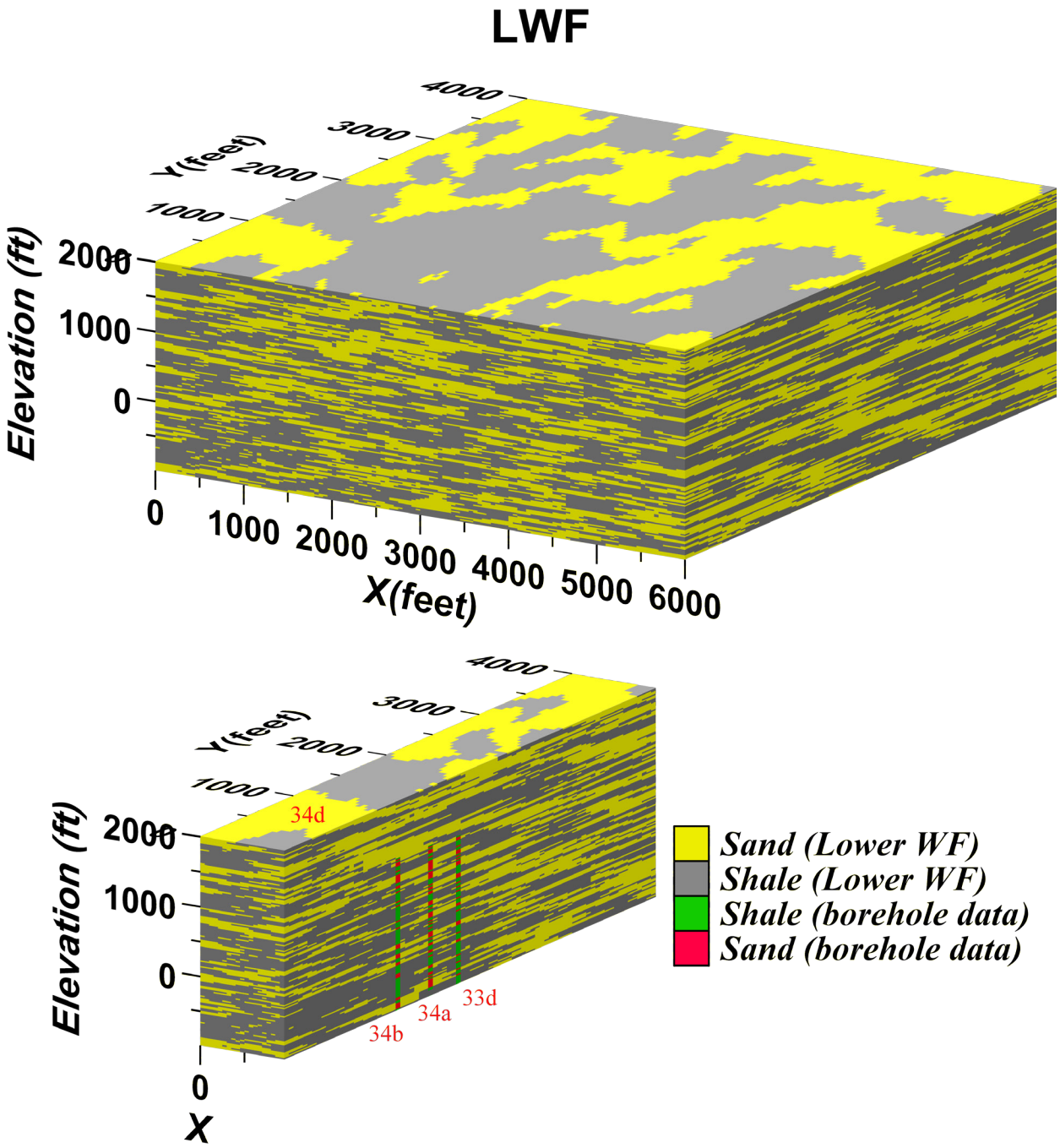

Figure 7. Rulison-LWF hydrofacies model (3-d view and the exploded view) built by TPROGS (using the Markov Chain models shown in Figure 5 and 6).

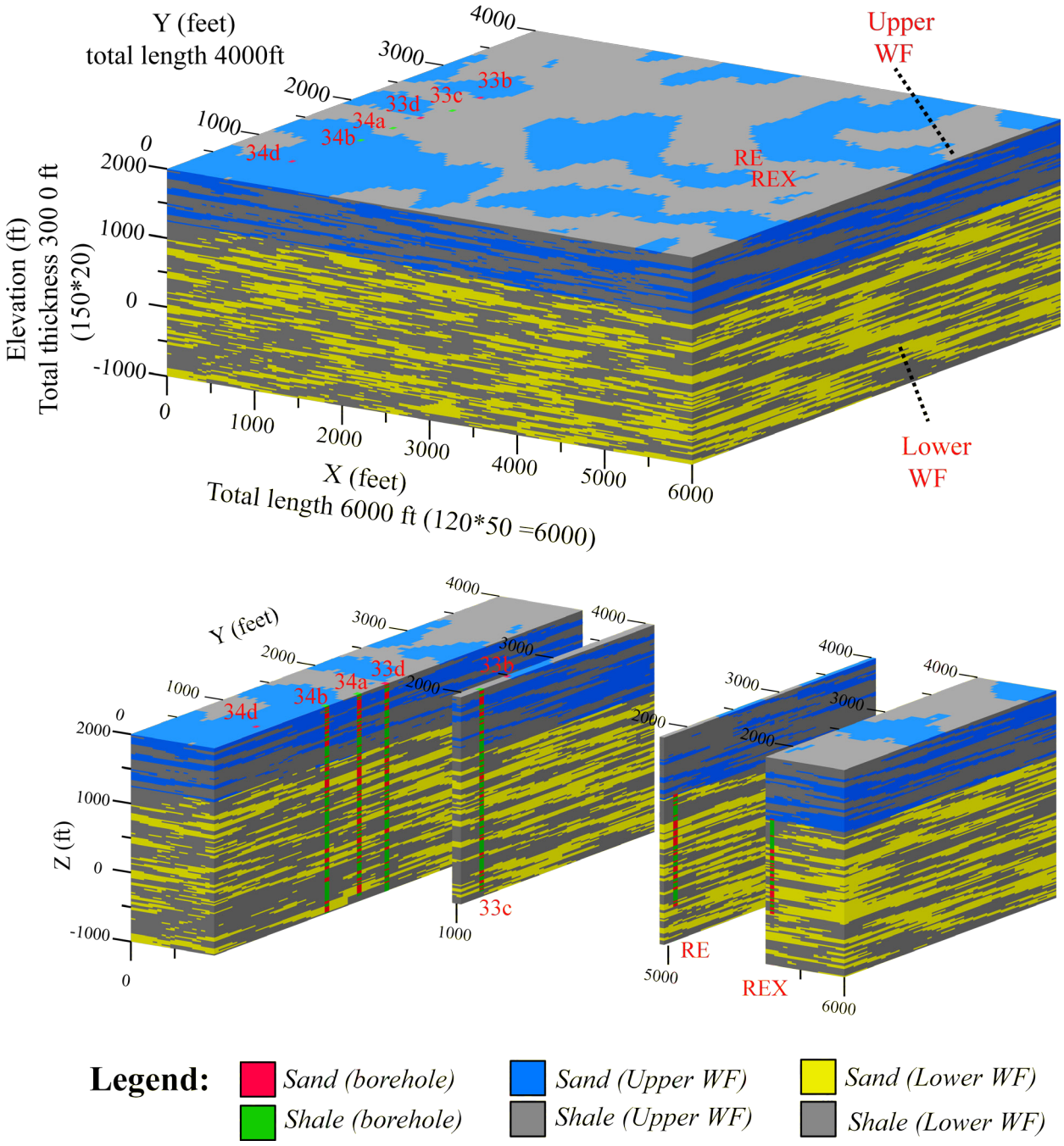

Figure 8. Combining Fig. 4 and Fig. 7 (with the interface shown by Fig. 3)) - Rulison facies model (3-d view and the exploded view) built by TPROGS. 8 wells (26-33b, 26-33c, 26-33d, 26-34a, 26-34b, 26-34d, RE, and REX) are used to build the transition probability model.

Reference

Carle, S. F., Labolle, E. M., Weissmann, G. S., Van Brocklin, D., and Fogg, G. E., 1998, Conditional simulation of hydrofacies architecture: a transition probability/Markov approach, In Fraser, G. S., and Davis, J. M., Concepts in Hydrogeology and Environmental Geology No. 1, SEPM (Society for Sedimentary Geology) Special Publication, p. 147-170.